

**SYNTHESIS AND E.S.R. STUDIES OF METAL IONS
IN LESS COMMON OXIDATION STATES :**

**(i) Chemistry of Dioxo-Bridged Manganese (III, IV)
Complexes and (ii) Chemistry of Bivalent Silver
Complexes with Sterically Hindered Ligands**

**A THESIS
SUBMITTED FOR THE DEGREE OF
DOCTOR OF PHILOSOPHY**

**By
G. SWARNABALA**



**SCHOOL OF CHEMISTRY
UNIVERSITY OF HYDERABAD
HYDERABAD - 500 134**

DECEMBER, 1988

CONTENTS

	Page No.
STATEMENT	i
CERTIFICATE	ii
ACKNOWLEDGEMENT	iii
PREFACE	iv
ABBREVIATIONS	viii
SECTION I	1
Chapter 1	2
Chapter 2	28
Chapter 3	34
References	112
SECTION II	120
Chapter 1	121
Chapter 2	127
Chapter 3	133
References	179
SUMMARY AND CONCLUSIONS	184

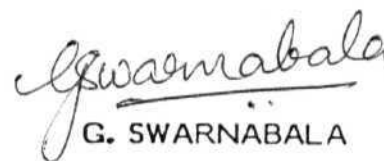
STATEMENT

I hereby declare that the matter embodied in the thesis is the result of investigations carried out by me in the School of Chemistry, University of Hyderabad, Hyderabad, under the supervision of Dr. M.V.Rajasekharan.

In keeping with the general practice of reporting scientific observations, due acknowledgement has been made whenever the work described is based on the findings of other investigators.

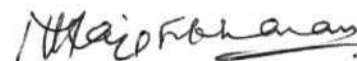
Hyderabad

December, 1988


G. SWARNABALA

CERTIFICATE

Certified that the work contained in this thesis entitled "Synthesis and e.s.r. studies of metal ions in less common oxidation states: (i) Chemistry of dioxo-bridged manganese (III, IV) complexes and (ii) Chemistry of bivalent silver complexes with sterically hindered ligands" has been carried out by G.Swarnabala, under my supervision and the same has not been submitted elsewhere for a degree.



M.V. Rajasekharan



Dean

School of Chemistry

(Thesis Supervisor)

ACKNOWLEDGEMENT

I thank Dr. M.V. RAJASEKHARAN for suggesting a topic of interest to me and for his help to learn the subject in a systematic, thoughtful and lucid fashion.

I wish to thank Prof. G. MEHTA and Prof. R. JAGANNATHAN, Deans, School of Chemistry during the tenure of my work in the University for their helpful cooperation.

I recall with happiness my acquaintance with all the staff of School of Chemistry, CIL and work shop and thank them for their timely cooperation.

It is a pleasure to remember all my colleagues of the School whose names form a volume of its own.

I thank all the University staff with whom I had contact for their help and enquiries.

I particularly recall the complete cooperation from my near and dear.

I greatly acknowledge financial assistance from U.G.C.

G. SWARNABALA

PREFACE

Mixed valent manganese complexes play an important role in the evolution of oxygen by water oxidation in Photosystem (PS II) of photosynthesis. Details regarding the structure of manganese site and the reaction mechanism are still ambiguous. However, some binuclear and tetranuclear complexes with polypyridyl, Schiff-base and related ligands in which the manganese is in (III, IV) oxidation states are proposed as good models. We desired to take advantage of the substitutional lability of $\text{Mn(III)}(d^4)$ site to prepare and characterise unsymmetrically ligated complexes. This has resulted in the isolation of complexes of the type $(\text{Mn}_2\text{O}_2\text{L}_3\text{A}_2)^{3+}$ where $\text{A}=\text{dmf}$, py and $(\text{Mn}_2\text{O}_2\text{L}_3\text{A})^{3+}$ where $\text{A}=\text{bpy}$, $\text{L}=\text{phen}$ and $\text{A}=\text{phen}$, $\text{L}=\text{bpy}$. They have been characterised by i.r, electronic and e.s.r spectra. The studies on oxygen evolution in presence of Ce^{4+} suggest that the unsymmetrical complexes are better catalysts for water oxidation.

We had also planned to synthesise new Mn(III, IV) complexes with ligands related to bpy viz., dmbp , dmp , mmbp , tmbp , daf and daf-one with a view to modify the electron transfer rate. However, all our attempts in this direction using Mn^{2+} and oxidizing agents like MnO_4^- , $\text{S}_2\text{O}_8^{2-}$ as well as substitution on Mn(urea)_6^{3+} followed by disproportionation and dimerisation, were unsuccessful.

Since we have prepared several sterically hindered ligands for the above purpose, we surveyed the chemistry of other complexes of these ligands. The interesting aspects of the copper chemistry of these ligands especially their marked influence in the $\text{Cu}^+/\text{Cu}^{2+}$ potential prompted

us to prepare and study analogous silver complexes. We have obtained magnetically dilute double salts, $[\text{AgLNO}_3]\text{PF}_6 \cdot \text{NH}_4\text{PF}_6$, with dmp and dmbp ligands while other ligands formed magnetically concentrated complexes. Detailed e.s.r studies were carried out on the double salts. These complexes were unstable and slowly disintegrated to give radicals which gave uninterpretable e.s.r spectra suggesting a novel electron transfer from PF_6^- to Ag^{2+} ion.

Our studies on the two different metals are separated into Section I and Section II for a convenient presentation.

In Section I the chemistry of dioxo-bridged manganese (III, IV) complexes are reported, beginning with a chapter giving details on mixed valent complexes in general, their historical importance, theory, classification and the literature on Mn(III, IV) complexes. The next chapter deals with the experimental section in which preparative methods are described along with the techniques used for the physical measurements and the computer simulation program used. The last chapter in this section gives a detailed discussion on the results of various analytical and spectral studies, as well as catalytic water oxidation in the presence of $(\text{NH}_4)_2\text{Ce}(\text{NO}_3)_6$.

In Section II, complexes of bivalent silver with sterically hindered ligands are reported. The first chapter gives a brief introduction to Ag(II) chemistry including a survey on bivalent silver complexes of heteroaromatic ligands. This is followed by a discussion on the analogous copper complexes with the above mentioned sterically hindered ligands. The second chapter describes the experimental proce-

dures adopted and the program for the computer simulation of e.s.r spectra. The last chapter gives the discussion of various analytical and spectral results obtained including a detailed interpretation of the e.s.r results on Ag(II) complexes of heteroaromatic ligands. These double salts lead to the formation of radicals which resulted in an uninterpretable e.s.r spectra. A survey of literature ruled out the possibility of silver cluster formation. Electron transfer from PF_6^- to Ag^{2+} is proposed and various radicals involving P and F, including the hitherto unknown PF_6 radical are considered as possible sources for the complex spectrum.

Some of the results presented in this thesis have been published or communicated in preliminary form.

- (i) "EPR studies of mixed valence interactions in Mn(III, IV) complexes", G. Swarnabala, M. Umashankar and M. V. Raja Sekharan, *Proc. XXII Congress Ampere on Magnetic Resonance and Related Phenomena, Zürich (1984)p.457-458.*
- (ii) "Water Oxidation by dioxo-bridged Mn(III, IV) Complexes", G. Swarnabala and M.V. Rajasekharan, *Proc. National Symposium on Unusual Valency States in Coordination Compounds, BARC, Bombay (1987) p.C-18.*
- (iii) "Chemistry of the Less Common Oxidation States of Manganese and Silver in their Complexes with N-heterocyclic ligands", G. Swarnabala and M.V. Rajasekharan, *Proc. National Symposium on Modern Trends in Inorganic Chemistry, IIT, Madras (1988)p.ML-4.*

- (iv) "Silver(II) Complexes of Hindered N-heterocyclic ligands. Electron Spin Resonance of Nitrato (6,6'-dimethyl-2,2'-bipyridyl) silver(II) and Nitrato (2,9-dimethyl-1,10-phenanthroline) silver(II) ions", G. Swarnabala and M.V. Rajasekharan, *Inorg. Chem.* (1989) in press.

ABBREVIATIONS

acac	: acetylacetone
bpy	: 2,2'-bipyridine
busalen	: N,N'-ethylenebis(4-sec-butyl salicylaldehyde)
busaltm	: N,N'-trimethylenebis(4-sec-butyl salicylaldehyde)
cat	: catechol
daf	: 4,5-diazafluorene
daf-one	: 4,5-diazafluorene-9-one
dedtc	: diethyldithiocarbamate
4,4'-dmbp	: 4,4'-dimethyl-2,2'-bipyridine
5,5'-dmbp	: 5,5'-dimethyl-2,2'-bipyridine
6,6'-dmbp(dmbp)	: 6,6'-dimethyl-2,2'-bipyridine
dmp	: 2,9-dimethyl-1,10-phenanthroline
dmf	: dimethylformamide
dmsO	: dimethylsulfoxide
4,4'-dpbp	: 4,4'-diphenyl-2,2'-bipyridine
4,7-dpp	: 4,7-diphenyl-1,10-phenanthroline
DPPH	: diphenylpicrylhydrazine
mmbp	: 6-monomethyl-2,2'-bipyridine
nicotin	: nicotinic acid
Oac	: acetate
phen	: 1,10-phenanthroline
N ₄ -pyridine	: tris(2-pyridylmethyl)amine
py	: pyridine

pz	: pyrazine
H ₂ sal	: salicylic acid
H ₂ salen	: N,N'-ethylenebis(4-sec-butyl salicylaldimine)
H ₂ saltn	: N,N'-trimethylenebis(salicylaldimine)
SB	: Schiff-base
tmbp	: 4,4',6,6'-tetramethyl-2,2'-bipyridine
tmtc	: N,N',N''-trimethyl-1,4,7-triaza cyclononane
TPP	: tetraphenylporphyrin
terpy	: 2,2',2''-terpyridine
TBA-PF ₆	: tetrabutylammoniumhexafluorophosphate

SECTION - I

CHEMISTRY OF DIOXO-BRIDGED MANGANESE (III, IV) COMPLEXES

CHAPTER -1
INTRODUCTION TO MIXED-VALENCE CHEMISTRY
AND A SURVEY OF THE LITERATURE ON
MANGANESE (III, IV) COMPLEXES

1. 1 General introduction to mixed-valence compounds:-

Compounds containing a given element in more than one formal oxidation state have been known for a long time. They usually have intense colours as exemplified by Prussian Blue which has been in use as an ink and dye-stuff for a few hundred years¹. Werner proposed² variable valency for the brightly coloured complexes prepared in the early 19th century. The development of crystal field theory and new physical techniques have provided deeper insight into the electronic structure of the mixed-valence compounds. Consequently, around 1967, several review articles have appeared which emphasised the optical properties and developed a scheme of classification based on electronic delocalisation³. These reviews as well as the earlier results on controlled valency semi-conductors⁴ which illustrated the correlation between structure and physical properties have stimulated much theoretical and experimental investigation. It is now recognised that mixed-valency plays an important role in several areas of science ranging from mineralogy to biology. Many of these various aspects are discussed in a recent volume on the subject edited by D.B.Brown⁵. Mixed-valency involving copper centers is believed to be of crucial importance in the recently discovered high temperature ceramic superconductors⁶. The next three sub-sections contain a brief review of the present theoretical understanding with reference to certain well studied mixed-valence systems.

1. 2 Classification of mixed-valence compounds:-

The mixed-valence complexes were classified by Robin and Day^{3e} on the basis of the strength and symmetry of the ligand fields about metal ions and their relationship to α , the valence delocalisation coefficient appropriate to a particular system, into three groups.

Class I: The different valence sites have quite different symmetry and ligand field strength, so that the energy difference is large and α approaches zero. An example would be the spinel, Co_3O_4 , in which the Co(III) ions are in octahedral ligand fields with low-spin configurations while the Co(II) ion is in tetrahedral ligand field with high-spin configuration. The two sites are so different that the properties of this compound can be thought of as a superposition of both the ions taken separately. The intervalence transition $\text{Co(II) Co(III)} \rightarrow \text{Co(III) Co(II)}$ has such a high energy that it does not contribute to the colour of this black compound. Another example⁵ is $\text{Cu(en)}_2(\text{CuBr}_2)_2$ containing Cu(I) and Cu(II) ions having different geometry.

Class II: The compounds belonging to this class are characterised by an absorption band in the visible region of the spectrum (14-27kK) which is absent in the constituent ions taken separately. The two A and B sites in this class of compounds are crystallographically distinguishable. For example they may both be octahedral, but with small differences in bond length or angle. Then the valence bond configuration A(IV) B(III) has an energy not too much greater than A(III) B(IV) . In simple terms, the energy of the transition can be written as

$$h\nu = E_A + E_B + E_{\text{mad}} \quad \dots 1.$$

where E_A and E_B are the changes in internal energy at sites A and B respectively, on transferring an electron from A to B and E_{mad} is the Madelung energy expended in moving the optical electron from A to B in the electrostatic field of all the other electrons in the molecule.

If the compound is a discrete dimer electron transfer takes place within

the molecule, but if it is a solid, bulk charge migration may be detected as semiconductivity. The properties of one of the most famous class II compounds, Prussian Blue, have been fully characterised and described⁷. Another set of examples⁸ are the compounds containing octahedral SbX_6^{3-} and SbX_6^- ions, where X is a halogen. Depending on the cation they are either blue or red, colours which are not found in any other Sb compounds. The compounds are diamagnetic. Both the far i.r and Mössbauer spectra show separate peaks characteristic of Sb (III) and Sb (V).

Mn (III, IV) μ -dioxo-bridged complexes⁹ also form good examples of this class of compounds. Both the ions are of octahedral geometry but differ in bond lengths and also show an intervalence absorption band which gives a green colour to the complexes.

Class III: Polynuclear mixed-valence anions, cations and neutral species whose structures do not contain crystallographically distinguishable sites where the oxidation sites might be localised are classified as class III-A compounds. They differ from class II systems where the distinction between A and B sites is lost completely so that $E_A = -E_B$ and E_{mad} is zero. The excitation energies are dependent on ligand field splittings and molecular orbital resonance integrals, just as they are in an ordinary polynuclear complex having metal-metal bonds. An example of this class would be $\text{Nb}_6\text{Cl}_{12}^{2+}$ ion¹⁰. Class III-B systems are metals and as such show an absorption edge, usually in the i.r and are opaque with a metallic sheen in the visible region. These show differences of two units in the oxidation states of the ions exemplified by Pd and Pt compounds. The non-stoichiometric tungsten bronzes¹¹ Na_xWO_3 ($x = 0.4$ to 0.9) and the

'molecular metals' of the type $K_2Pt(CN)_4Br_{0.3} \cdot 3H_2O$ (KCP)¹² are important members of this class. The bronzes are metallic, their specific conductivities proportional to x and their optical and magnetic properties are typical of metals. These are known to be three-dimensional lattices. In KCP the Br ions are non-stoichiometrically distributed in channels between the chains of square $Pt(CN)_4$ groups stacked plane to plane. The partial oxidation leaves the d_z^2 band incompletely occupied leading to metallic conductivity along the Pt chains.

- 1.3 **Theoretical description of mixed-valence compounds:-** A summary of the theoretical treatment with special reference to the PKS model¹³ for binuclear systems is given in this section. The two possible states of the binuclear system A-B can be written as,

$$\Psi_a = \Psi_A(M) \Psi_B(N) \quad \dots 2.$$

$$\Psi_b = \Psi_A(M-n) \Psi_B(N+n) \quad \dots 3.$$

where M and N are the oxidation states of site A and B respectively. Ψ_b differs from Ψ_a in that n electrons have been transferred from B to A . The electronic Hamiltonian, $\hat{H}_e = \hat{H}_e A + \hat{H}_e B + \hat{V}$, in which \hat{V} is the interaction term, will mix the two mixed-valence states to give

$$\Psi_1 = C_a \Psi_a + C_b \Psi_b \quad \dots 4.$$

$$\Psi_2 = C_b \Psi_a - C_a \Psi_b \quad \dots 5.$$

with energies

$$W_1 = 1/2 [E_I - \sqrt{E_I^2 + 4V^2}] \quad \dots 6.$$

$$W_2 = 1/2 [E_I + \sqrt{E_I^2 + 4V^2}] \quad \dots 7.$$

where, $E_I = H_{bb} - H_{aa}$. The important quantity here is the ratio of the energy difference between the two sites to the interaction energy, viz., $R = E_I/V_{ab}$. The coefficients in Ψ_1 and Ψ_2 can be written as,

$$C_b / C_a = 1/2 (R - \sqrt{R^2 + 4}). \quad \dots 8.$$

Class I compounds: $R \gg 1$, $C_b^2 / C_a^2 \sim \frac{1}{R^2}$

Class II compounds: $R \ll 1$, $C_b^2 / C_a^2 \sim 1 - \frac{R}{2}$

The valence delocalisation coefficient is defined as $\alpha^2 = C_a^2$.

Piepho, Krausz and Schatz¹³ (PKS) have shown that inclusion of vibronic coupling gives a more complete picture of mixed-valence delocalisation.

1.3.1 Basic assumptions of the PKS model:-

1. Overlap between the orbitals on the two centres, A and B is negligible.
2. A single antisymmetric mode is involved in coupling the two centres. This mode is assumed to be a combination of the totally symmetric normal modes of the two sites with identical force constants.
3. The electronic ground states for A and B belong to non-degenerate representations.
4. The energy of interaction between the two centres is small compared to electronic binding energies i.e. the influence of excited state potential surfaces can be neglected.

1.3.2 Results of the PKS model for the static case:-

The parameters in the model are the dimensionless quantities λ , ϵ and δ . The quantities ϵ and δ are related to the previously defined V_{ab} and E_1 , $\epsilon = V_{ab} / h\nu$ and $\delta = 1/2 E_1 / h\nu$.

λ is the linear force constant which is responsible for displacing the potential surface for the two centres from their equilibrium value along

the antisymmetric coupling mode, q , having frequency, $h\nu$.

The potential surfaces are given as (Figure 1),

$$\frac{W_a}{h\nu} = \lambda q + \frac{1}{2}q^2 \quad \dots 9.$$

$$\frac{W_b}{h\nu} = -\lambda q + \frac{1}{2}q^2 \quad \dots 10.$$

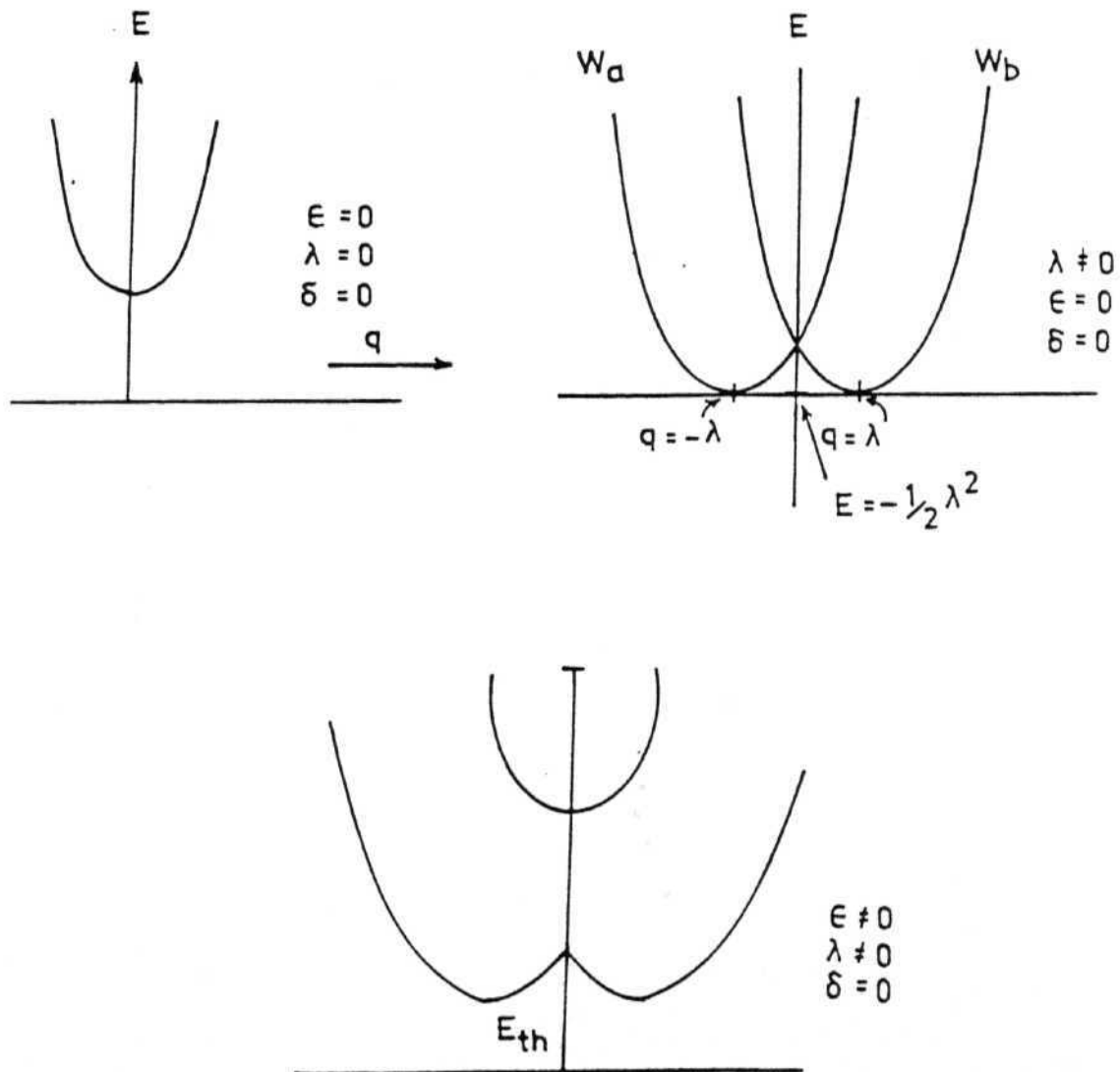


Figure 1: Potential surfaces for static case

with energies

$$W_{1,2} = \frac{q^2}{2} \mp \sqrt{\epsilon^2 + (\lambda q + \delta)^2} \quad \dots 11.$$

$$\text{and } \frac{C_b}{C_a} = \frac{\epsilon - \lambda q - \delta - \sqrt{\epsilon^2 + (\lambda q + \delta)^2}}{\epsilon + \lambda q + \delta - \sqrt{\epsilon^2 + (\lambda q + \delta)^2}} \quad \dots 12.$$

When $\epsilon = 0$, $\lambda = 0$, the potential surfaces are centered at $q = 0$ and displaced from each other by 2δ , and Ψ_a and Ψ_b are not mixed. When $\epsilon \neq 0$, $\lambda \neq 0$, Ψ_a and Ψ_b are mixed and are dependent on q . The q -dependence vanishes when either $\lambda = 0$ ($\Psi_{1,2} = \frac{1}{\sqrt{2}} (\Psi_a \pm \Psi_b)$) or $\epsilon = 0$ ($\Psi_{1,2} = \Psi_b, \Psi_a$).

When $\delta = 0$, the barrier height (activation energy for thermal electron transfer) is given by

$$\frac{E_{th}}{h\nu} = \frac{1}{2} \lambda^2 - |\epsilon| + \frac{\epsilon^2}{2\lambda^2}, |\epsilon| \leq \lambda^2 \quad \dots 13.$$

when E_{th} is large, λ^2 is large, $\epsilon/\lambda^2 \ll 1$, we have localised (class I) system. When $E_{th} \rightarrow \text{zero}$, $|\epsilon|/\lambda^2 \gtrsim 1$ it corresponds to class III.

In the static case the vibronic wave function can be written as Born-Oppenheimer products.

$$\Psi_n^{(1)}(r, q) = \Psi_1(r) \chi_{1,n}(q); \Psi_n^{(2)} = \Psi_2(r) \chi_{2,n}(q), n = 1, 2, \dots, \infty \quad \dots 14.$$

The nuclei are confined to individual potential surfaces, and the inter-valence transfer absorption can be thought of as a Frank-Condon transition from the minimum of one surface to an excited vibrational level of the other potential surface.

1. 3. 3 Results of the PKS model for the dynamic case:-

Born-Oppenheimer approximation is no longer valid when λ and ϵ are both non-zero. The deviations are expected to be especially large when $\lambda \sim \epsilon$.

The nuclei will be moving on both potential surfaces and the vibronic wave function will have to be written as a linear combination of Born-Oppenheimer products.

$$\Psi_n(r,q) = \Psi_a(r) \chi_a(q) + \Psi_b(r) \chi_b(q) \quad \dots 15.$$

where
$$\chi_{a,b}(q) = \frac{1}{\sqrt{2}} \left\{ \sum_{k=0}^{\infty} (r_{n,k} \pm r'_{n,k}) \chi_k(q) \right\}, \quad \dots 16.$$

$\chi_k(q)$ are harmonic oscillator wave functions. The vibronic energies and the coefficients r and r' have to be determined by numerical diagonalisation of a suitably truncated matrix of the Hamiltonian including nuclear kinetic energy, $\hat{H} = \hat{H}_e + \hat{T}_n(q)$. Typical vibronic energy level diagram for the symmetrical case ($\delta = 0$) is shown in Figure 2.

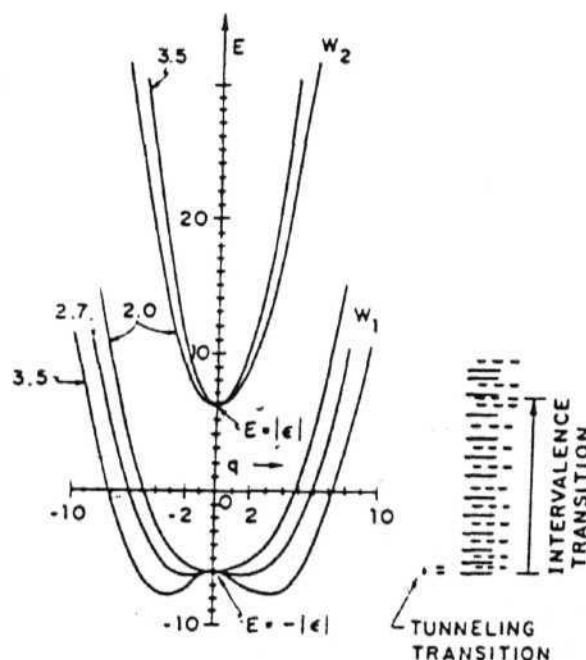


Figure 2: Vibronic energy level diagram for ($\delta = 0$) symmetrical case. The long vertical arrow shows the strongest single intervalence transition at low temperature. Tunneling transitions occur primarily between successive low-lying vibronic levels, the short vertical arrow showing the one from the ground vibronic state (Ref. 13b).

The criterion for localised and delocalised cases can be defined by calculating the nuclear and electronic probability distributions $P_n(q)$ and $P_n(r)$,

$$P_n(q) = \int |\Psi_n|^2 d\tau_e = \sum_{k,k'} \chi_k(q) \chi_{k'}(q) (r_{nk} r_{nk'} + r'_{nk} r'_{nk'}) \quad \dots 17.$$

$$P_n(r) = \int |\Psi_n|^2 dq = \frac{1}{2} (\Psi_a^2 + \Psi_b^2) + (\Psi_a^2 - \Psi_b^2) \sum_{k=0}^{\infty} r_{nk} r'_{nk} + \Psi_a \Psi_b \sum_{k=0}^{\infty} (r_{nk}^2 - r'_{nk}^2) \quad \dots 18.$$

The occurrence of two maxima against one in a plot of $P_n(q)$ versus q distinguishes a localised system from a delocalised one. Analogous to α^2 , a delocalisation coefficient $\beta_d(n)$ can be defined as the coefficient of the cross term in $P_n(r)$

$$\beta_d^2(n) = \left[\sum_k (r_{nk}^2 - r'_{nk}{}^2) \right]^2 \sim \frac{\epsilon^2}{\lambda^2 + \delta^2} = 4\sigma_d^2 \quad \dots 19.$$

in the localised limit.

3.4 Optical transitions in mixed-valence systems:

Two types of optical transitions are predicted by the vibronic model - the well known IVTA and the lesser known tunneling transition in the ground vibronic manifold (See Figure 2). The latter transition which is predicted to occur in the far i.r. region has not been observed so far. The band contours for the IVTA can be calculated once the parameters (λ , ϵ and δ) are known. In actual practice, comparison of calculated and experimental band contours is complicated by the possible presence of low symmetry splittings and spin-orbit coupling effects. Many features of the IVTA have been analysed since long using the Hush formulae¹⁴ which do not require detailed knowledge of the wave functions. The vibronic model predicts that these formulae are valid only in the strongly localised situations

i.e., $\lambda^2 + \delta$ large and $\gg \epsilon^2$. The Hush formulae are summarised below:

$$\frac{h\nu_{\max}}{E_{\text{th}}} = 4 \quad \dots 20.$$

$$(h\Delta\nu_{1/2})^2 = 16 kT(\ln 2)(h\nu_{\max} - 2\delta h\nu) \quad \dots 21.$$

$$\alpha_d^2 = \frac{4.24 \times 10^{-4} \epsilon_{\max} \Delta\nu_{1/2}}{\nu_{\max} R} \quad \dots 22.$$

where ϵ is the molar extinction coefficient and R is the distance between the two centres (in \AA).

The PKS model also makes definite predictions regarding the resonance Raman effect¹⁵, but the RR transitions have not so far been explored in detail experimentally.

1.3.5 Improved models:-

In addition to the approximations listed in 1.3.1, the PKS model has the serious drawback that it is essentially a two-site model. Experiments on the Creutz-Taube ion $[(\text{NH}_3)_5\text{Ru}(\text{pz})\text{Ru}(\text{NH}_3)_5]^{5+}$, have shown that the bridging ligand interacts strongly with the two Ru centres¹⁶. A three-site model which explicitly includes the bridging species has been proposed recently¹⁷. It was shown that in the strongly coupled case the totally symmetric vibrational mode has to be included in the vibronic coupling problem. A ligand field model which includes spin-orbit coupling and low-symmetry components have also been put forward to explain the electronic properties of the Creutz-Taube ion¹⁸. This again has the drawback that orbitals on the bridging species are excluded from the treatment. It appears that the ligand field model will be suitable for treating the electronic structure, while the inclusion of all the coupled vibrations will be necessary

to account for the IVTA band profiles.

1.4 Study of two model complexes:

Two well studied mixed-valence systems are discussed here in order to illustrate the several experimental methods as well as to highlight the potential difficulties in characterising a system as localised or delocalised.

1.4.1 Creutz-Taube ion:-

The Creutz-Taube complex¹⁹, μ -pyrazine-bis(pentaammine ruthenium)⁵⁺ ion, provided a suitable starting point for theoretical analysis of binuclear mixed-valence complexes, since the two coupled Ru centres are identical and only a single bridging ligand is involved. The electronic spectra showed^{19(a)} band at 17.7 kK for the metal to ligand charge transfer and an intense broad band around 6.4 kK ($\epsilon = 5500 \text{ cm}^{-1} \text{ m}^{-1}$) characteristic of IVTA. The electron transfer was expected to be rapid, $k_{th} > 10^9 \text{ sec}^{-1}$. However, n.m.r studies¹⁹ gave $k_{th} > 10^7 \text{ sec}^{-1}$. Mössbauer measurements²⁰ made on p-toluenesulfonate salts at 4K and interpreted in terms of class II behaviour were later found to be in error¹⁶. ESCA spectra²¹ exhibited one $3d_{5/2}$ Ru(II) peak and $3d_{3/2}$ and $3d_{5/2}$ Ru(III) peaks, expected for class II ion; but this behaviour was later²² shown to be compatible with that of a class III ion as well. The resonance Raman spectrum²³ was found to be very similar to the fully reduced ion, with the exception of a band at 1070 cm^{-1} which was attributed to pz bound to Ru(III) thus indicating a class II system. Powder e.s.r. studies²⁴ implicating a localised electronic structure were contradicted by single crystal studies²⁵ consistent with valence delocalisation. A crystal structure²⁶ of mixed halide salt gave results consistent with both descriptions.

Recently Fürholz et al.¹⁶ have made a comprehensive restudy of the Creutz-Taube complex involving single crystal, optical, resonance Raman, x-ray crystallographic, Mössbauer and e.s.r. techniques. The main conclusions from the above work are (i) there is more than one transition under the IVTA band envelope, (ii) the system is not localised on the Mössbauer time scale, however, the isomer shift is close to that of Ru (III, III), (iii) in the chloride salt the two Ru centres are crystallographically equivalent, while for the tosylate the centres are significantly different; the structure of (II, III) closely resembles that of (II, II), (iv) e.s.r. shows considerable rhombic splitting implying strong interaction between the metal centres and the pyrazine bridge, (v) Raman and e.s.r. studies do not establish ground state symmetry, and (vi) the experiments do not "allow one to decide whether the odd electron is trapped on one Ru or delocalised equally over both".

2 **Prussian Blue:-** Another widely studied complex is Prussian Blue which was studied first in 18th century¹. The several studies carried out for the assignment of oxidation states of this complex have been reviewed by Sharpe⁷. The structure of this complex was derived from x-ray powder data²⁷. Powder neutron diffraction studies²⁸ have put an upper limit of about 5% for the spin delocalisation in the electronic ground state. Single crystal x-ray work confirmed the cubic polymeric structure with 25% of Fe(II) sites being vacant leading to an inherent structural disorder.

Robin³⁰ has assigned an intervalence band at 14.1 kK whose intensity

suggested a value of valence delocalisation coefficient $\alpha = 0.1$ consistent with estimated³¹ $\alpha = 0.11$ from the perturbation model. Magnetic moment measured between 10 and 300 K corresponded to $\mu_{\text{eff}} = 5.98 \text{ BM}$ /Fe(III) high-spin and a diamagnetic low-spin Fe(II) atom³². Mössbauer spectra showed separate transitions from the Fe(II) and Fe(III) sites³³. It was necessary to resort to selective isotopic substitutions to resolve the overlapping signals. A ferromagnetic transition is assumed below 5.5 K where the exchange pathway lies through N-C-Fe^{II}-C-N.

In summary one can conclude that Prussian Blue contains trapped valences at Fe(II) and Fe(III) sites.

Mn(III), Mn(IV) and dinuclear mixed-valence complexes.

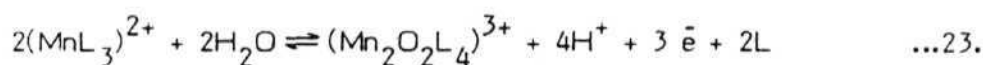
- 1 **Complexes with heteroaromatic ligands:-** The first proposed complex of a binuclear cation was $(\text{Mn}_2\text{O}_2 \text{ bpy}_4)^{3+}$ by Nyholm and Turco in 1960³⁴. They have determined the oxidation state by reacting the complex with oxalic acid in the presence of silver sulphate and also by potentiometry. They also determined the magnetic moment to be 1.7 BM at 25°C. Stoufer et al³⁵, in 1972, determined the crystal structure of the perchlorate salt. The monoclinic greenish black crystal contains two manganese centres with different metal-ligand bond distances - the one with shorter distance is considered to be Mn(IV) (d^3) and the other Mn(III) (d^4 high-spin). The difference in the average bond length is 0.138 Å.

This complex and the phenanthroline analogue have been prepared and studied in detail by Cooper et al³⁶ in 1977. They have characte-

rised them by i.r., electronic spectra and electrochemistry. A 680cm^{-1} band observed in i.r. was attributed to MnO_2Mn bridge in the dimer. The three shoulders at 19.0, 18.0 and 14.6 kK observed in electronic spectra were assigned to high-spin Mn(III) ion and the band in near-i.r. around 12.1 kK to IVTA. The solution studies have shown that the original green solution of the dimer turned red on acidification and was found reversible upon addition of sodium acetate solution. At lower pH, the IVTA band disappeared and reappeared only on making the solution pH 4.5. They have also measured solution magnetic moments by n.m.r and found consistent with the value for a single electron. The electrochemical studies in acetonitrile revealed that these dimers participate in one-electron oxidation processes. By using Hush's formulae¹⁴ they have calculated the electron delocalisation coefficient α^2 as 0.01 which implied that the electron spends 99% of the time on the Mn(III) atom. They have compared with selected data³⁷ of (III, IV) dimers and showed that the extent of delocalisation in these dimers is high due to the short metal-metal distance (2.7\AA). It is quite evident in comparison³⁸ with $\alpha^2 = 0.0026$ for $[(\text{NH}_3)_5\text{Ru}(\text{pz})\text{RuCl}(\text{bpy})_2]^{4+}$ where the metal-metal distance is approximately 7\AA . A thermal activation energy of 8.6 kcal m^{-1} was calculated from which a maximum thermal electron transfer rate of 10^6 s^{-1} was estimated assuming no activation entropy and a transmission coefficient of unity.

Single crystal e.s.r. studies of $(\text{Mn}_2\text{O}_2\text{bpy}_4)(\text{ClO}_4)_3$ complex were reported by Inoue³⁹ in 1978. He observed weak signals at $g = 4$

attributable to excited states and at $g = 2$ for ground state. The hyperfine splitting in the ground doublet state showed at least 16 lines with 70-100G spacings. Hence the odd electron in Mn(III, IV) was said to be mostly localised on one of the manganese atoms and unequally distributed between both the manganese in the dimer. In the same year Morrison et al⁴⁰ reported the formation of Mn (III, IV) complexes with bpy, phen, 4,4'-dmbp, 4,4'-dpbp, 4,7-dpp and terpy by electrochemical oxidation of Mn(II)L₂ complexes in acetonitrile. Except terpy, all other complexes were oxidised quantitatively. They have suggested that the oxidation of Mn (II) complexes and the subsequent dimerisation of the product species require release of four protons to yield the Mn (III, IV) dimers as follows:-



The redox potentials for bpy complexes were found to be more than phen complexes. They have also reported⁴⁰ e.s.r. spectra with 6 lines attributing them to broadening due to super-exchange between the two metal centres. They have also prepared⁴¹ mononuclear Mn(II), Mn(III) and Mn (IV) complexes of bpyO₂ and terpyO₃ electrochemically in acetonitrile. These complexes were found stabilised against dimerisation unlike in the case of bpy and phen ligands.

At the same time Cooper et al⁹ have examined the e.s.r. spectra of Mn (III, IV) dimers in acetonitrile with a 16 line pattern. They have suggested two inequivalent manganese ions at room temperature with hyperfine splitting values $A_1 = 167 \pm 3$ G and $A_2 = 79 \pm 3$ G. The hyperfine splitting pattern with $|A_1| \approx 2 |A_2|$ and the small g anisotropy were found consistent with Mn(III) high-spin antiferro-

magnetically coupled to Mn(IV) producing an $s=1/2$ ground state. These dimers are expected to yield 11 lines in the fast exchange limit and upto 36 lines in slow exchange. Hence the 6 line pattern suggested by Morrison et al⁴⁰ was shown to be consistent with Mn(II) impurity and not Mn (III, IV) dimers. The temperature dependence data of magnetic susceptibility of this $s = (2, 3/2)$ pair was found in good agreement with the isotropic Heisenberg exchange Hamiltonian $H = -2 J s_1 \cdot s_2$, yielding $J = -150 \pm 7 \text{ cm}^{-1}$ for the bpy dimer and $J = -134 \pm 5 \text{ cm}^{-1}$ for phen dimer.

Very recently Stebler et al⁴² have reported crystal and molecular structure of $(\text{Mn}_2\text{O}_2\text{phen}_4)(\text{PF}_6)_3 \cdot \text{CH}_3\text{CN}$. The orthorhombic crystal was found to have crystallographically equivalent manganese ions. Detailed analysis of anisotropic atomic displacement parameters indicated static or dynamic disorder between a Mn(III) - Mn(IV) and a Mn(IV) - Mn (III) ion. Optical absorption band around 12.5 kK, assigned to IVTA, was found to be temperature dependent with an increase in intensity when the temperature was decreased and the band at 14.7 kK was found to be independent. From the magnetic data, based on isotropic Heisenberg operator, exchange coupling constant was calculated as $J = -148 \text{ cm}^{-1}$ in close agreement with Cooper et al⁹.

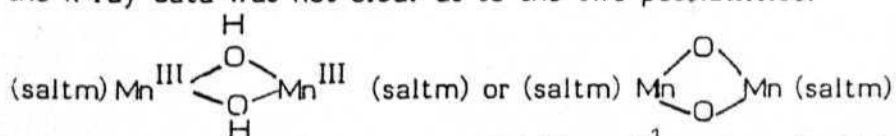
Recently, Pavacik et al⁴³ have reported the formation of a $(\text{Mn}(\text{Sal})_2\text{bpy})$ where H_2Sal = salicylic acid. They have treated $(\text{Mn}_2\text{O}_2\text{bpy}_4)(\text{ClO}_4)_3 \cdot 2\text{H}_2\text{O}$ ⁹ with NaHSal (4 equiv.) in acetonitrile solution which led to a rapid precipitation of a brown microcrystalline material which was not identified. However it was found soluble

in dimethylformamide to give a deep red solution. Crystals of $(\text{Mn sal}_2 \text{ bpy})$ were isolated and structurally characterised. Magnetic moment obtained by Evans method⁴⁴ in dimethylsulfoxide was 3.83 BM consistent for a Mn(IV) ion. The Mn(IV) complex might have formed by the substitution of two sal^{2-} groups for one of the bipyridine groups and both of the oxides. Identification of the initially formed brown crystalline material would make this aspect of its chemistry clearer.

Very recently Ramaraj et al⁴⁵ have reported oxygen evolution by water oxidation with $(\text{Mn}_2\text{O}_2 \text{ bpy}_4) (\text{ClO}_4)_3$ complex in heterogeneous medium in the presence of $(\text{NH}_4)_2 [\text{Ce} (\text{NO}_3)_6]$. They have observed gas bubbles over a period of 4 hrs. The experiment was done in argon atmosphere. The gas evolved was analysed gas-chromatographically. They have carried out c.v. experiments in water and reported that the complexes are stable in water contrary to the observation of Cooper et al⁹.

Complexes with Schiff-bases:-

A number of monomeric Mn(III) Schiff-base complexes are known⁴⁶. Crystal structure of manganese complexes of tetradentate Schiff-bases $\text{H}_2 \text{ salen}$ and $\text{H}_2 \text{ saltm}$ have been reported⁴⁷. It was shown that the Mn(II) complexes react with oxygen irreversibly to yield various oxidation products. A dimer for $\text{Mn}(\text{saltm})\text{H}_2\text{O}$ complex with bridging oxygen atoms (Mn - Mn distance 2.7 Å) is also known⁴⁷. But the x-ray data was not clear as to the two possibilities:



However, i.r absorption around $650\text{-}600 \text{ cm}^{-1}$ region for MnO_2Mn

ring was reported⁴⁸. The dimer has magnetic moment of $\mu = 2.13$ BM at room temperature consistent with antiferromagnetic coupling of either high-spin Mn(III) or high-spin Mn(IV) atoms. Reaction of oxygen with Mn(salen) yielded a sparingly soluble product $[\text{Mn}_2(\text{salen})_2\text{O}_2]$ which displayed similar properties, i.e., i.r. absorptions at 645 and 631 cm^{-1} and $\mu = 1.96$ BM⁴⁹. The reaction of excess oxygen with Mn(salen) and Mn(saltm) in benzene or dimethylsulfoxide yields a second insoluble product which was formulated as a polymeric μ -oxo - manganese (IV) complex, $[\text{Mn}(\text{salen})\text{O}]_n$.

Five coordinate cationic complexes of Mn(III), $[\text{Mn}(\text{SB})\text{H}_2\text{O}]\text{ClO}_4$, where SB is the dianion of the tetradentate Schiff-base busalen and busaltm have been synthesized and characterised by Boucher et al⁵⁰ in 1975. Hydrolysis by 0.005 M NaOH, of chloroform solutions of these complexes in air led to the formation of six-coordinate species $[(\text{Mn}_2(\text{busalen})_2\text{O}_2) \cdot \text{H}_2\text{O}]$ and $[\text{Mn}_2(\text{busaltm})\text{O}_2] \cdot 2\text{H}_2\text{O}$. These Mn(IV) complexes are dimeric in chloroform solutions and show reduced room temperature magnetic moments, $\mu = 2.5$ BM. I.r and visible bands were inconsistent with $\text{Mn}_2(\text{IV})\text{O}_2$ ring in these complexes.

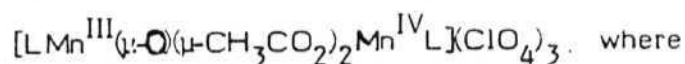
The same authors have synthesised and characterised⁵¹ several optically active complexes of Mn(III), $[\text{Mn}(\text{SB})\text{H}_2\text{O}]\text{ClO}_4$ and $[\text{Mn}(\text{SB})\text{Cl}]$ and the Mn(III, IV) dimers, $[\text{Mn}_2(\text{SB})_2(\text{OH})^-(\text{O})] \cdot n\text{H}_2\text{O}$ where SB was a dianion of the optically active tetradentate Schiff-base derived from (-) -1,2- diaminopropane and 4-sec - butylsalicylaldehyde or 4-sec-butyl-2- acetylphenol. The electronic absorption bands around 14-21 kK, 21 - 30 kK and 30-45 kK were observed

The band around 22 kK was assigned to mixed-valence intervalence transition.

Complexes with other ligands:

Oxo-bridged dimeric manganese(IV) porphyrin complexes have been reported⁵² including crystal and molecular structures. The complexes were found to be e.s.r. silent. These were found to oxidise cyclohexane at room temperature to give cyclohexyl azide. Thermal decomposition of these μ -oxo-bridged $[X Mn(IV) TPP]_2 O$ ($X = N_3^-, OCN^-$) complexes yielded deeply trapped mixed-valence dimeric complexes which show 16 line e.s.r. spectrum⁵³.

Very recently Wieghardt et al⁵⁴ have reported dinuclear



$L = tmtc$. Crystal and molecular structure have been reported. On oxidation of $Mn_2(II)$ complex synthesised it formed $Mn_2(III)$ complex, the $Mn(III, IV)$ mixed-valence complex and a $Mn_2(IV)$ complex. The $Mn_2(II)$ complex was found to show weak antiferromagnetic coupling where $J = -9 \text{ cm}^{-1}$. However, the $Mn(II, III)$ complex remained unisolable. The same authors have isolated⁵⁵ $Mn_2(III)$ complex which on electrochemical oxidation yields $Mn(III, IV)$ mixed-valence dimer. This dimer was also obtained by chemical oxidation and was isolated in crystalline form. The $Mn_2(III)$ was found to be ferromagnetically coupled where $J = +18 \text{ cm}^{-1}$. The electronic spectra of the mixed-valent dimer in acetonitrile had IVTA band at 12.7 kK. Interestingly, there was another IVTA band around 7.14 kK. Similar electronic

spectra were recorded⁵⁶ for manganese containing metalloprotein of a pseudocatalase isolated from *Lactobacillus planarum* suggesting this complex to be a model for water oxidation in photosystem II of photosynthesis in plants. Magnetic data for the Mn (III, IV) complex was calculated which found that the atoms are intramolecularly coupled antiferromagnetically. Further electrochemical oxidation of this complex led to the formation of Mn_2 (IV) complex which was unstable. C.v in liquid SO_2 (0.1M TBA - PF_6) at $-40^\circ C$ showed two reversible one-electron transitions at 1.25 V and 1.92 V (with NHE). The first corresponds to Mn_2 (III) \rightarrow Mn (III, IV) and the second to Mn (III, IV) \rightarrow Mn_2 (IV). Mn_2 (IV) complex was found unstable even in liquid SO_2 .

Nair et al⁵⁷ have attempted the preparation of a mixed-valent manganese species with β -cyclodextrin ligand. They have synthesised a Mn_2 (III) complex which was soluble in water, dimethylformamide and dimethylsulfoxide. However in water it was found unstable decomposing to hydrated oxides of manganese. The electronic spectra were recorded in dimethylformamide and magnetic moments were determined by the n.m.r. method which was found to be 3.51BM/Mn at 302K decreasing to 3.38BM/Mn at 224K, well below spin-only value (4.9BM) for a mononuclear species suggesting a weak antiferromagnetic coupling of the manganese spins. The c.v. studies in dimethylformamide showed a quasi-reversible two electron oxidation wave. No mixed-valent Mn (III, IV) product expected for a one-electron oxidation of Mn_2 (III) was formed. Mn_2 (IV) obtained was unstable and at room temperature decomposed within a few hours.

Matsushita et al⁵⁸ have prepared binuclear manganese complexes by using bridging quadridentate bis (Schiff-bases) and dipicolinates and with bis(μ -oxo) groups and one or two picolinate ligands per manganese. Their redox chemistry has been characterised by c.v and controlled-potential coulometry. They indicate that the electron-transfer mechanisms are ligand-centered rather than metal-centered. They show that the bpy ligands in the bis (μ -oxo) bridged complexes can be substituted by 2 or more picolinate anions like $(\text{Mn}_2\text{O}_2\text{bpy}_3\text{PA}_2)^+$ and $(\text{Mn}_2\text{O}_2\text{PA}_4)^-$. Several of these complexes were thought to be good models for water oxidation in photosystem II.

Suzuki et al⁵⁹ reported preparation of dinuclear manganese (III, IV) and manganese (IV, IV) complexes with N_4 -pyridine. The analytically pure samples were determined by redox titrations and their conductivity was measured. C.v in CH_3CN was recorded and magnetic moments at 300 K - 80 K were measured. They were found to exhibit strong antiferromagnetic interaction with $J \sim -159$ and -137 cm^{-1} , respectively. E.s.r spectrum of the (III, IV) complex showed a 16-line ^{55}Mn hyperfine pattern at $g=2$ indicating a trapped valence state. Absorption bands in CH_3CN in the visible region were shown. A preliminary simulation of the spectrum was also given. The resonance fields were almost reproduced. Introduction of small anisotropies in g and A tensors caused no significant change in spectrum. Little anisotropy in g and A tensors implies that the structures of two manganese units are close to the regular octahedron. This complex was reported not to oxidise water under similar conditions as that reported by Ramaraj et al⁴⁵.

Manganese complexes as models for photosystem II:-

Current literature on photo-synthesis in green plants has accepted the involvement of manganese in the evolution of oxygen. Kok et al⁶⁰ have proposed the 'S states' mechanism to account for the periodic release of O_2 from chloroplasts. Short pulses of light oxidise each reaction centre by one electron producing one electron oxidation of the O_2 evolving centres on each flash that yields states S_2 , S_3 , S_4 , S_0 , S_1etc. in a cycle. By using light of sufficient intensity to turn over all reaction centres on each flash this synchronization is preserved. Water is then oxidised to O_2 with a yield that reaches a maximum every fourth flash of light eventually damping to a steady state level. S_4 is the state associated with O_2 release. This behaviour established that the O_2 evolving centres function independently, yielding intermediate states which can persist for tens of seconds and longer before deactivation.

Just after Cooper et al⁹ have studied e.s.r. of the Mn (III, IV) dimers in detail, Dismukes et al⁶¹ in 1981, have proposed them as models for photosynthetic oxidation of water. They have performed e.s.r. of spinach chloroplasts giving a series of laser flashes, $n = 0, 1, \dots, 6$ at room temperature and rapidly cooling to -140°C revealing 16 lines and possibly 21 or more hyperfine lines when observed below 35 K. The spectrum was consistent with a pair of antiferromagnetically coupled manganese ions, or possibly a tetramer of manganese ions, in which Mn (III) and Mn (IV) ions are present. The intensity of the signals from these flashes indicated that the paramagnetic signal was monitoring oxidation state changes in the enzyme involved in oxidation of water.

Goodin et al.⁶² in 1984 reported e.s.r. and x-ray absorption K-edge measurements of a spinach photosystem II preparation in S_1 , S_2 or S_3 states. The changes observed in the edge properties between samples prepared in S_1 to S_3 states were in direct agreement with changes of signal intensity in e.s.r. A Mn (II, III) complex was suggested for S_1 state and Mn (III, IV) complex for a S_2 or S_3 state. A mechanism was proposed to show the changes of oxidation states of manganese in the S-states model (Sub-section 1.6.2).

Continuous power saturation and temperature dependence of e.s.r. signals which are generated by low-temperature illumination of dark-adapted photosystem II membranes associated with S_2 state of the O_2 evolving complex of photosynthesis were reported by Paula et al.⁶³ in 1985. The data showed that the S_2 state e.s.r. signals arise from more than one paramagnetic site. A model was proposed for the species giving rise to the S_2 state e.s.r. signal in which an antiferromagnetically exchange coupled Mn(III, IV) dimer which is ferromagnetically exchange coupled to another site with $s = 1$ was likely to be present. The second site could be low-spin Mn (III), low-spin Fe (IV), or even a second manganese dimer.

Spectroscopic evidence for manganese:-

E.s.r. spectroscopy has revealed the presence of multiline signal attributed to an oxidised form of the terminal electron donor in the S_2 state in thalokoid membranes. By comparison with synthetic manganese complexes⁶⁴ and from simulations of the e.s.r. spectrum it has been identified with a cluster of two, or possibly four, interacting manganese ions present in a mixed-valence oxidation state

Mn_2 (III, IV) or Mn_4 (3 III, IV) respectively. The Mn_2 (II, III) oxidation state was also proposed⁶⁵ based on e.s.r. simulations.

2

Mechanism for the role of manganese:-

Goodin et al⁶² have proposed a scheme for the change in manganese oxidation associated with S states cycle. In state S_0 , the metal centres are in the Mn(II, III) state. Transition from S_0 to S_1 occurs by the oxidation of one of the donor species which releases a proton. This transition occurs first by oxidation of the unstable intermediate S_1^* . This state relaxes to S_2 after two charge equivalents are transferred from the donor species to manganese, giving the Mn (III, IV) complex with no net proton release. Transition from S_2 to S_3 is analogous to the S_0 to S_1 step. The final light-induced step proceeds as before with the formation of an unstable intermediate S_3^* , which relaxes to a peroxo-bridged species with the Mn(III, IV) species containing the reduced donors. A water to ligand exchange reaction may then accompany the release of O_2 , regenerating S_0 . The last step proposes the release of two protons, one before and one after release of O_2 . The mechanism is shown in figure 3.

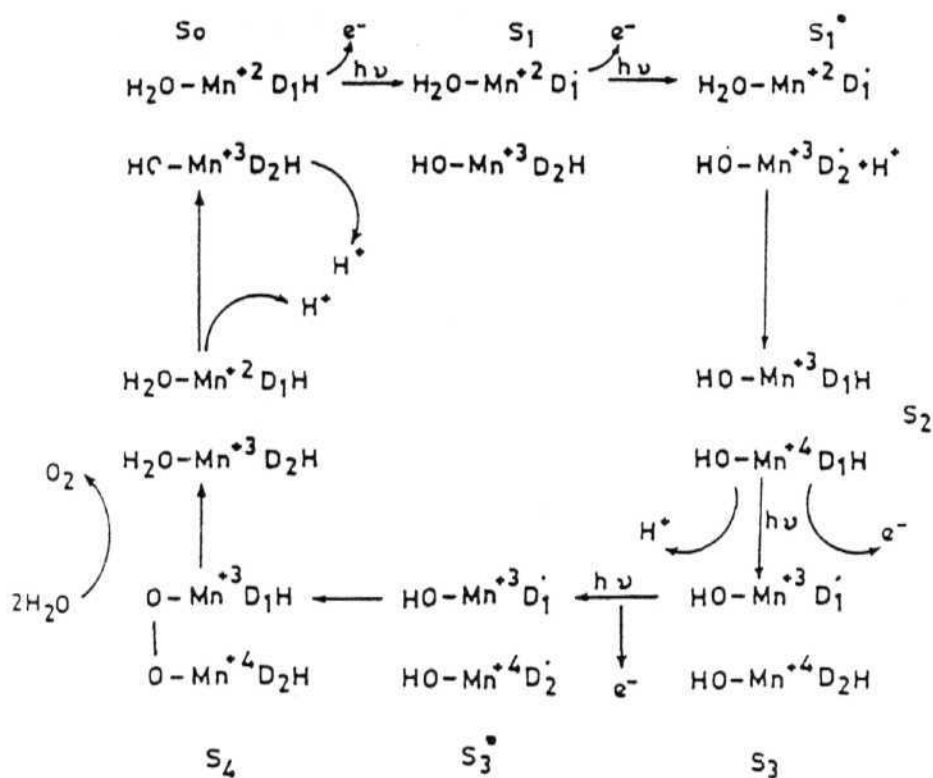


Figure 3: Higher oxidation states of manganese suggested for Oxygen evolution by water oxidation associated with S states cycle (Ref.62).

CHAPTER - 2

EXPERIMENTAL SECTION

Chemicals:-

The starting materials for the preparation of ligands were either bought from Aldrich or Fluka. Other solvents and common chemicals were of reagent grade or better quality. All the organic solvents were purified by standard procedures described in Vogel⁶⁶. Ether was stored over sodium, pyridine over potassium hydroxide pellets, acetonitrile over Type 4A molecular sieves and dimethylformamide was vacuum distilled in dry nitrogen atmosphere and stored over Type 4A molecular sieves.

Preparation of ligands:-

2,2'-bipyridine (bpy), 1,10-phenanthroline (phen) and 2,9-dimethyl-phenanthroline (dmp) were bought from Aldrich Chemicals. 4,4'-dimethylbipyridine(4,4'-dmbp) and 5,5'-dimethylbipyridine(5,5'-dmbp) were prepared from γ -picoline and β -picoline respectively by coupling over W7-J Raney nickel freshly made from nickel-aluminium alloy⁶⁷. Our attempts to prepare 6,6-dimethylbipyridine (dmbp) from α -picoline by the same method resulted in very low yields (< 1%). Hence a recently reported method⁶⁸ was used to obtain high yields by phase-transfer catalysis. In this procedure, freshly prepared 2-bromo-6-picoline was coupled over 5% Pd/C and benzyltriethylammonium chloride. The ligand was recrystallised from methanol. 6-methylbipyridine (mmbp) was prepared⁶⁹ by methylating 2,2'-bipyridine using freshly prepared methyl lithium. The oil obtained was crude and attempts to obtain a pure sample by steam distillation were unsuccessful. It was purified by column chromatography (ethyl acetate and hexane, 75:25).

4,5-diazafluorenone (daf-one) was prepared^{70a,b} by oxidation of 1,10-phenanthroline with alkaline KMnO_4 . 4,5-diazafluorene (daf) was prepared^{70a,c} by reducing the fluorenone by heating with hydrazine hydrate in a sealed glass tube at 165°C for 18 hours. 4,4',6,6'-tetramethylbipyridine (tmbp) was prepared⁷¹ by treating freshly distilled 2,4-dimethylpyridine with sodium.

Preparation of $[\text{Mn}_2\text{O}_2\text{L}_4]^{3+}$ complexes:-

$[\text{Mn}_2\text{O}_2\text{L}_4] \text{X}_3$ where $\text{L}=\text{bpy}$, phen, 4,4'-dmbp, 5,5'-dmbp, and $\text{X}=\text{ClO}_4^-$, BF_4^- or PF_6^- were prepared by the earlier known procedure³⁶ for $\text{Mn}_2\text{O}_2(\text{bpy})_4(\text{ClO}_4)_3$. The bpy complexes were recrystallised from acetonitrile, and all others were recrystallised in the following manner: the complex was dissolved in minimum amount of acetonitrile, filtered, and was precipitated with dry ether to give a pure green coloured fine powder. This was repeated 3-4 times to obtain an analytically pure sample. Crystallisation by the usual evaporation method resulted in decomposition while recrystallisation from ligand buffer resulted in ligand coprecipitation. Analytical data are given below with calculated values in parantheses.

$\text{Mn}_2\text{O}_2(\text{phen})_4(\text{ClO}_4)_3$: 2Mn, 14O, 3Cl, 8N, 32H, 48C, C=50.00(49.61), H=2.49(2.78), N=9.86(9.65), phen(by spectrophotometry)=62(62.09)%.

$\text{Mn}_2\text{O}_2(\text{phen})_4(\text{PF}_6)_3$: 2Mn, 2O, 3P, 18F, 8N, 32H, 48C, C=44.86(44.43), H=2.75(2.49), N=8.68(8.64)%.

$\text{Mn}_2\text{O}_2(\text{bpy})_4(\text{ClO}_4)_3$: 2Mn, 14O, 8N, 40C, 32H, 3Cl, C=44.28(45.11), H=2.97(3.03), N=10.87(10.52), bpy(by spectrophotometry)=57(58.66)%.

$\text{Mn}_2\text{O}_2(\text{bpy})_4(\text{PF}_6)_3 \cdot 2\text{Mn}, 2\text{O}, 8\text{N}, 40\text{C}, 32\text{H}, 3\text{P}, 18\text{F}, \text{C}=39.66(39.98),$
 $\text{H}=2.69(2.67), \text{N}=9.30(9.33)\%.$

$\text{Mn}_2\text{O}_2(4,4'\text{-dmbp})_4(\text{PF}_6)_3 \cdot 4,4'\text{-dmbp}(\text{by spectrophotometry})=51(54.40)\%.$

$\text{Mn}_2\text{O}_2(5,5'\text{-dmbp})_4(\text{PF}_6)_3 \cdot 5,5'\text{-dmbp}(\text{by spectrophotometry})=57(56.10)\%.$

Preparation of $[\text{Mn}_2\text{O}_2\text{L}_3\text{A}_2] \text{X}_3$:-

The complexes with $\text{A} = \text{N}$, N-dimethylformamide (dmf) or pyridine (py) were prepared. Preparation of $[\text{Mn}_2\text{O}_2\text{L}_3\text{Y}] \text{X}_3$ where $\text{L}=\text{bpy}$, $\text{Y}=\text{phen}$ and $\text{L}=\text{phen}$, $\text{Y}=\text{bpy}$ was also attempted.

1 Dmf substitution:-

The parent olive green complex, $\text{Mn}_2\text{O}_2(\text{phen})_4(\text{PF}_6)_3$ was dissolved in a minimum amount of dmf to give a green coloured solution. This on standing for about 15-20 days in a desicator changes colour to red. The change in colour was monitored by optical spectra. The solution was then precipitated by using excess of dry ether. The red precipitate was washed several times with dry ether. This complex was found ^{to be} sensitive to moisture, turning to pink after standing for several weeks. The analogous procedure for the bpy complex resulted in an impure gummy material. Analytical data for $[\text{Mn}_2\text{O}_2(\text{phen})_3(\text{dmf})_2](\text{PF}_6)_3 \cdot 2\text{Mn}, 4\text{O}, 38\text{H}, 42\text{C}, 8\text{N}, 3\text{P}, 18\text{F}, \text{C}=39.95(39.92), \text{H}=2.88(3.03), \text{N}=8.80(8.87), \text{phen}(\text{by spectrophotometry})=43(42.79)\%.$

2 Pyridine substitution:-

The parent complex $[\text{Mn}_2\text{O}_2\text{L}_4](\text{ClO}_4)_3$, $\text{L}=\text{bpy}$ or phen was dissolved in pyridine and filtered. The clear green solution was left for crystallisation by slow evaporation. Pure green crystalline material was

collected after a few days, washed and dried. Analytical data,
 $[\text{Mn}_2\text{O}_2(\text{phen})_3(\text{py})_2](\text{ClO}_4)_3$: 2Mn, 14O, 8N, 34H, 46C, 3Cl, C=48.73
 (48.51), H=2.97(2.98), N=10.10(9.84)%;
 $[\text{Mn}_2\text{O}_2(\text{bpy})_3(\text{py})_2](\text{ClO}_4)_3$: 2Mn, 14O, 8N, 40C, 34H, 3Cl, C=44.48
 (45.03), H=3.02(3.21), N=9.31 (10.50)%.

Bpy or phen substitution:-

The parent complex $[\text{Mn}_2\text{O}_2(\text{phen})_4](\text{ClO}_4)_3$ was dissolved in bpy/
 (bpyH) NO_3 buffer (pH=4.5). To the clear green solution obtained
 after filtration, a few drops of concentrated aqueous solution of
 sodium perchlorate was added. Immediate precipitation occurred
 giving a product contaminated with ligand. It was washed with metha-
 nol to remove major amounts of free ligand and then recrystallised
 from acetonitrile. Analogous procedure was employed to precipitate
 $[\text{Mn}_2\text{O}_2(\text{bpy})_4](\text{ClO}_4)_3$ from phen/(phen H) NO_3 buffer. Analytical
 data,

$[\text{Mn}_2\text{O}_2(\text{phen})_3(\text{bpy})](\text{ClO}_4)_3$: 2Mn, 14O, 3Cl, 8N, 32H, 46C, C=49.41
 (48.55), H=2.96(2.84), N=10.65(9.85)%;
 $[\text{Mn}_2\text{O}_2(\text{bpy})_3(\text{phen})](\text{ClO}_4)_3$: 2Mn, 14O, 3Cl, 8N, 32H, 42C, C=47.60
 (46.29), H=2.84(2.94), N= 10.47(10.29)%.

Physical measurements:-

The C,H,N analyses were performed on Perkin-Elmer 240C analyser.
 Infra-red spectra in the range $600\text{-}4000\text{ cm}^{-1}$ were recorded on Perkin
 Elmer IR 1310 or 297 instruments. Electronic spectra were measured
 on Perkin-Elmer LAMBDA-3 spectrophotometer. Ligand estimations
 were carried out on Shimadzu UV-visible spectrophotometer (ε for

phen in methanol containing 25% 5N HCl = $0.5479 \times 10^5 \text{ m}^{-1} \text{ cm}^{-1}$ at 272 nm; bpy in methanol = $0.2596 \times 10^5 \text{ m}^{-1} \text{ cm}^{-1}$ at 280 nm; 4,4'-dnbp in methanol containing 25% 5N HCl = $0.2755 \times 10^5 \text{ m}^{-1} \text{ cm}^{-1}$ at 299 nm). E.s.r. spectra were recorded on JEOL Fe 3X spectrometer equipped with a variable temperature cryostat. DPPH was used as a standard for calibration ($g=2.0036$). Photoacoustic spectra (p.a.s) were recorded on PARC photoacoustic spectrometer using MgCO_3 as a standard diluent.

Computer simulation of e.s.r. spectra:-

A previously described computer program⁷² was modified to include ligand hyperfine interaction in first order. For simulating the hyperfine interaction in dimeric manganese spectrum, one Mn nucleus was taken as a central atom and the other Mn nucleus was treated as 'ligand'. The calculations were carried out on a WIPRO Machines IBM compatible personal computer. Further details are given in Chapter 3.

CHAPTER - 3
RESULTS AND DISCUSSION

I.r. spectra of manganese (III, IV) complexes.

I.r. spectra of phen complexes:-

The i.r. frequencies of all the phen complexes are tabulated in Table I. In dioxo-bridged manganese complexes one of the vibrations of the MnO_2Mn unit is expected to have a frequency around 700 cm^{-1} . For the Mn(III, IV) and Mn(IV, IV) complexes with phen the band was reported³⁶ at 686 and 692 cm^{-1} respectively. We have observed a band at about 680 cm^{-1} for all the ClO_4^- , BF_4^- and PF_6^- salts of the complexes. Bands corresponding to anions⁷³⁻⁷⁵ were observed around 1210 , 1138 , 1030 and 945 cm^{-1} for ClO_4^- ; 1070 and 777 cm^{-1} for BF_4^- and 840 , 745 and 555 cm^{-1} for PF_6^- in all the complexes.

In the dmf substituted complex formulated as $(\text{Mn}_2\text{O}_2\text{phen}_3\text{dmf}_2)(\text{PF}_6)_3$, dmf bands were observed at 2900 , 1660 , 1420 and 1095 cm^{-1} , the latter two bands overlapping with those in the parent complex (Figure 4). The band at 680 cm^{-1} is very weak in this complex casting some doubt on the formulation of the product as a dioxo-bridged compound. However, e.s.r. (sub-section 3.4) as well as analytical results (Chapter 2, sub-section 2.4.1) are in favour of such a structure. All the other bands corresponded to those in the parent phen complex.

The ClO_4^- salt has been substituted by py to obtain $(\text{Mn}_2\text{O}_2\text{phen}_3\text{py}_2)(\text{ClO}_4)_3$ complex (Figure 5). Bands at 3020 , 1600 , 1440 , 1140 and 700 cm^{-1} correspond to py and band at 680 cm^{-1} corresponds to the dioxo-bridge. All other bands correspond to those in the parent complex.

$(\text{Mn}_2\text{O}_2\text{phen}_3\text{bpy})(\text{ClO}_4)_3$ complex formed by crystallisation of the phen complex from bpy buffer has a sharp band at 670 cm^{-1} which is assigned to MnO_2Mn bridge. Both the symmetrical phen and bpy

TABLE I: I.r. spectra of phen complexes.

$(\text{Mn}_2\text{O}_2\text{phen}_4)(\text{ClO}_4)_3$	$(\text{Mn}_2\text{O}_2\text{phen}_4)(\text{BF}_4)_3$	$(\text{Mn}_2\text{O}_2\text{phen}_4)(\text{PF}_6)_3$	$(\text{Mn}_2\text{O}_2\text{phen}_4)(\text{dmf}_2)(\text{ClO}_4)_3$	$(\text{Mn}_2\text{O}_2\text{phen}_3)(\text{dmf}_2)(\text{BF}_4)_3$	$(\text{Mn}_2\text{O}_2\text{phen}_3)(\text{dmf}_2)(\text{PF}_6)_3$	$(\text{Mn}_2\text{O}_2\text{phen}_3)(\text{py}_2)(\text{ClO}_4)_3$	$(\text{Mn}_2\text{O}_2\text{phen}_3)(\text{bpy})(\text{ClO}_4)_3$
3400 (b)	3425 (b)	3400 (b)	3440 (b)	3425 (b)	3400 (b)	3420 (b)	3450 (b)
3050	3060	3050	3075	3055	3050	3020	3010
1630	1630	1620	2950	2925	2900 (w)	1620	1615
1610	1610	1600	1680	1690 (sh)	1660 (s)	1600 (s)	1595
1580	1585	1580	1640	1650	1620	1580	1575
1510	1525	1510	1620	1612	1600	1510	1510
1425	1498	1485 (w)	1590	1598	1580	1440 (s)	1480
1340	1458	1450	1520	1518	1510	1420	1460
1310	1425	1420 (s)	1500 (w)	1420	1485 (sh)	1330	1435
1220	1345	1335	1430	1400 (sh)	1450	1300	1420
1210 (sh)	1308	1300	1400	1340	1420 (vs)	1210 (s)	1320
1140 (s)	1260 (w)	1218	1340	1300	1380	1140 (s)	1300
1070	1225	1140	1310	1220	1335	1030 (b)	1230
1030 (sh)	1210	1095	1280	1140	1218	1000 (w)	1210
945 (sh)	1140 (w)	1050	1230	1050 (b)	1140	745	1140 (sh)
840	1070 (b)	1020 (w)	1210 (w)	840	1095	700	1070 (b)
770 (w)	865 (w)	980 (w)	1150 (w)	760 (w)	840 (b)	680	850 (w)
710	845	950 (w)	1080 (b)	718	765	600	835
680	770 (s)	830 (b)	842	680 (sh)	740 (sh)		750 (s)
650 (sh)	740 (w)	765 (w)	770 (w)	625	718		710
610	728	740 (sh)	720				670

Contd....

$(\text{Mn}_2\text{O}_2\text{phen}_4)(\text{ClO}_4)_3$	$(\text{Mn}_2\text{O}_2\text{phen}_4)(\text{BF}_4)_3$	$(\text{Mn}_2\text{O}_2\text{phen}_4)(\text{PF}_6)_3$	$(\text{Mn}_2\text{O}_2\text{phen}_4)(\text{dmf}_2)(\text{ClO}_4)_3$	$(\text{Mn}_2\text{O}_2\text{phen}_3)(\text{dmf}_2)(\text{BF}_4)_3$	$(\text{Mn}_2\text{O}_2\text{phen}_3)(\text{dmf}_2)(\text{PF}_6)_3$	$(\text{Mn}_2\text{O}_2\text{phen}_3)(\text{py}_2)(\text{ClO}_4)_3$	$(\text{Mn}_2\text{O}_2\text{phen}_2)(\text{bpy})(\text{ClO}_4)_3$
<u>680</u>	<u>680</u>	705	<u>680</u>	<u>680</u> (w)	<u>680</u> (w)		640
655		<u>680</u> (s)	<u>660</u> (w)		625		605
630		640	640				
		625	620				

b: broad, sh: shoulder, s: sharp, w: weak, vs: very sharp.

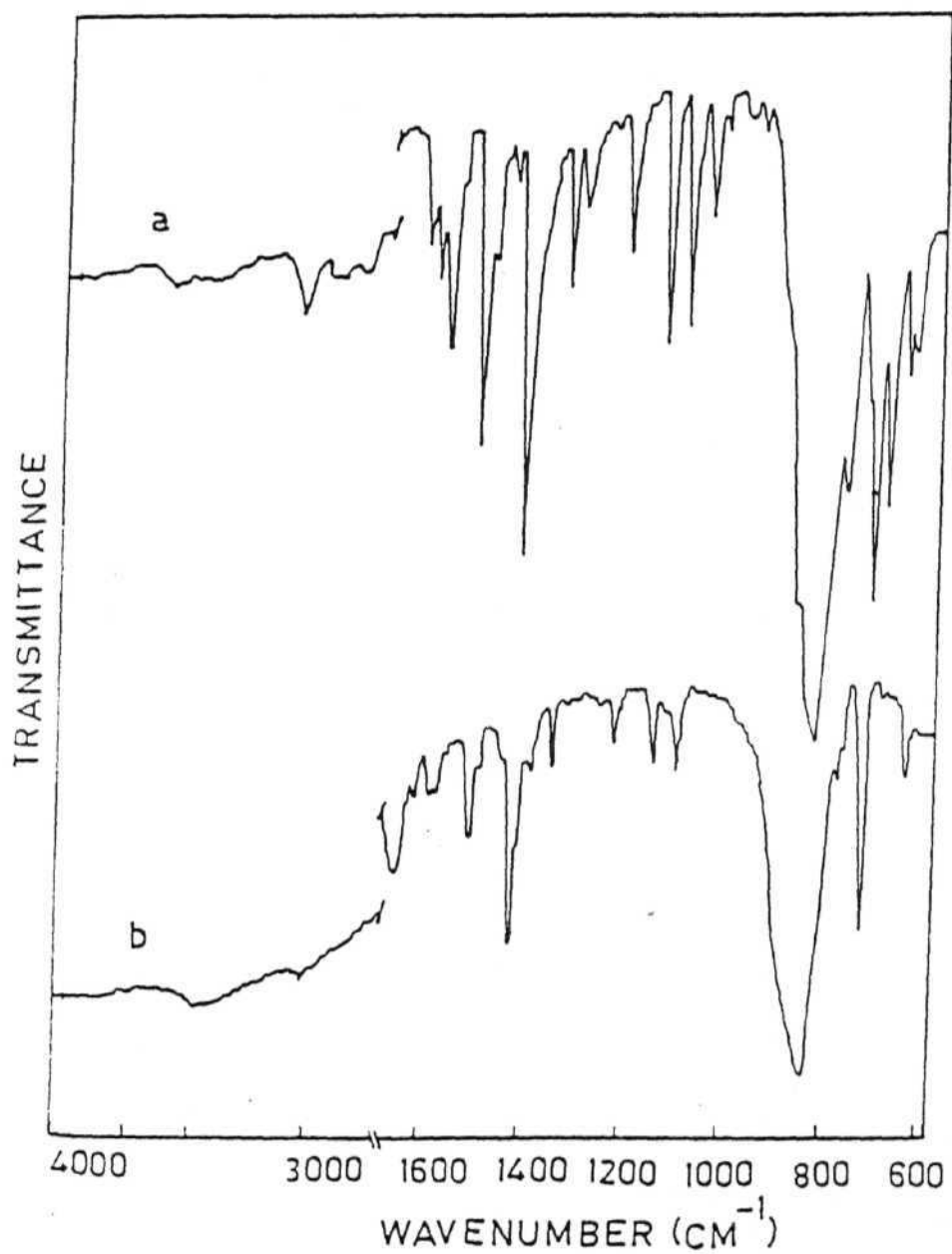


Figure 4: I.r spectra of (a) $(\text{Mn}_2\text{O}_2\text{phen}_4)(\text{PF}_6)_3$ and (b) $(\text{Mn}_2\text{O}_2\text{phen}_3\text{dmf}_2)(\text{PF}_6)_3$

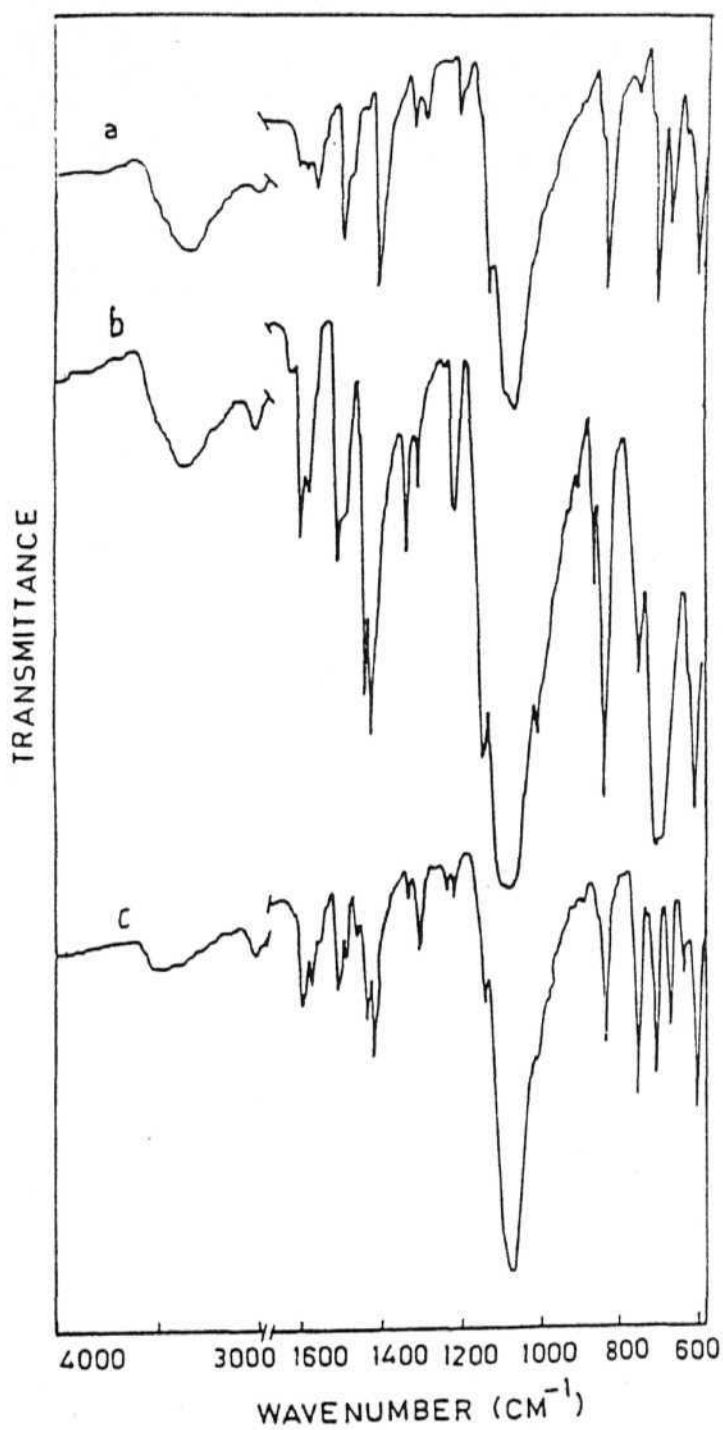


Figure 5: I.r spectra of (a) $(\text{Mn}_2\text{O}_2\text{phen}_4)(\text{ClO}_4)_3$,
 (b) $(\text{Mn}_2\text{O}_2\text{phen}_3\text{py}_2)(\text{ClO}_4)_3$ and
 (c) $(\text{Mn}_2\text{O}_2\text{phen}_3\text{bpy})(\text{ClO}_4)_3$.

complexes have a band at 1420 cm^{-1} . In the unsymmetrical complex this band is split into two bands at 1435 and 1420 cm^{-1} . In addition new bands at 1480 and 1460 cm^{-1} are observed which can be assigned to bpy. A sharp band at 750 cm^{-1} which was weak in the parent complex and several features common to both the parent phen and bpy complexes were observed.

1. 2 I.r. spectra of bpy complexes:-

The frequencies corresponding to ClO_4^- , BF_4^- and PF_6^- salts of $(\text{Mn}_2\text{O}_2\text{bpy}_4)^{3+}$ complexes are listed in Table II. All the salts have bands around $680\text{-}690\text{ cm}^{-1}$ corresponding to MnO_2Mn bridge. All other bands correspond to ligand and anions.

The ClO_4^- salt has been substituted by py (Figure 6). Bands corresponding to py were observed at 3030 , 1598 , 1460 , 1140 and 720 cm^{-1} . The band at 685 cm^{-1} corresponds to the dioxo-bridge.

The substituted complex obtained from phen buffer, $(\text{Mn}_2\text{O}_2\text{bpy}_3\text{phen})(\text{ClO}_4)_3$, shows a band at 675 cm^{-1} for MnO_2Mn bridge (Figure 6). The 1420 cm^{-1} band is not split in this complex. Otherwise the features are similar to that of $(\text{Mn}_2\text{O}_2\text{phen}_3\text{bpy})(\text{ClO}_4)_3$ analogue.

1. 3 I.r. spectra of 4,4'-dmbp and 5,5'-dmbp complexes:-

The i.r. spectra of 4,4'-dmbp and 5,5'-dmbp complexes are listed in Table III. The former complex shows a band at 688 cm^{-1} corresponding to the dioxo-bridge. All other bands correspond to ligand and anion frequencies.

The 5,5'-dmbp complex and its dmf derivative show bands due to

Table II. I.r. spectra of bpy complexes.

$(\text{Mn}_2\text{O}_2\text{bpy}_4)$ $(\text{ClO}_4)_3$	$(\text{Mn}_2\text{O}_2\text{bpy}_4)$ $(\text{BF}_4)_3$	$(\text{Mn}_2\text{O}_2\text{bpy}_4)$ $(\text{PF}_6)_3$	$(\text{Mn}_2\text{O}_2\text{bpy}_3\text{py}_2)$ $(\text{ClO}_4)_3$	$(\text{Mn}_2\text{O}_2\text{bpy}_3\text{phen})$ $(\text{ClO}_4)_3$
3400 (b)	3400 (b)	3620 (s)	3375 (b)	3405 (b)
3050	3060	3480 (b)	3030	3060
1650	1600	3180 (w)	1598	1620
1620	1560	3100	1560	1600
1580	1490	3060	1490	1580
1510	1460	1600	1460 (s)	1500
1490	1440	1560	1440	1480
1460	1310	1490	1420	1445
1420	1270 (w)	1470	1310	1420
1340	1240	1440	1240	1330
1300	1150 (w)	1310	1210	1300
1210	1035 (b)	1270	1140 (w)	1210
1140 (sh)	760 (vs)	1240	1080 (b)	1135 (sh)
1070 (b)	720	1170	1000	1075 (b)
840	680	1150	960	850
765	620	1105	880	835
710	610	1055	810	760
680		1010	760 (s)	700
610		820 (b)	720	675
		745	685	640
		710	610	600
		670		
		640		
		618		

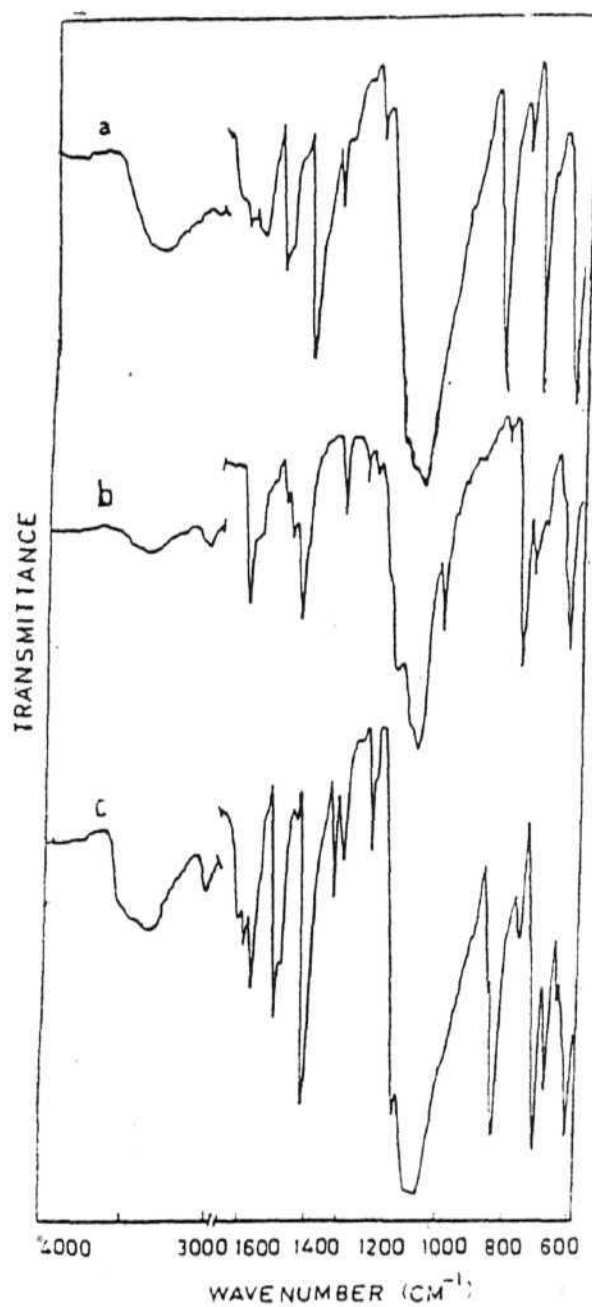


Figure 6: I.r spectra of (a) $(\text{Mn}_2\text{O}_2\text{bpy}_4)(\text{ClO}_4)_3$,
(b) $(\text{Mn}_2\text{O}_2\text{bpy}_3\text{py}_2)(\text{ClO}_4)_3$ and
(c) $(\text{Mn}_2\text{O}_2\text{bpy}_3\text{phen})(\text{ClO}_4)_3$.

Table III. I.r. spectra of complexes of methyl substituted ligands.

$(\text{Mn}_2\text{O}_24,4'\text{dmbp}_4)(\text{PF}_6)_3$	$(\text{Mn}_2\text{O}_25,5'\text{dmbp}_4)(\text{PF}_6)_3$	$(\text{Mn}_2\text{O}_25,5'\text{dmbp}_3\text{dmf}_2)(\text{PF}_6)_3$
3680	3660	3680 (b)
3110 (w)	3060 (w)	3080 (w)
1640	1600	2925 (w)
1558	1582 (w)	1675
1480	1570	1618
1450	1500	1545 (w)
1418	1472	1485
1375 (w)	1390	1400 (w)
1325	1312	1320 (w)
1310	1280 (w)	1295 (w)
1285	1245	1255
1248	1160	1240
1225	1050	1170
1210 (w)	840	1055
1080 (w)	745	840
1020	720	725
925 (w)	680	700
830	655	650
740 (w)	555	600
688	430	
635	390	
550	370	

w: weak, b: broad.

MnO₂Mn bridge at 680 and 700 cm⁻¹ respectively (Figure 7). The dmf derivative shows bands around 2925, 1675, 1400 and 1055 cm⁻¹ corresponding to dmf.

Electronic spectra of manganese (III, IV) complexes.

1 Origin of electronic bands in Mn(III), Mn(IV) and dinuclear Mn(III,IV) complexes in octahedral crystal fields:-

In the cis-distorted octahedral unit, MnN₄O₂ of the Mn(III, IV) mixed-valence complexes Mn(III)(d⁴) ion is in high-spin state corresponding to the free ion term, ⁵D. As the next quintet state (⁵F derived from d³s configuration) lies ~ 110,000 cm⁻¹ above the ⁵D ground state of the free ion⁷⁶, only one spin-allowed absorption band (⁵E_g → ⁵T_{2g}) is expected in the visible region (figure 8a). However, due to static and dynamic Jahn-Teller interaction, as well as rhombic distortion the simple octahedral splitting will not be applicable. The true symmetry at each manganese site is not higher than C_{2v}. A large distortion is expected since the configuration (t_{2g})³e_g contains a σ-antibonding electron and the splitting of the ⁵E_g ground term may be large enough to yield a transition in near i.r or visible region (Figure 8b).

Weak spin forbidden quintet - triplet transitions are expected in the visible region. As Mn(III) ion is moderately oxidising in nature the LMCT will occur at lower energies which may sometimes obscure the d-d transitions. Thus the complexes of Mn(III) display a low energy transition around 10.0kK and two higher energy transitions around 16.0-21.0kK, the former corresponding to the transition between the

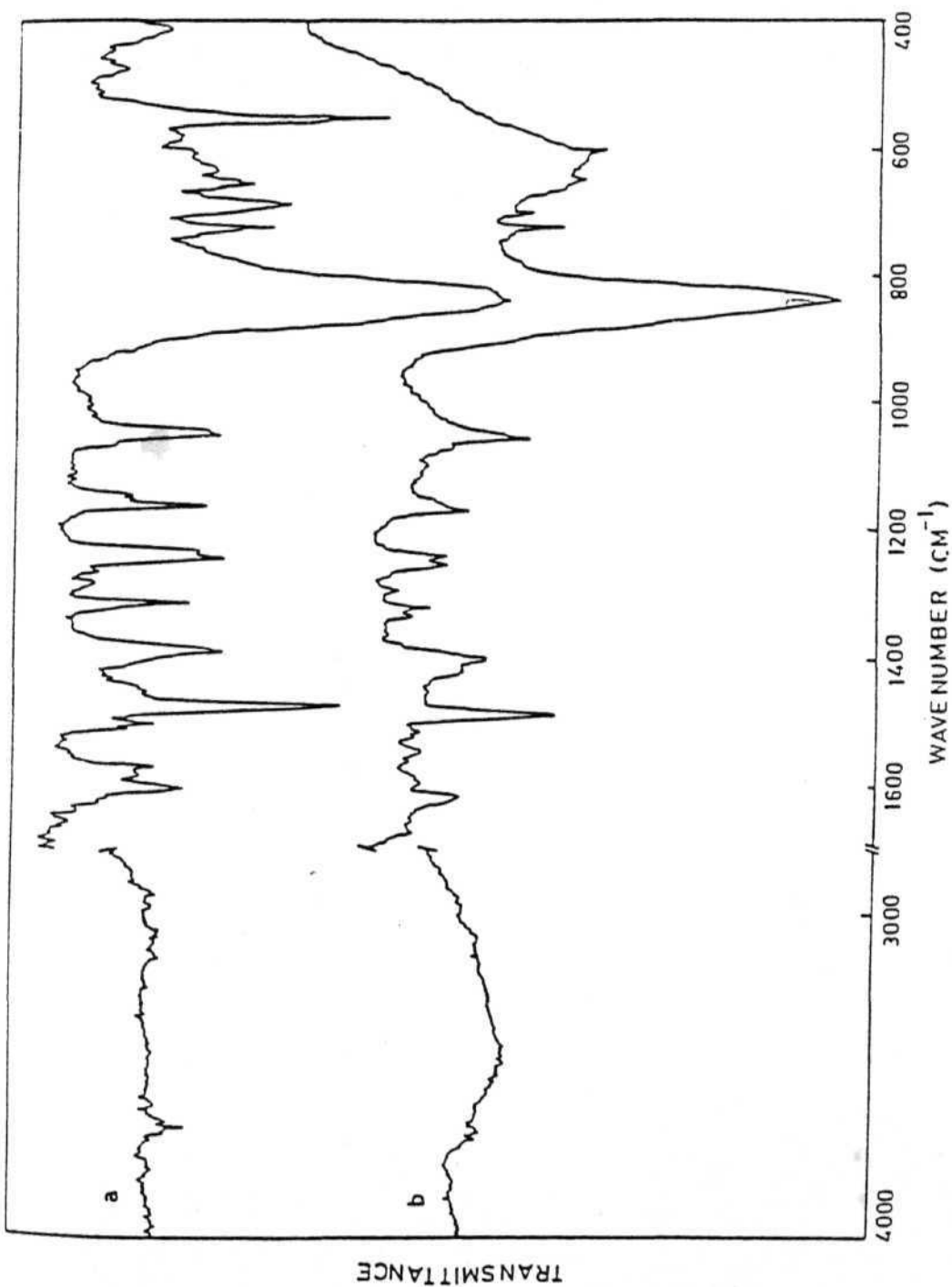


Figure 7: I.r spectra of (a) $(\text{Mn}_2\text{O}_2)_5,5\text{-dmbp}_4(\text{PF}_6)_3$ and (b) $(\text{Mn}_2\text{O}_2)_5,5\text{-dmbp}_3\text{dmf}_2(\text{PF}_6)_3$.

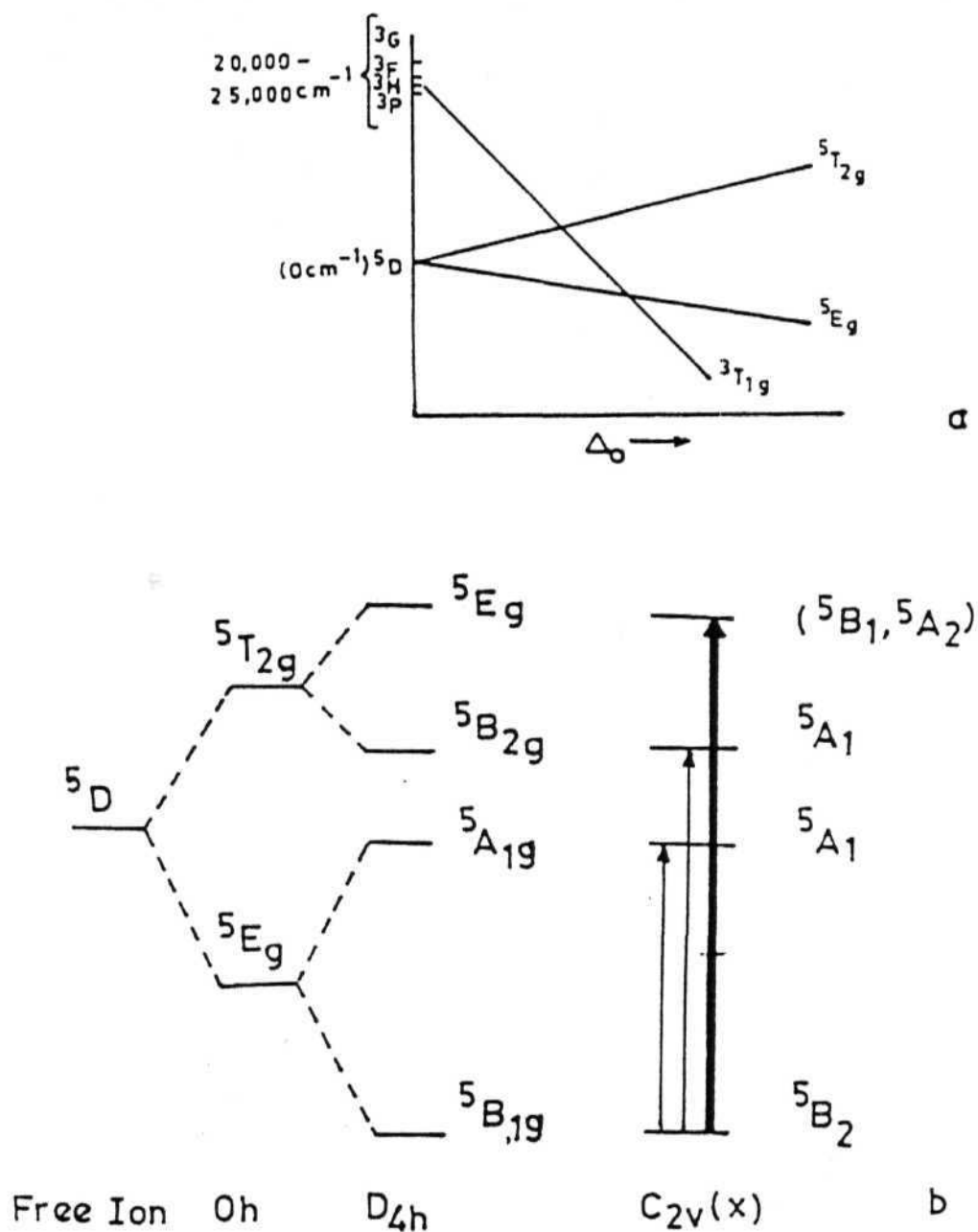


Figure 8: (a) Simplified energy level diagram (Tanabe-Sugano) for the d^4 system Mn(III) in Octahedral surroundings.

(b) Low symmetry splitting. The notation corresponding to D_{4h} and $C_{2v}(x)$ point groups are given.

split components of 5E_g , and the latter broad band (which is resolved into two bands at low temperatures) corresponding to the transition from the ground state to the components of ${}^5T_{2g}$.

These transitions for some of the Mn(III) complexes are listed in Table (IV).

Relatively, few manganese (IV) complexes have been studied. The manganese (IV)(d^3) ion has a ground term 4F which in octahedral geometry splits into ${}^4A_{2g}$, ${}^4T_{2g}$ and ${}^4T_{1g}$ levels. The energy level diagram for a d^3 ion in octahedral geometry is shown in figure 9. The spin-allowed d-d transitions shown are expected to be at higher energies because of the higher oxidation states compared to the isoelectronic Cr(III) ion and are mostly shifted to the UV region where they are obscured by the much more intense charge transfer and intraligand transitions. Optical transition energies for some of the Mn(IV) complexes are listed in Table V.

In a mixed-valent dinuclear complex containing interacting Mn(III) and Mn(IV) centres, in addition to the transitions belonging to these centres, a new absorption is expected corresponding to the Frank-Condon hopping of an electron between them. This may occur anywhere from very low energies in the near i.r to high energies in the UV. In a symmetric mixed-valence complex, eg. $(Mn_2O_2L_4)^{3+}$, the transition may be thought of as taking the molecule from, say, LMn(III)-LL-Mn(IV)L to LMn(IV)-LL-Mn(III)L. The free energy for net electron transfer is zero since clearly the initial and final products

Table IV Absorption bands (kK) in Mn(III) complexes^a

Complex	${}^5A_{1g} + {}^5B_{1g}$	$({}^5E_g, {}^5B_{2g}) + {}^5B_{1g}$
$Mn(H_2O)_6^{3+}$		21.0
$Mn(dmsO)_6^{3+}$	14.8	16.7 20.0
$Mn(dmf)_6^{3+}$	15.4	17.9 20.8
$Mn(acac)_3$	9.5	17.9 21.5
$Mn(Oac)_3$	11.4	22.0

^aRef.77

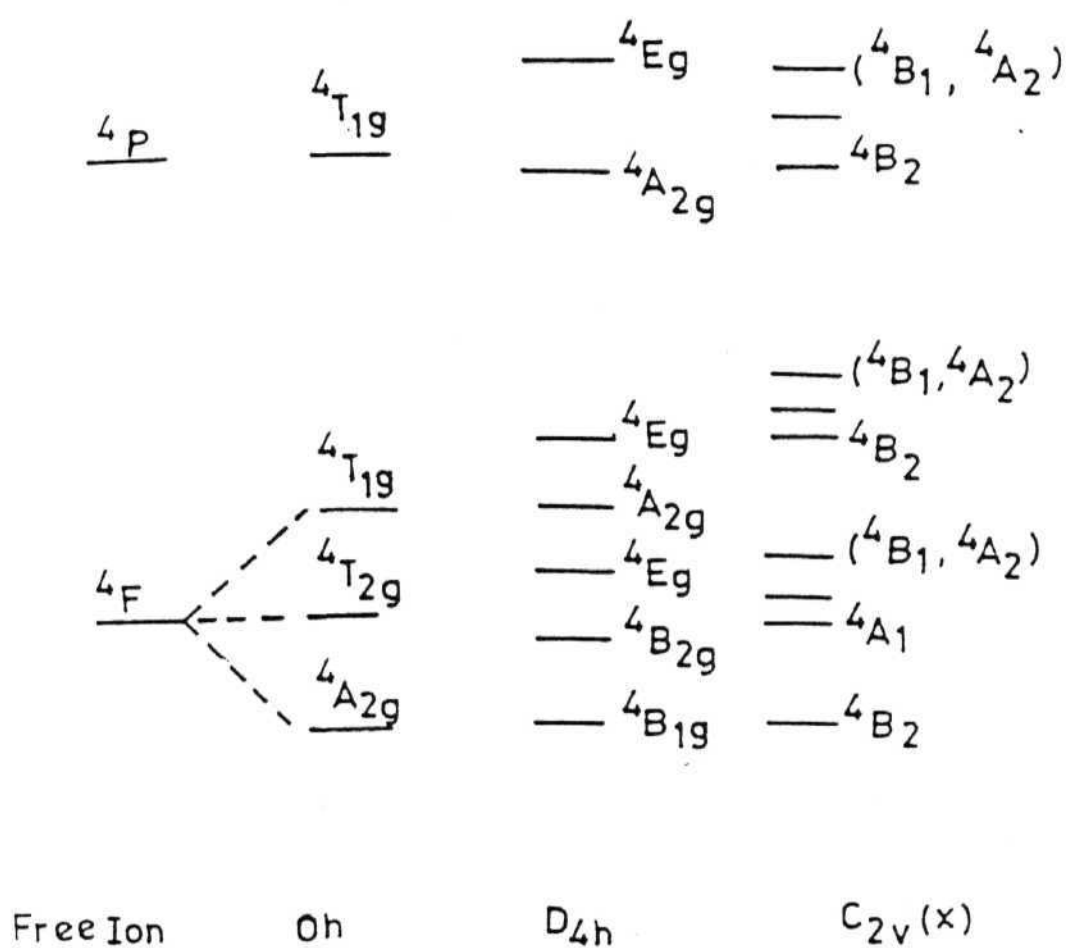


Figure 9: Energy level diagram for a d^3 ion (Mn IV) in Octahedral geometry.

Table V Absorption bands (kK) in Mn(IV) complexes.^a

Complex	$(^2E_g, ^2T_{1g}) \leftarrow ^4A_{2g}$	$^2T_{2g} \leftarrow ^4A_{2g}$	$^4T_{2g} \leftarrow ^4A_{2g}$	$^4T_{1g} \leftarrow ^4A_{2g}$
MnF_6^{2-}	16.0 17.3	25.7	21.8	28.1
$MnCl_6^{2-}$	12.0		18.2	25.5
$Mn(CN)_6^{2-}$	14.9		31.9	
$MnB(OH)_4$	17.9?		15.9	19.2

^aRef. 77

are the same. However the intervalence transition is a Frank-Condon transition which will not have zero energy. Thus the Mn(III)L distance is different from Mn(IV)L distance and the solvation spheres around the two ions will be different. During the electronic transition there is no time for nuclear motion. Thus after electron transfer, the Mn(III) ion finds itself in an Mn(IV) environment (hence higher energy) and Mn(IV) ion finds itself in an Mn(III) environment, also of higher energy. Therefore there is activation energy for the optical electron transfer and a non-zero value for the energy of the IVTA transition.

The absorption spectra of Mn(III, IV) complexes have been reported earlier³⁶ to show broad bands around 14.6, 17.9 and 19.0kK corresponding to Mn(III)(d⁴) high-spin ion where the low energy band is due to ${}^5B_{1g} \rightarrow {}^5A_{1g}$ transition and the two higher energy bands are due to ${}^5B_{1g} \rightarrow {}^5T_{2g}$ transition. The spin-allowed d-d bands due to Mn(IV)(d³) ion are shifted into UV region and are obscured by π - π^* bands of the ligand. The IVTA band was observed as a very broad band at around 12.0kK in $(Mn_2O_2L_4)(ClO_4)_3$ complexes where L=bpy or phen in the corresponding ligand buffer solution³⁶. Small shifts due to solvent were reported in CH₃CN and nitrobenzene.

2.2

Electronic spectra of phen complexes:-

The optical spectra for $(Mn_2O_2phen_4)^{3+}$ complexes and its derivatives are listed in Table VI. Two higher energy bands and one lower energy band are observed in CH₃CN which may be assigned to transitions of the Mn(III) ion (figure 8b). These bands are practically the same as those seen in aqueous phen buffer³⁶. But the IVTA band reported at 12.0kK in phen buffer solution was found shifted to 13.4kK

Table VI Electronic spectra of phen complexes.

Complex	λ (nm)	$\bar{\nu}$ (kK)	ϵ ($\text{m}^{-1}\text{cm}^{-1}\text{l}$)	Solvent
$(\text{Mn}_2\text{O}_2\text{phen}_4)(\text{ClO}_4)_3$	735 (sh)	13.6		CH_3CN
	685	14.6		
	562 (sh)	17.8		
	530 (sh)	18.9		
	830	12.0		phen ^a buffer
	684	14.6	509.0	
	555	18.0	427.0	
	525	19.0	553.0	
	740 (sh)	13.4	102.2	py
	604 (sh)	16.6	254.8	
$(\text{Mn}_2\text{O}_2\text{phen}_4)(\text{PF}_6)_3$	735 (sh)	13.6	804.3	CH_3CN
	685	14.6	827.1	
	565 (sh)	17.7	819.5	
	530 (sh)	18.9	1077.5	
	680 (sh)	14.7		dmf
$(\text{Mn}_2\text{O}_2\text{phen}_3\text{py}_2)(\text{ClO}_4)_3$	764 (sh)	13.1	667.2	CH_3CN
$(\text{Mn}_2\text{O}_2\text{phen}_3\text{bpy})(\text{ClO}_4)_3$	735 (sh)	13.6	775.1	CH_3CN
	688	14.5	794.0	
	562 (sh)	17.8	608.3	
	525	19.0	781.7	
$(\text{Mn}_2\text{O}_2\text{phen}_3\text{dmf}_2)(\text{ClO}_4)_3$ red solution	680	14.7		CH_3CN
	560	17.9		
	528	18.9		

^aRef. 36

(figures 10b, 11a). The solvent effect on the band position appears to be more than the solvent effect on intensity. If the intensity is appreciably affected we have to postulate that the IVTA band (13.4kK) in CH_3CN is very weak and 14.6kK band appears as a doublet due to two d-d transitions or due to spin-orbit coupling. This is unlikely because (i) only one low energy band is expected from Mn(III) even in the presence of moderate rhombic distortion, (ii) spin-orbit splitting is not expected for this band and (iii) in aqueous buffer upon lowering the pH the IVTA band disappears and only one weak band remains at 14.6kK³⁶.

In the unsymmetrical complex formed by substituting dmf, no IVTA band was observed (figures 11b, 12). The figure 12 shows the change in the spectrum with time corresponding to change in colour from green to red. The visible band is very much reduced in intensity and the higher energy shoulders are masked by the tail of intense UV band which moves into the visible region. The solid state p.a.s spectra do show the visible band as a shoulder at 13.2kK. The p.a.s. spectra of $(\text{Mn}_2\text{O}_2\text{phen}_4)(\text{BF}_4)_3$ and $(\text{Mn}_2\text{O}_2\text{phen}_3\text{dmf}_2)(\text{PF}_6)_3$ are compared in figure 13. It is noteworthy that upon dissolution of the red dmf substituted complex in aqueous phen buffer the solution turns green and the spectral bands correspond to the parent phen complex (figure 14).

The py substituted $(\text{Mn}_2\text{O}_2\text{phen}_3\text{py}_2)(\text{ClO}_4)_3$ complex dissolved in CH_3CN shows broad features resembling the spectra of the parent complex dissolved in pyridine (figure 15). Here again, the low energy

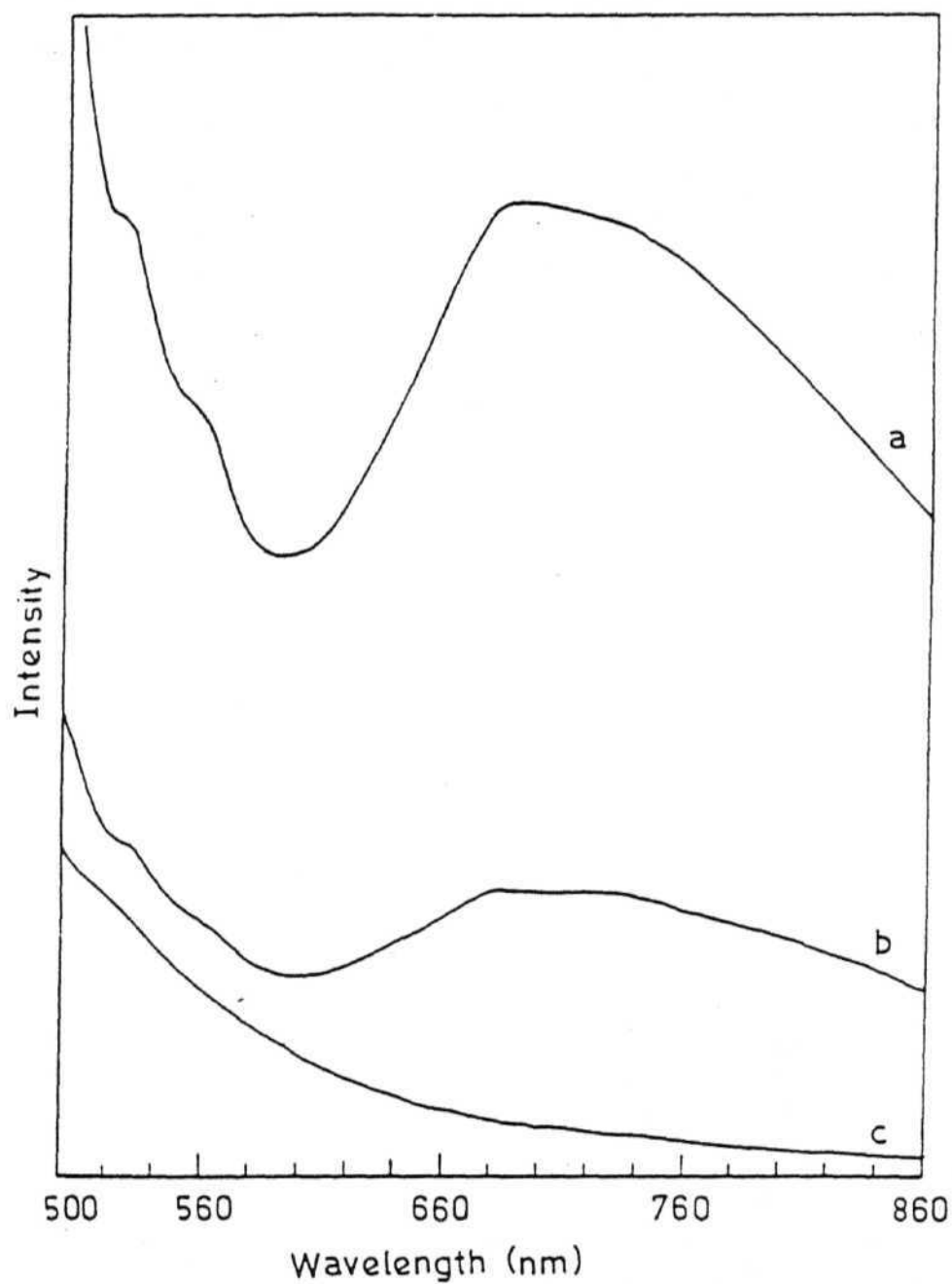


Figure 10: Electronic spectra of (a) $(\text{Mn}_2\text{O}_2\text{phen}_3\text{bpy})(\text{ClO}_4)_3$ in CH_3CN , (b) $(\text{Mn}_2\text{O}_2\text{phen}_4)(\text{ClO}_4)_3$ in CH_3CN and (c) $(\text{Mn}_2\text{O}_2\text{phen}_4)(\text{ClO}_4)_3$ in dmf.

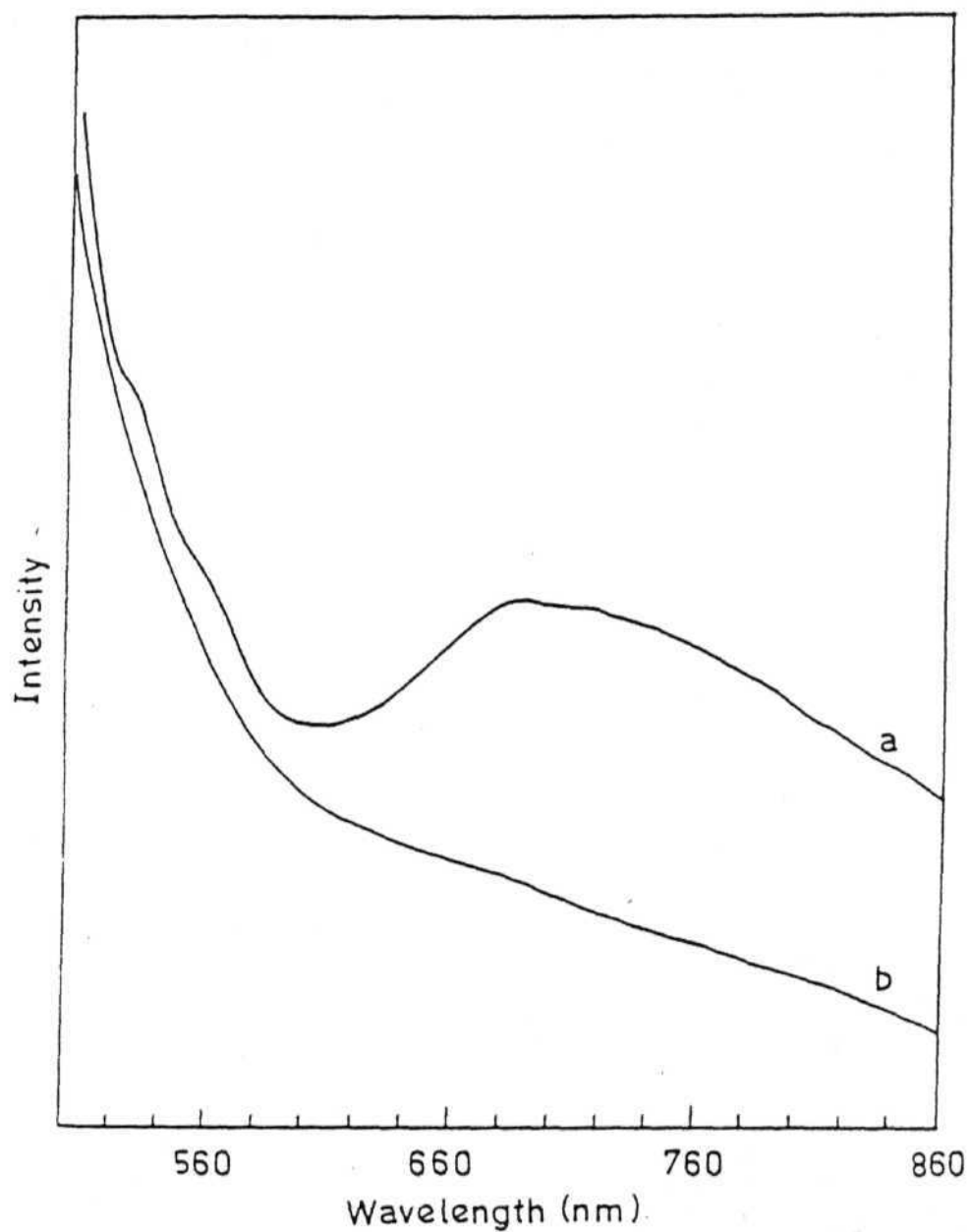


Figure 11: Electronic spectra of (a) $(\text{Mn}_2\text{O}_2\text{phen}_4)(\text{PF}_6)_3$ in CH_3CN and (b) $(\text{Mn}_2\text{O}_2\text{phen}_4)(\text{PF}_6)_3$ dissolved in dmf immediately.

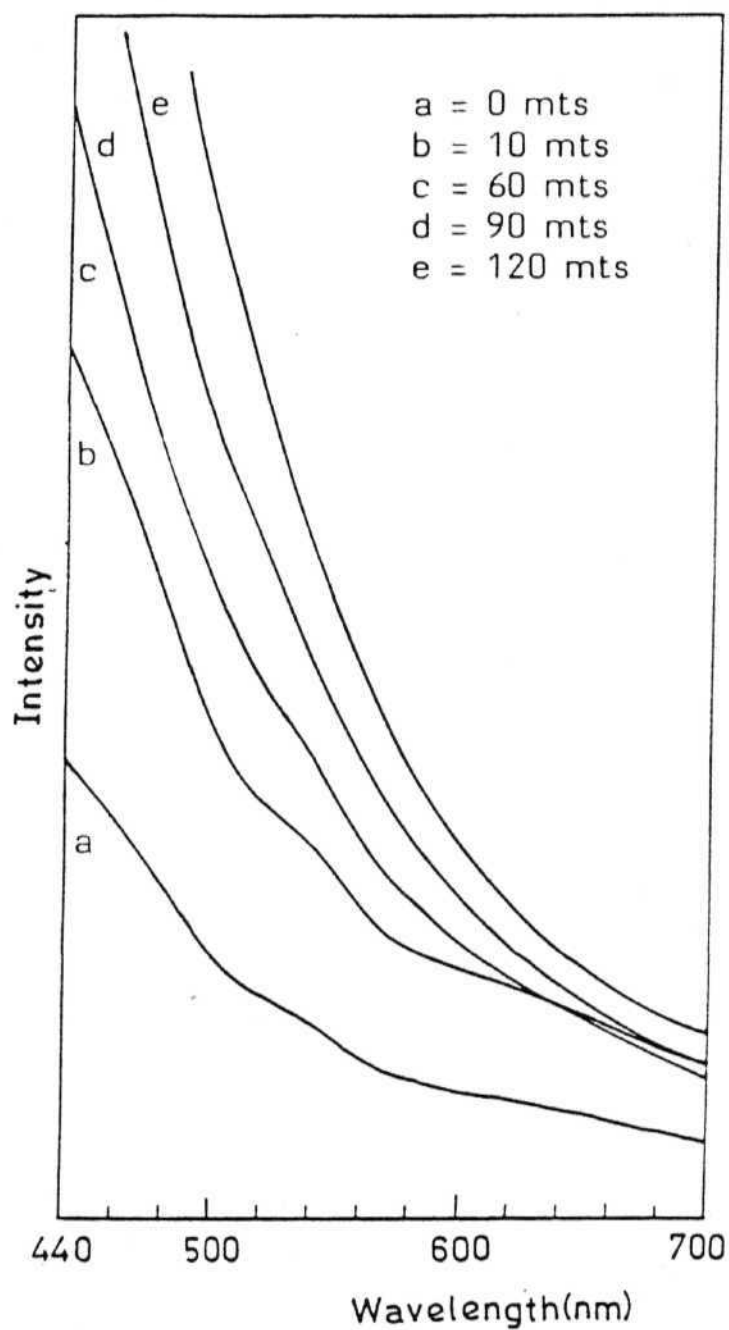


Figure 12

Electronic spectra of $(\text{Mn}_2\text{O}_2 \text{phen}_4)(\text{ClO}_4)_3$ dissolved in dmf showing gradual change in the intensity of the bands corresponding to colour change from green to red.

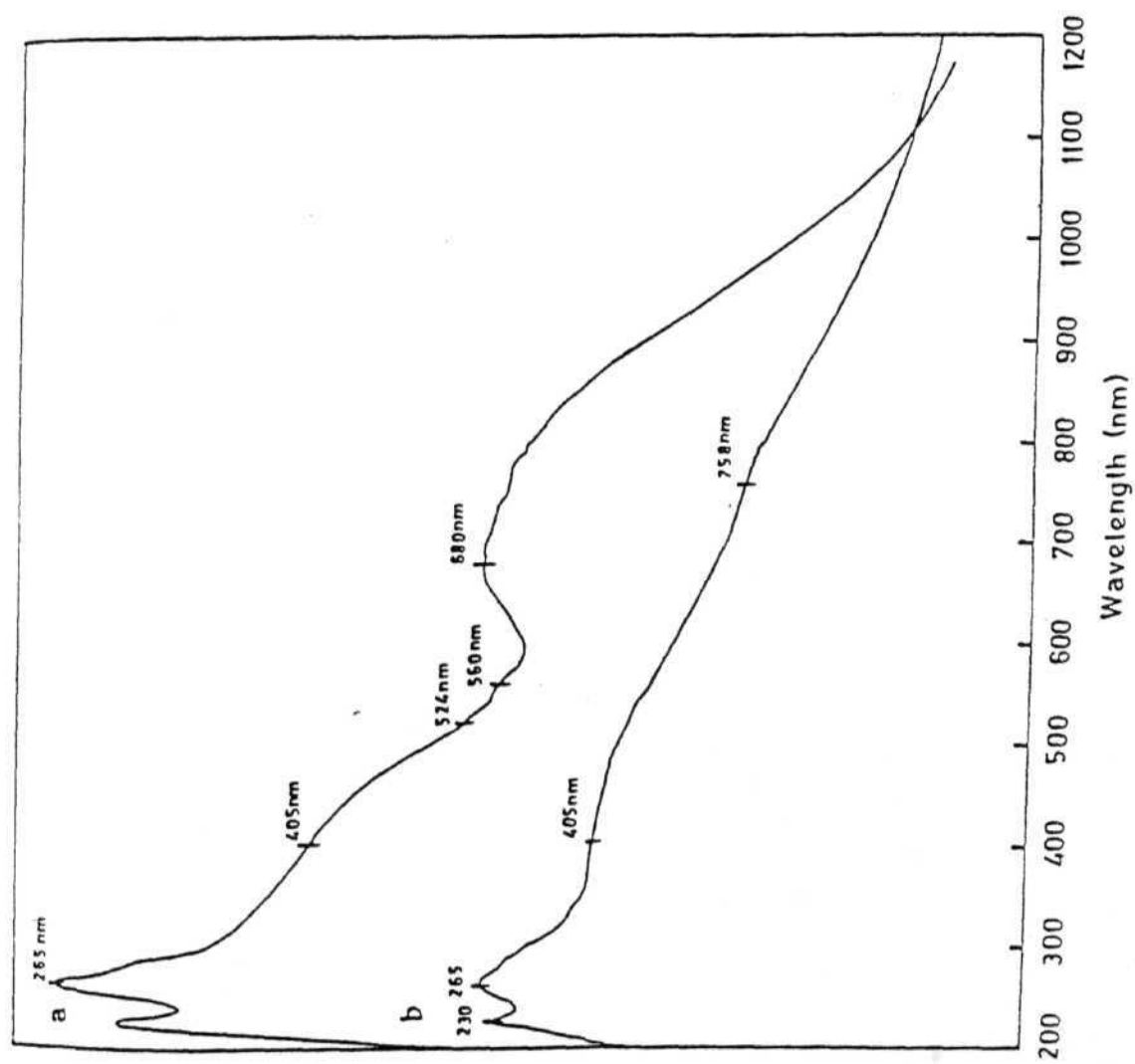


Figure 13: P.a.s. spectra of (a) $(\text{Mn}_2\text{O}_2\text{phen}_4)(\text{BF}_4)_3$ and (b) $(\text{Mn}_2\text{O}_2\text{phen}_3\text{dmf}_2)(\text{PF}_6)_3$.

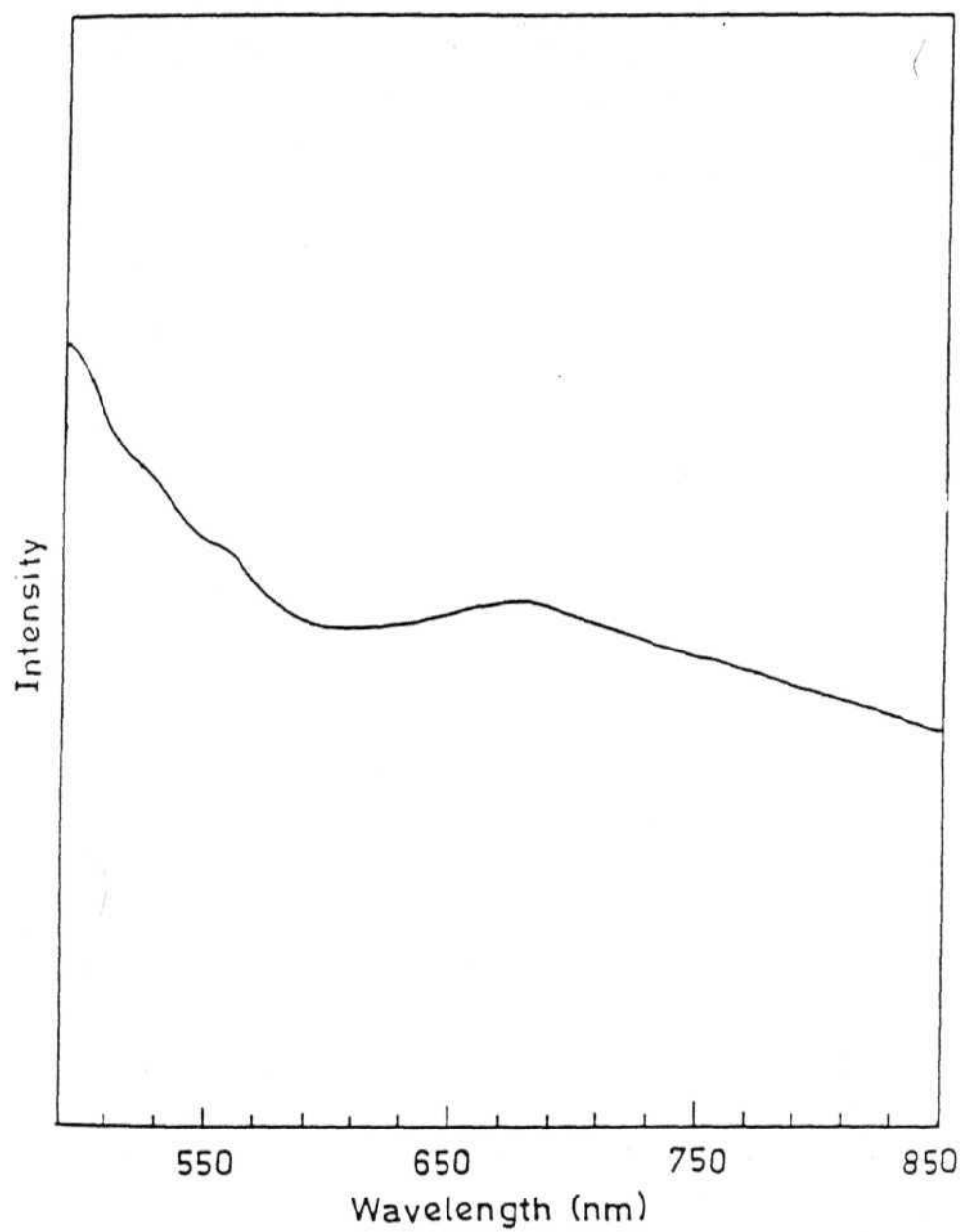


Figure 14: Electronic spectrum of $(\text{Mn}_2\text{O}_2\text{phen}_3\text{dmf}_2)\text{ClO}_4)_3$ dissolved in phen buffer.

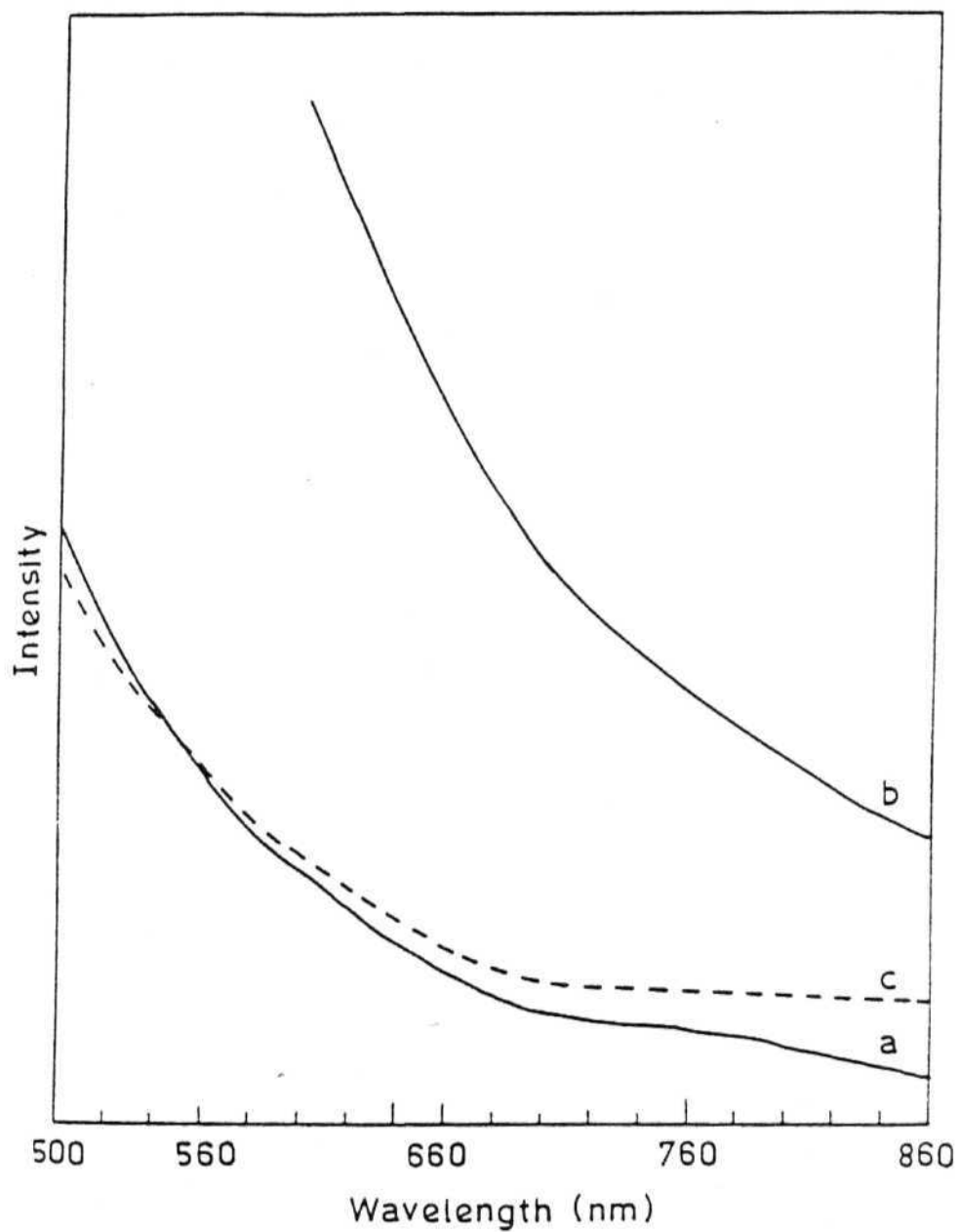


Figure 15: Electronic spectra of (a) $(\text{Mn}_2\text{O}_2\text{phen}_4)(\text{ClO}_4)_3$ in py, (b) $(\text{Mn}_2\text{O}_2\text{phen}_3\text{py}_2)(\text{ClO}_4)_3$ in CH_3CN and (c) $(\text{Mn}_2\text{O}_2\text{phen}_4)(\text{PF}_6)_3$ in py.

band is reduced in intensity and the intense UV band masks the high energy shoulders.

In conclusion it can be said that partial substitution by dmf and py considerably inhibits the mixed-valent delocalisation as implied by the low intensity of the IVTA band. Since the major contribution to the low energy band arises from the very broad IVTA, the substituted complexes have relatively featureless optical absorption spectra.

2.3 Electronic spectra of bpy complexes:-

The electronic spectra of all the bpy complexes are listed in Table VII. The bands corresponding to the three transitions in Mn(III) ion are observed. In CH_3CN the IVTA band shifted into the higher energy region compared to the values reported for the buffer solution³⁶ (figures 17a, 18a and 19a). All other features are essentially same as in the case of phen complexes (figures 16-19). The solution spectra may be compared with the p.a.s spectrum shown in figure 20.

2.4 Electronic spectra of unsymmetrical complexes containing both phen and bpy ligands:-

The spectra of CH_3CN solution of ligand exchanged products, $[\text{Mn}_2\text{O}_2(\text{bpy})_3\text{phen}](\text{ClO}_4)_3$ and $[\text{Mn}_2\text{O}_2(\text{phen}_3\text{bpy})](\text{ClO}_4)_3$ (figures 10a, 19b) are remarkably similar in band positions as well as intensities (Tables VI and VII). The band maxima are also same as those observed for the parent symmetrical complexes. However, the visible band in the unsymmetrical complexes has increased in intensity relative

Table VII Electronic spectra of bpy complexes.

Complex	λ (nm)	$\bar{\nu}$ (kK)	ϵ ($\text{m}^{-1}\text{cm}^{-1}\text{l}$)	Solvent
$(\text{Mn}_2\text{O}_2\text{bpy}_4)(\text{ClO}_4)_3$	732	13.7	602.2	CH_3CN
	688	14.5	618.9	
	562 (sh)	17.8	563.2	
	530 (sh)	18.9	701.4	
	740 (sh)	13.5	208.5	py
	610 (sh)	16.4	488.8	
	542 (sh)	18.5	793.7	bpy buffer ^a
	830	12.0		
	684	14.5	561.0	
	555	18.0	455.0	
	525	19.0	530.0	
$(\text{Mn}_2\text{O}_2\text{bpy}_4)(\text{BF}_4)_3$	738 (sh)	13.6	613.6	CH_3CN
	688	14.5	638.2	
	560 (sh)	17.9	594.9	
	525 (sh)	19.0	767.1	
	732 (sh)	13.7	201.7	dmf
	532 (sh)	18.8	981.6	
$(\text{Mn}_2\text{O}_2\text{bpy}_4)(\text{PF}_6)_3$	738 (sh)	13.6	687.7	CH_3CN
	688	14.5	709.4	
	562 (sh)	17.8	613.5	
	525 (sh)	19.0	805.3	
	738 (sh)	13.6	192.2	dmf
	538 (sh)	18.6	909.7	
$(\text{Mn}_2\text{O}_2\text{bpy}_3\text{py}_2)(\text{ClO}_4)_3$	684 (sh)	14.6	1376.8	CH_3CN
	565 (sh)	17.7	1425.9	
	535 (sh)	18.7	1561.2	
Contd...				

Complex	λ (nm)	$\tilde{\nu}$ (kK)	ϵ ($\text{m}^{-1}\text{cm}^{-1}\text{l}$)	Solvent
$(\text{Mn}_2\text{O}_2\text{bpy}_3\text{phen})(\text{ClO}_4)_3$	732 (sh)	13.7	792.3	CH_3CN
	688	14.5	814.8	
	558 (sh)	17.9	649.6	
	525	19.0	803.5	

^aRef. 36

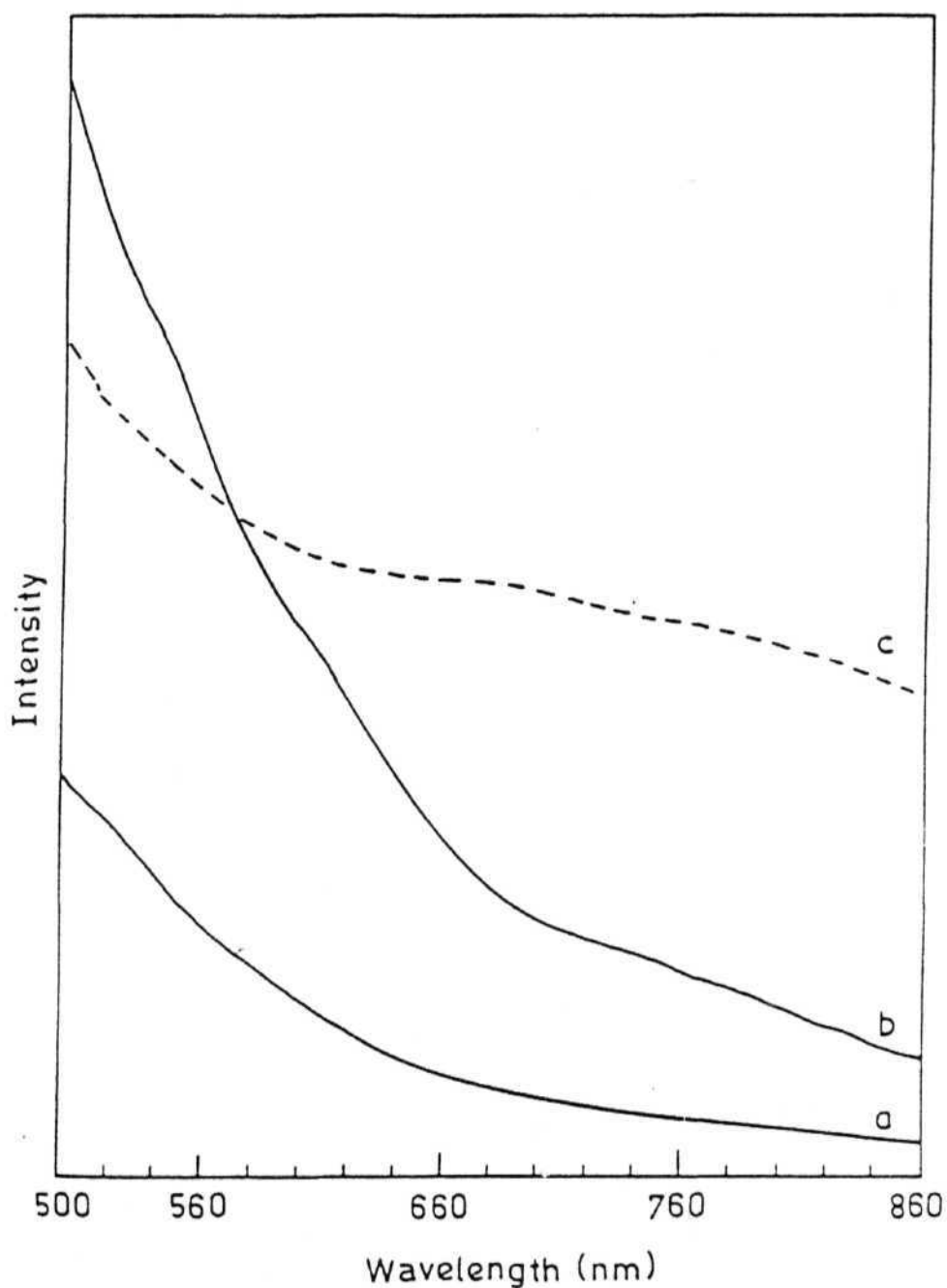


Figure 16: Electronic spectra of (a) $(\text{Mn}_2\text{O}_2\text{bpy}_4)(\text{ClO}_4)_3$ in dmf, (b) $(\text{Mn}_2\text{O}_2\text{bpy}_4)(\text{ClO}_4)_3$ in py and (c) $(\text{Mn}_2\text{O}_2\text{bpy}_3\text{py}_2)(\text{ClO}_4)_3$ in CH_2CN .

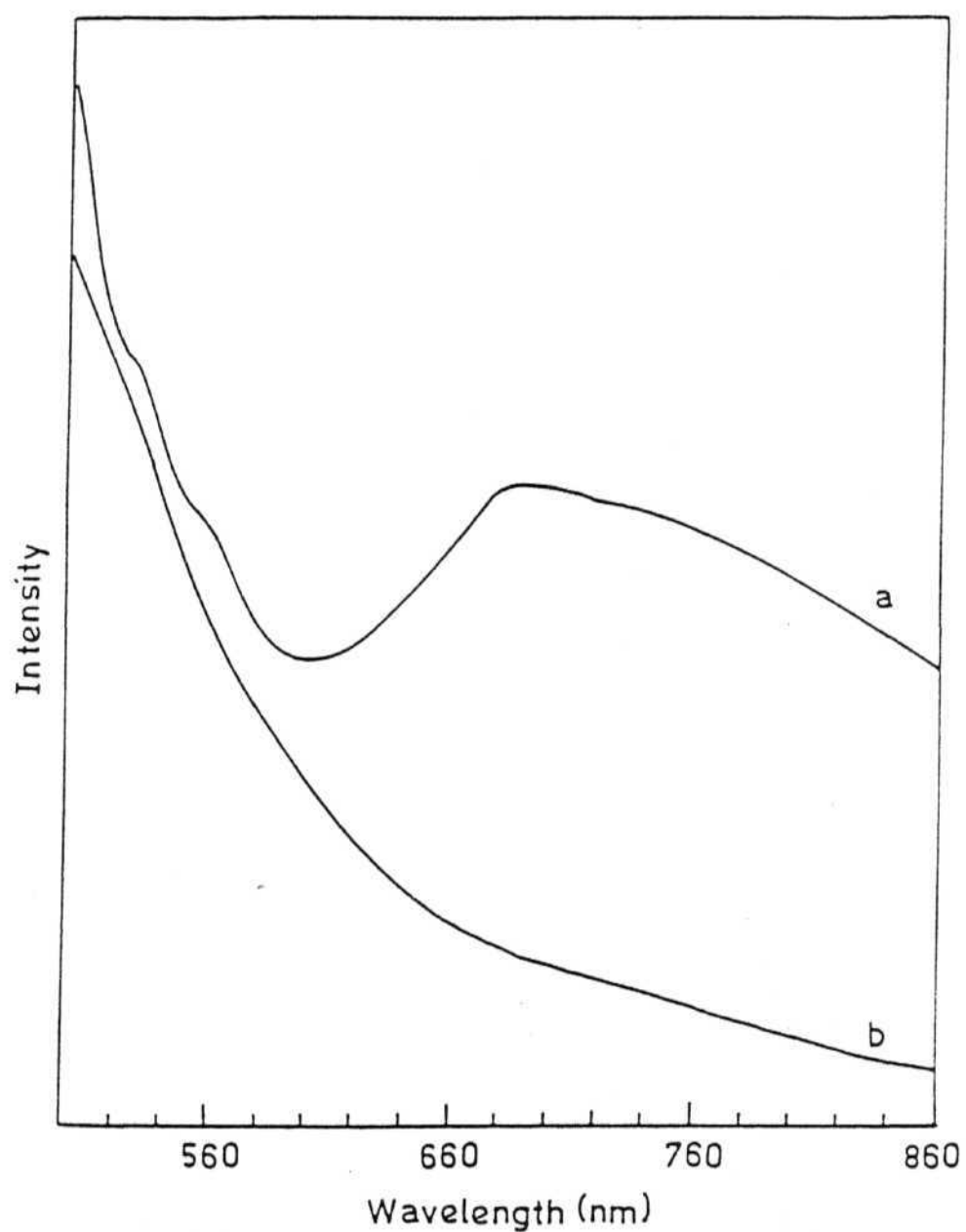


Figure 17: Electronic spectra of (a) $(\text{Mn}_2\text{O}_2\text{bpy}_4)(\text{BF}_4)_3$ in CH_3CN and (b) $(\text{Mn}_2\text{O}_2\text{bpy}_4)(\text{BF}_4)_3$ in dmf .

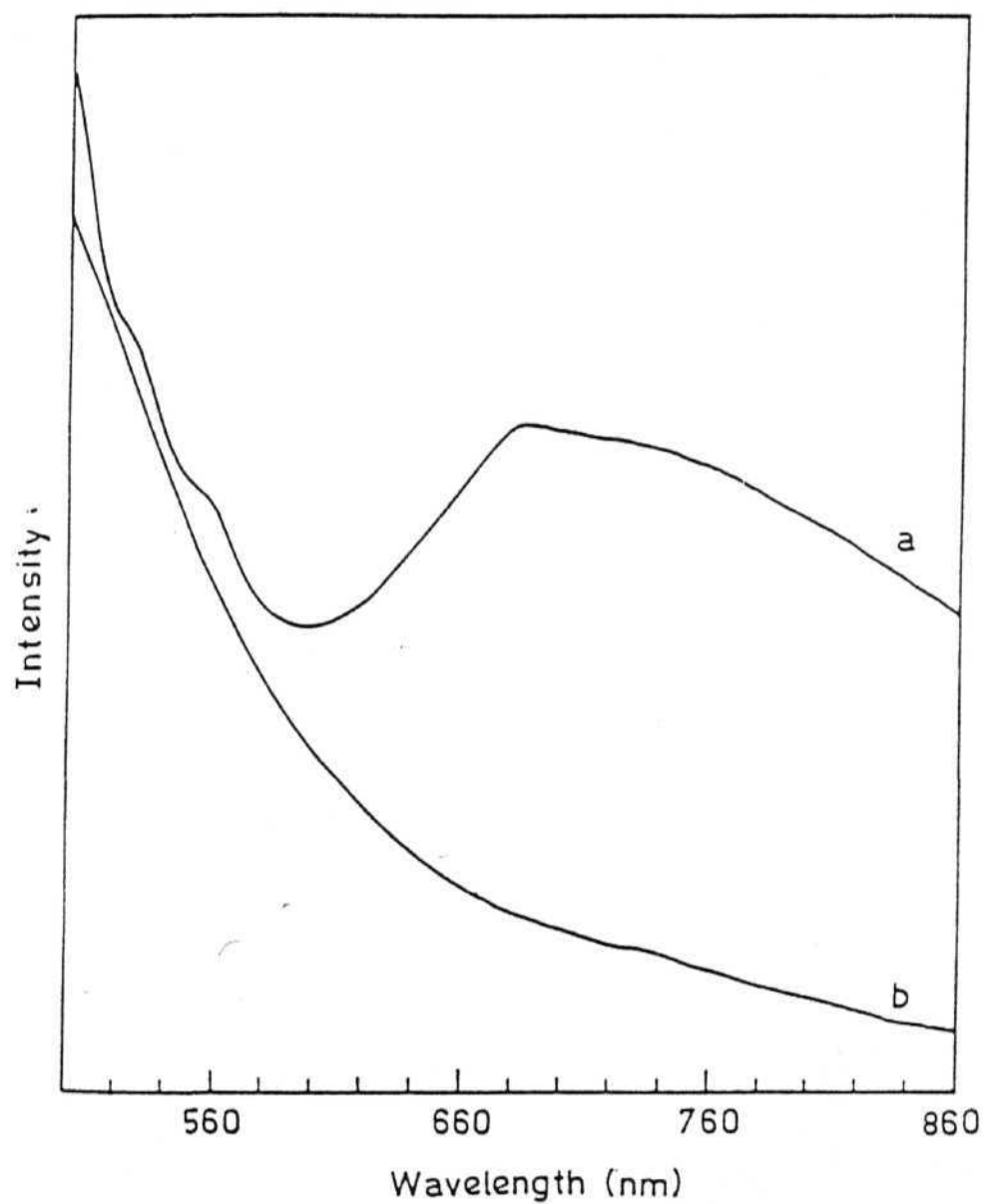


Figure 18; Electronic spectra of (a) $(\text{Mn}_2\text{O}_2\text{bpy}_4)(\text{PF}_6)_3$ in CH_3CN and (b) $(\text{Mn}_2\text{O}_2\text{bpy}_4)(\text{PF}_6)_3$ in dmf.

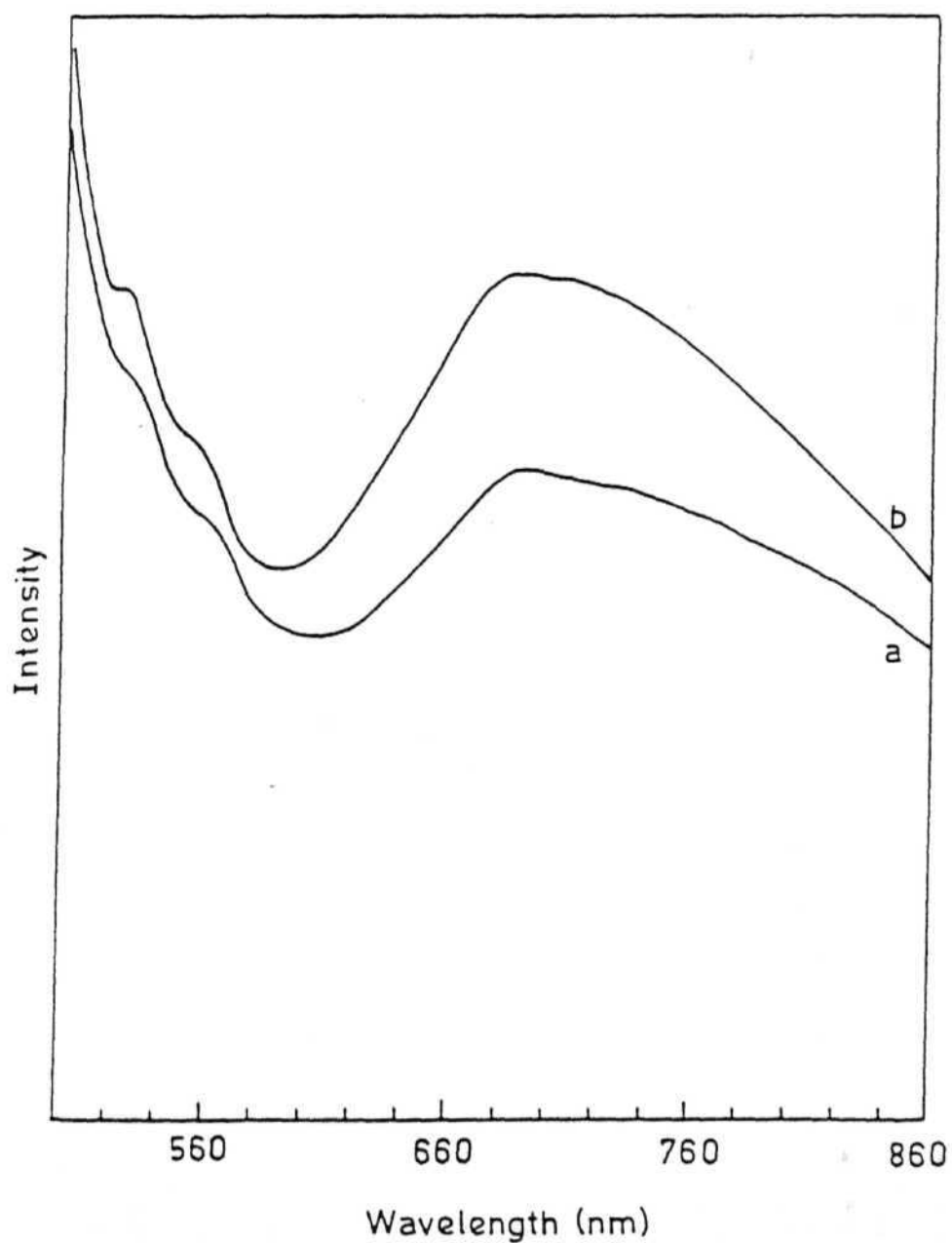


Figure 19: Electronic spectra of (a) $(\text{Mn}_2\text{O}_2\text{bpy}_4)(\text{ClO}_4)_3$ in CH_3CN and (b) $(\text{Mn}_2\text{O}_2\text{bpy}_3\text{phen})(\text{ClO}_4)_3$ in CH_3CN .

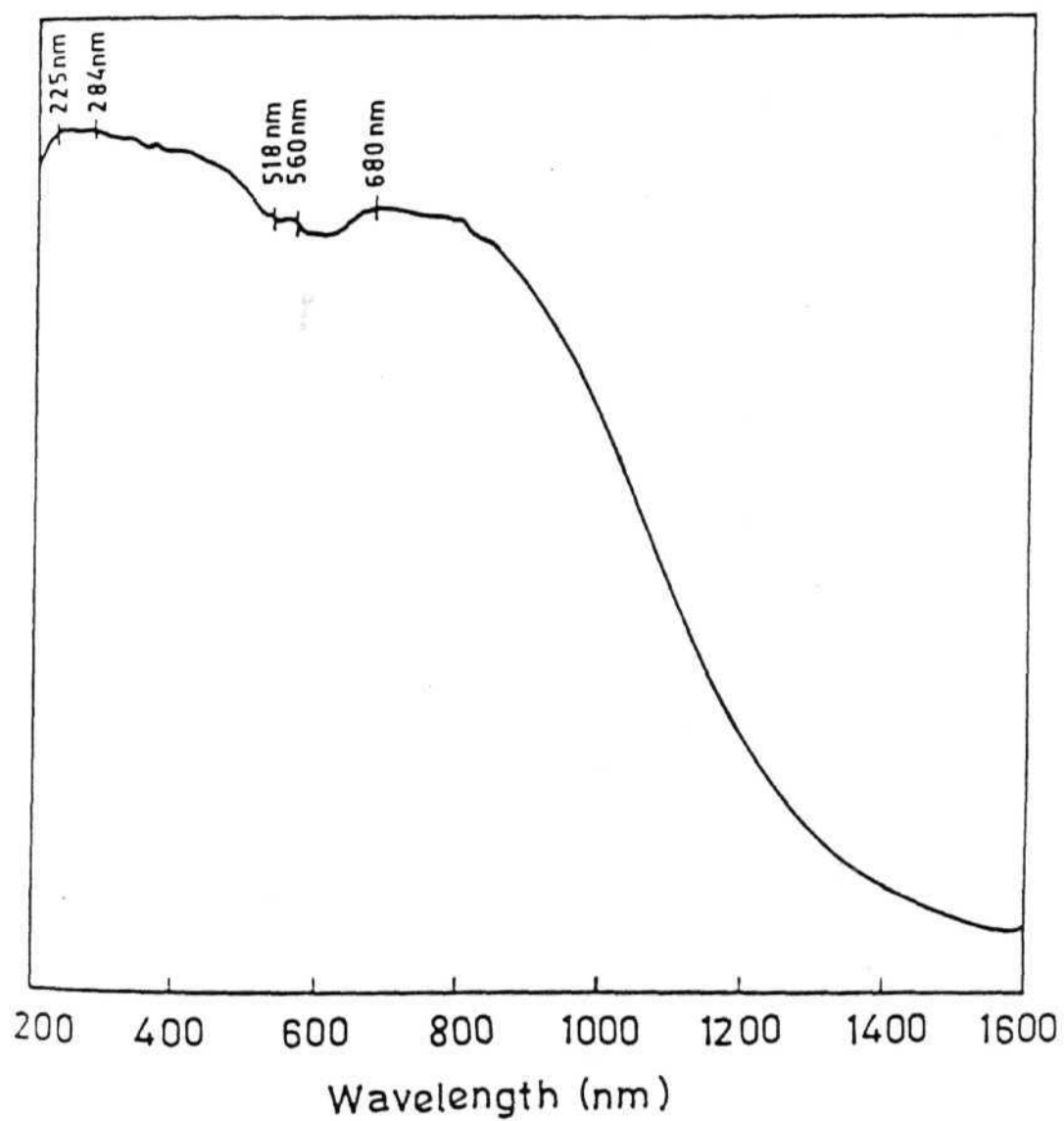


Figure 20: P.a.s spectrum of $(\text{Mn}_2\text{O}_2\text{bpy}_4)(\text{ClO}_4)_3$.

to the high energy bands. The parent phen complex has more intense bands than the bpy complex. Substitution by phen on the bpy complex is found to increase the intensity of all the absorption bands. Similarly substitution by bpy on the phen complex leads to reduction in the intensity. In both cases the visible band is affected more than the high energy bands. Based on the simple model of mixed valent delocalisation one would expect the unsymmetrical dinuclear complex to have lesser delocalisation and correspondingly lesser intensity for the IVTA band. In fact this is what is observed upon substitution by dmf and py. However, in the case of exchange of bpy by phen having very similar bonding characteristics (basicity, π -acceptor ability) there appear to be other factors which control the extent of mixed valent delocalisation.

2.5 Electronic spectra of methyl substituted bpy ligand complexes:-

The optical spectra of 4,4'-dmbp and 5,5'-dmbp complexes are listed in Table VIII. These complexes show bands due to the three Mn(III) transitions (figures 21 and 22). The dmf substituted complexes of these ligands also are observed to behave similarly in CH_3CN as that of the unsubstituted ligand complexes. The p.a.s spectra of these complexes are in concurrence with the solution spectra (figures 23 and 24).

Table VIII Electronic spectra of methyl substituted bpy complexes.

Complex	λ (nm)	$\bar{\nu}$ (cm ⁻¹)	Solvent
(Mn ₂ O ₂ 4,4'-dmbp ₄)(PF ₆) ₃	684	14.6	CH ₃ CN
	560(sh)	17.9	
	530(sh)	18.9	
(Mn ₂ O ₂ 4,4'-dmbp ₃ dmf ₂)(PF ₆) ₃	764	13.1	CH ₃ CN
	558(sh)	17.9	
(Mn ₂ O ₂ 5,5'-dmbp ₄)(PF ₆) ₃	684	14.6	CH ₃ CN
	564(sh)	17.7	
	535(sh)	18.7	

sh = shoulder

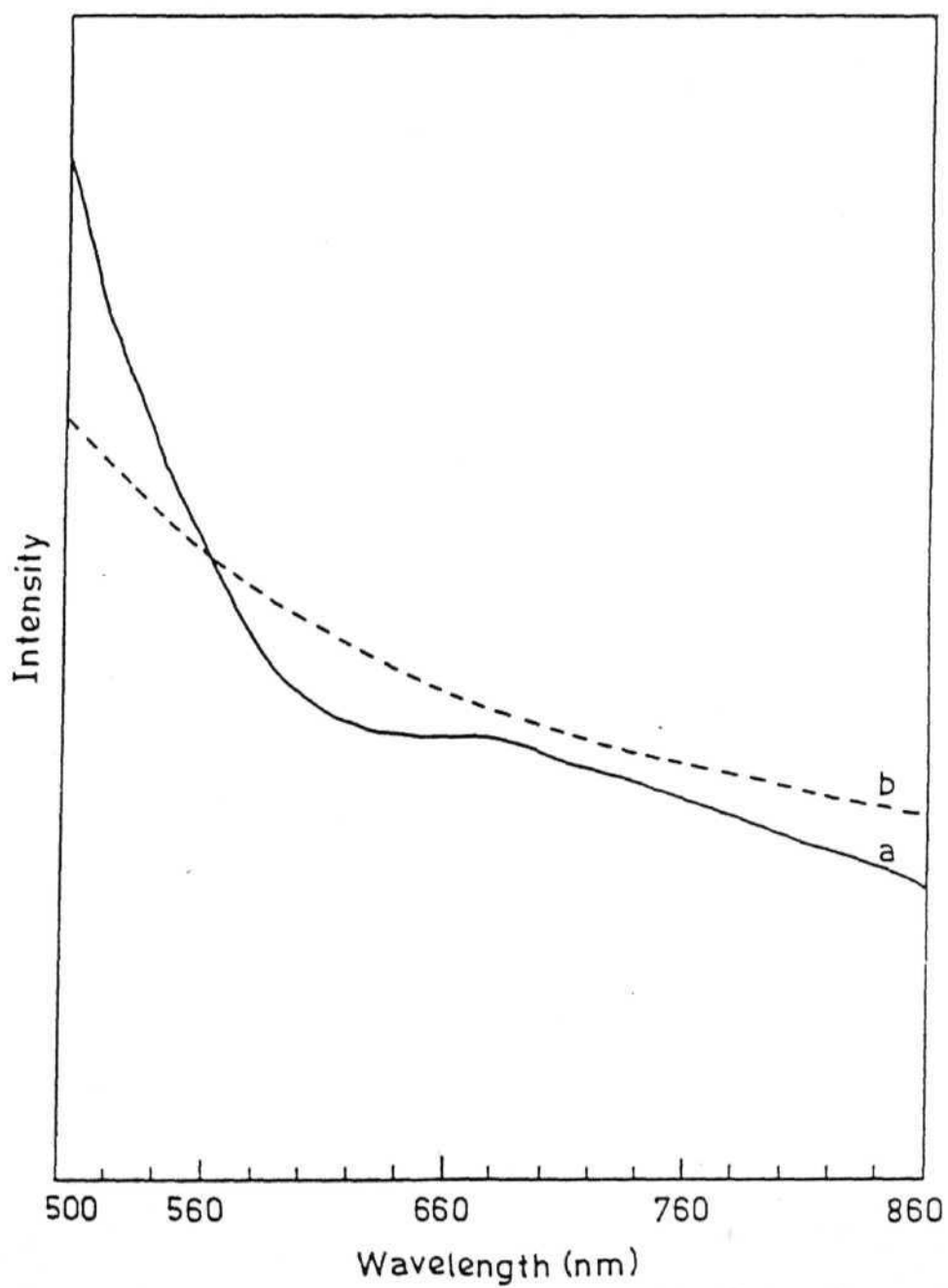


Figure 21: Electronic spectra of (a) $(\text{Mn}_2\text{O}_2 4,4'\text{-dmbp}_4)(\text{PF}_6)_3$ in CH_3CN and (b) $(\text{Mn}_2\text{O}_2 4,4'\text{-dmbp}_3 \text{ dmf}_2)(\text{PF}_6)_3$ in CH_3CN .

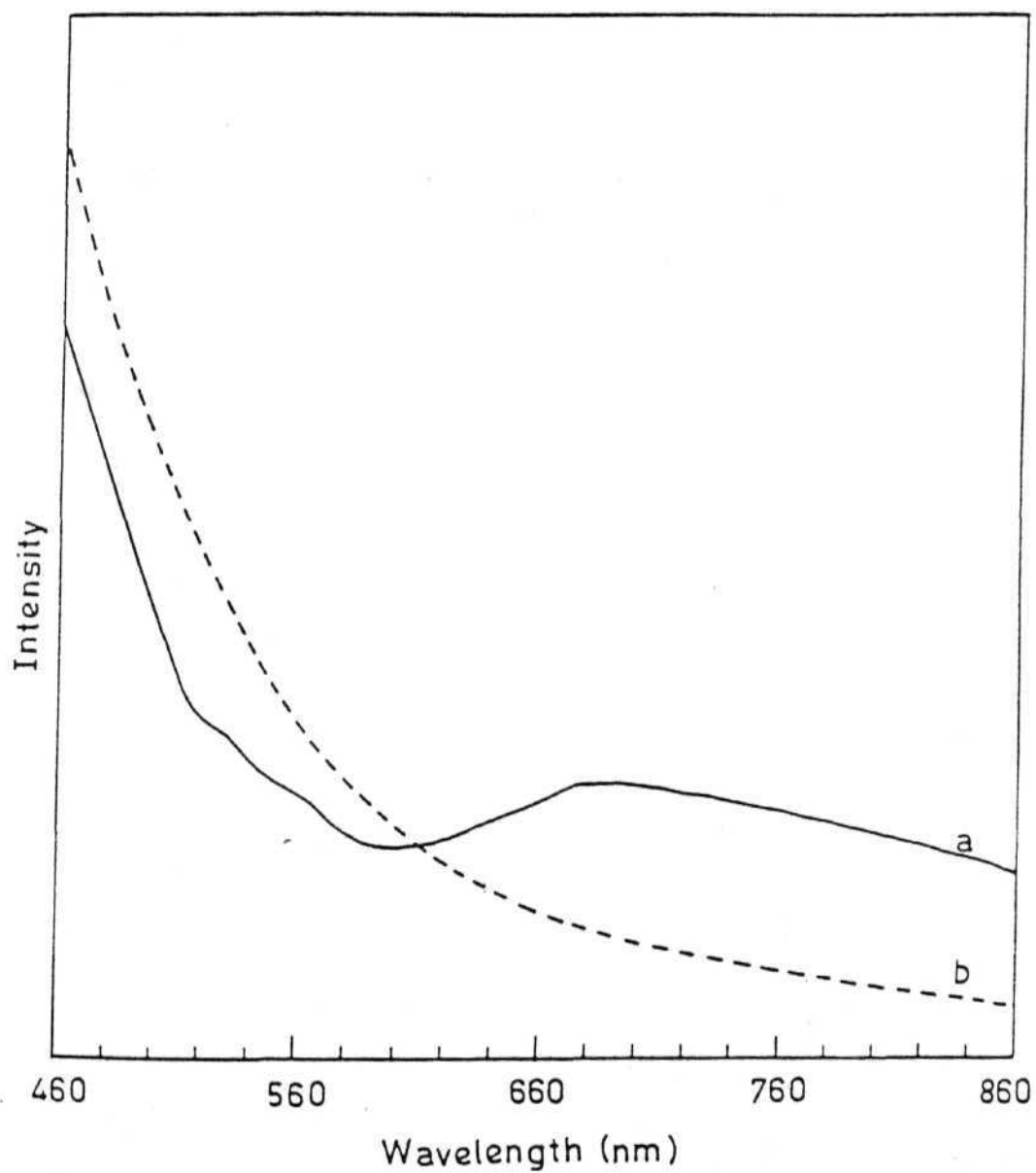


Figure 22: Electronic spectra of (a) $(\text{Mn}_2\text{O}_2 5,5\text{-dmbp}_4)(\text{PF}_6)_3$ in CH_3CN and (b) $(\text{Mn}_2\text{O}_2 5,5\text{-dmbp}_3\text{dmf}_2)(\text{PF}_6)_3$ in dmf.

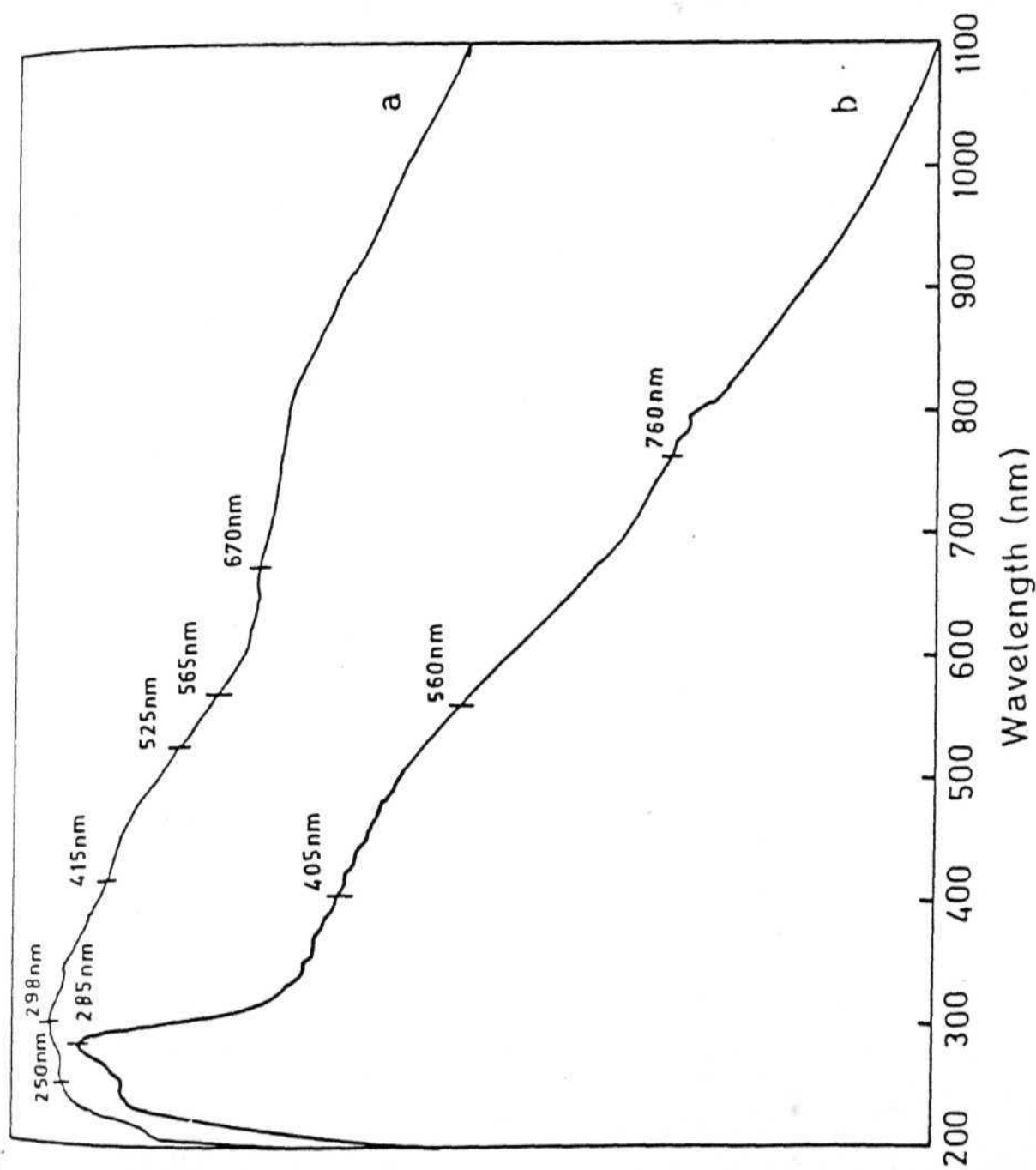


Figure 23: P.a.s spectra of (a) $(\text{Mn}_2\text{O}_{24,4}\text{-dmbp}_4)(\text{PF}_6)_3$ and (b) $(\text{Mn}_2\text{O}_{24,4'}\text{-dmbp}_3\text{dmf}_2)(\text{PF}_6)_3$.

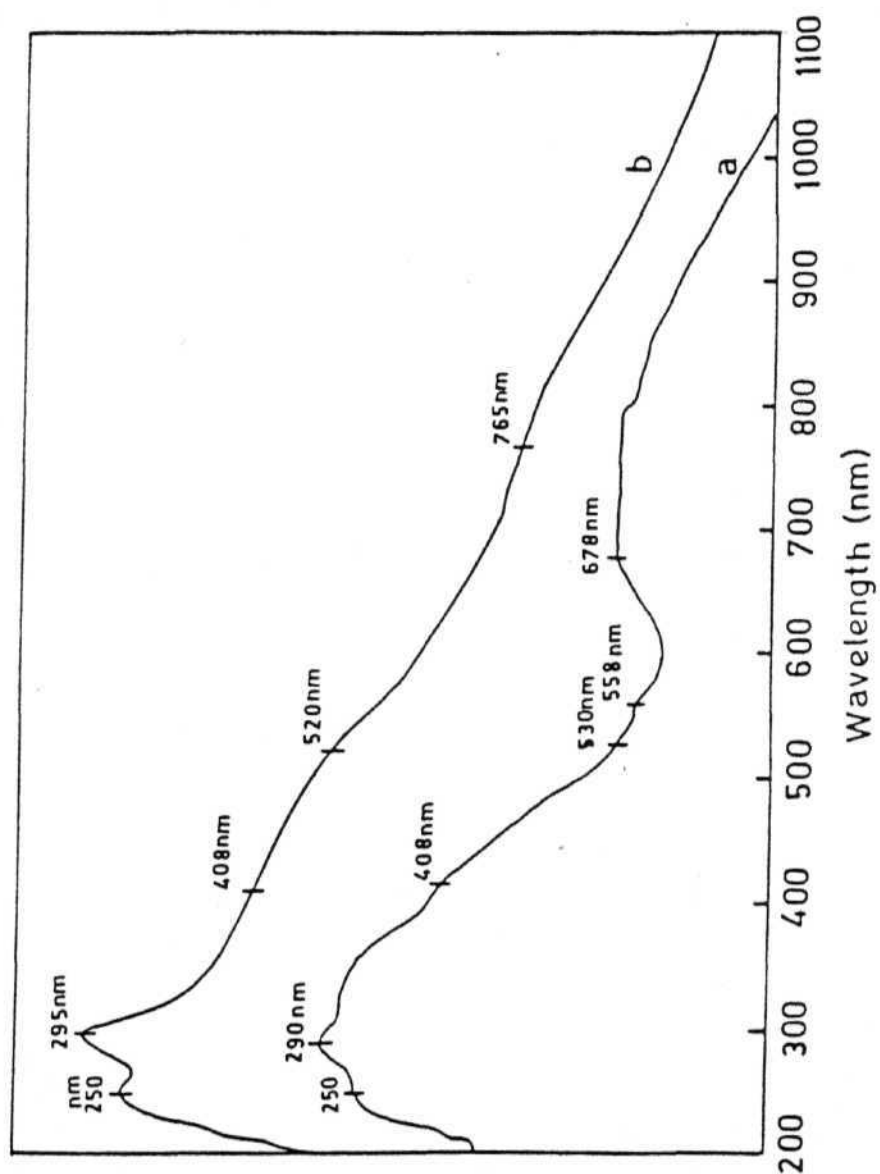


Figure 24: P.a.s spectra of (a) $(\text{Mn}_2\text{O}_2 \cdot 5,5'\text{-dmbp}_4)(\text{PF}_6)_3$ and (b) $(\text{Mn}_2\text{O}_2 \cdot 5,5'\text{-dmbp}_3\text{dmf}_2)(\text{PF}_6)_3$.

E.s.r spectra of the manganese complexes:

Theoretical Interpretation of E.s.r spectra:-

A binuclear complex may be considered as a total molecular complex consisting of two smaller units which are weakly interacting. To describe the magnetic behaviour of this whole molecular complex, a spin Hamiltonian is formulated for each unit and the spin-spin interaction terms are added. E.s.r presents a convenient probe to derive data for the ground and the first excited spin states. The interaction between the spins alters the single-spin values of g and hyperfine coupling constant A .

For an antiferromagnetic binuclear system with unpaired electrons the total spin Hamiltonian may be expressed as a function of the single ion Hamiltonians, \mathcal{H}_1 and \mathcal{H}_2 and the Heisenberg Hamiltonian \mathcal{H}_{12} as $\mathcal{H} = \mathcal{H}_1 + \mathcal{H}_2 + \mathcal{H}_{12}$ assuming the orbital angular momentum to be completely quenched. The isotropic Heisenberg Hamiltonian $\mathcal{H}_{12} = -2JS_1 \cdot S_2$ describes the spin-spin coupling and it is the largest term in the combined spin Hamiltonian. In the presence of large antiferromagnetic coupling (large negative J), $\text{Mn}^{(\text{III})}(S_1=2) - \text{Mn}^{(\text{IV})}(S_2=3/2)$ system will have a doublet ground state well removed from the other states (figure 25). The following treatment is strictly valid only when the magnitude of the exchange parameter, J is much greater than the zero-field splitting parameter, D . This condition is satisfied for the $\text{Mn}(\text{III}, \text{IV})$ complexes which have $|J| \gtrsim 100 \text{ cm}^{-1}$ ⁷⁸.

The spin-Hamiltonian for any state, S can be written in the coupled and uncoupled regimes as follows:

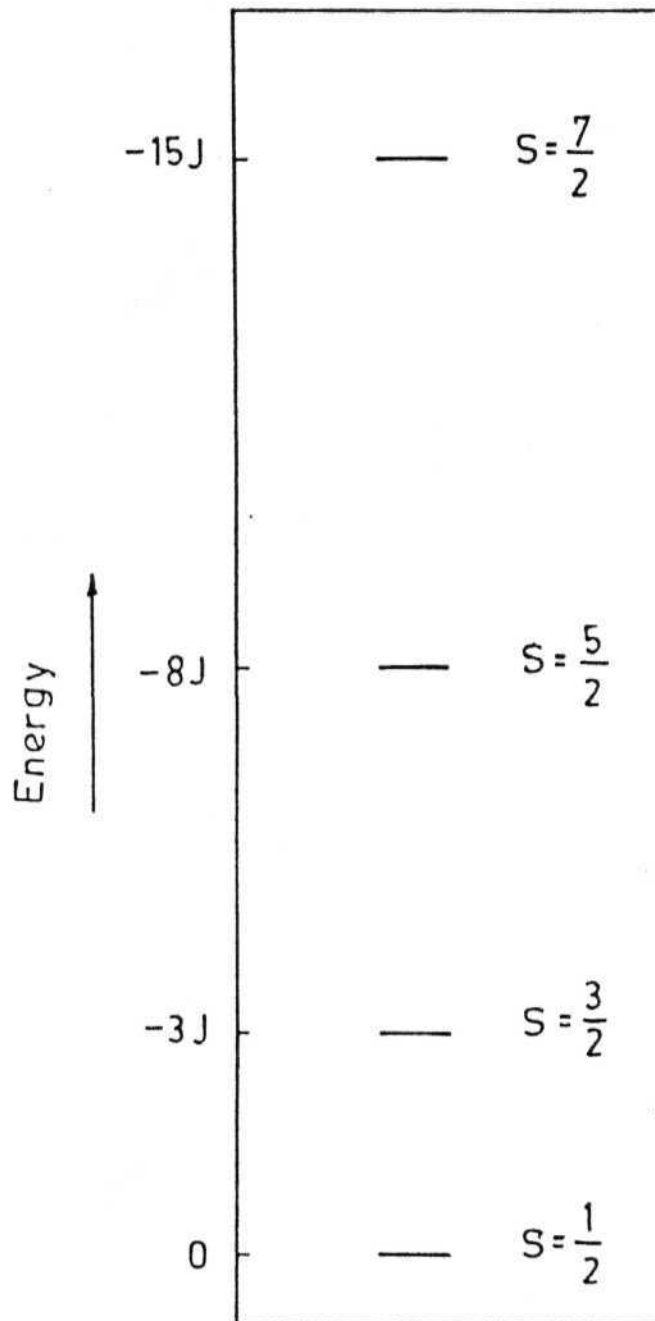


Figure 25: Energy level diagram showing the coupled spin states, $S=S_1+S_2$, for $S_1=2$, $S_2=3/2$.

$$\mathcal{H}_{\text{coupled}} = H \cdot \underline{g} \cdot S + S \cdot \underline{A}_1 \cdot I_1 + S \cdot \underline{A}_2 \cdot I_2, \quad \dots 24.$$

$$\mathcal{H}_{\text{uncoupled}} = H \cdot \underline{g}_1 \cdot S + H \cdot \underline{g}_2 \cdot S + S \cdot \underline{A}_1' \cdot I_1 + S \cdot \underline{A}_2' \cdot I_2 \quad \dots 25.$$

The coupled tensors \underline{g} , \underline{A}_1 and \underline{A}_2 can be related to those of the non-interacting ions via projection of S_1 and S_2 on S , and can be written as,

$$\underline{g} = \alpha \underline{g}_1 + \beta \underline{g}_2 \quad \dots 26.$$

$$\underline{A}_1 = \alpha \underline{A}_1' \quad \dots 27.$$

$$\underline{A}_2 = \beta \underline{A}_2' \quad \dots 28.$$

where

$$\alpha = \frac{S(S+1) + S_1(S_1+1) - S_2(S_2+1)}{2S(S+1)}$$

and

$$\beta = \frac{S(S+1) + S_2(S_2+1) - S_1(S_1+1)}{2S(S+1)}$$

The quantities, α and β for the various spin-states are as follows:-

S	α	β
1/2	2	-1
3/2	4/5	1/5
5/2	22/35	13/35
7/2	4/7	3/7

A treatment analogous to this has been employed by Gibson et al⁷⁹ for the analysis of the spinach ferredoxin system involving exchange coupled iron ions with bridging sulfur ligands.

$\text{Fe}^{3+}(\text{d}^5, S=5/2)$ -sulfur ligands- $\text{Fe}^{2+}(\text{d}^6, S=2)$ with $S = 1/2$.

Whenever the condition $|J| \gg |D|$ is not satisfied, S is no more a good quantum number and the above equations will have to be modified.

A treatment including zero-field parameter has been given by Euler⁸¹ for the cases $S_2 = \frac{1}{2}$ and $S_1 = 1, 3/2, 2$ and $5/2$.

The other less important terms in the Hamiltonian concern quadrupole interaction and nuclear Zeeman interaction. Quadrupole interaction results in shift in the energies of the different energy levels relative to one another. The nuclear Zeeman term represents the direct interaction between the external magnetic field and the nuclear magnetic moment. It cancels for transitions between states with identical values of m_I . It is considered when forbidden transitions are observed.

The g and A values for the Mn(III) and Mn(IV) ions in some crystals and complexes are collected in Table IX.

3.2 g and A values for mononuclear Mn^{3+} and Mn^{4+} complexes⁸³:-

$Mn^{3+}(d^4)$: In a distorted octahedral environment, the orbital singlet ground state (figure 8) will be coupled to the components of the excited T_2 state via spin-orbit interaction. To first order, the g -values can be written as

$$g_{||} = g_e - 8\lambda/\Delta \quad \dots 29.$$

$$g_{\perp} = g_e - 2\lambda/\Delta \quad \dots 30.$$

Where $g_e = 2.0023$ is the free-spin value, λ is the one-electron spin-orbit coupling constant for Mn^{3+} and Δ is the energy of the excited state (with splitting neglected) with respect to the ground orbital singlet state. The free electron value for $\lambda = 360 \text{ cm}^{-1}$ and the g -values are predicted to be less than 2.00.

The hyperfine tensor is expected to contain appreciable dipolar contribution. However, data on Mn^{3+} ion is scarce. In TiO_2 (Table IX) the

Table IX The g and A values for Mn(III) and Mn(IV) ions in some crystals and complexes

Ion	g_x		g_y		g_z		A_x		A_y		A_z		Ref
	(g_{\perp})	(g_{\parallel})	(g_{\perp})	(g_{\parallel})	(g_{\perp})	(g_{\parallel})	$(\times 10^{-4} \text{ cm}^{-1})$	(A_{\parallel})	$(\times 10^{-4} \text{ cm}^{-1})$	(A_{\perp})	$(\times 10^{-4} \text{ cm}^{-1})$	(A_{\parallel})	
Mn ³⁺ in TiO ₂	1.99	2.00			2.00		84.5		52.8		80.3		82
Mn ⁴⁺ in TiO ₂					1.99						71.5		82
Mn ⁴⁺ in SrTiO ₃					1.99						69.8		82
Mn ⁴⁺ in MgO					1.99						70.8		83
Mn ⁴⁺ in Al ₂ O ₃					1.99			70.4			69.6		83
Mn ³⁺ (cat) ₃ ²⁻	3.60	2.00											84
Mn ⁴⁺ (sub.heteropoly- molybdates and tungstates)	4.00	2.00											85
Mn ⁴⁺ TPP(OCH ₃) ₂	~5.43	2.40	1.60 (w)								~72G		86
Mn ⁴⁺ TPP(NCO) ₂	3.92	2.01									~69G		86
(Mn ³⁺ TPP Cl)ClO ₄	4.00	2.00											86

principal values range from 0.0053 to 0.0085 cm^{-1} .

$\text{Mn}^{4+}(\text{d}^3)$: The ground orbital singlet state (figure 9) is coupled, by spin-orbit interaction to the components of the excited T_2 , but not T_1 . In this case the g-values can be written as

$$g_{||} = g_e - 8\lambda/\Delta_0 \quad \dots 31.$$

$$g_{\perp} = g_e - 8\lambda/\Delta_1 \quad \dots 32.$$

where Δ_0 and Δ_1 are the energies of the components of T_2 , 4B_2 and 4E , respectively, in tetragonal symmetry. The spin orbit coupling constant is expected to be slightly larger in this case ($\sim 390 \text{ cm}^{-1}$) and g-values are predicted to be less than 2.00 as in the case of Mn^{3+} .

For the d^3 ion the hyperfine splitting is almost entirely due to core-polarisation which produces a field of $\sim -192 \text{ kG}$ at the nucleus with a small orbital contribution of -4 to -6 kG . The A tensor is, therefore, expected to be almost isotropic. The parameters in Al_2O_3 are $0.0069 \text{ cm}^{-1}(A_{||})$ and $0.00704 \text{ cm}^{-1}(A_{\perp})$ (Table IX).

3. 3. 3

Number of hyperfine splittings in manganese (III, IV) complexes:-
Hyperfine coupling with the two ${}^{55}\text{Mn}$ nuclei ($I=5/2$) will in general give a multiline e.s.r spectrum. The number of lines expected depends on the extent of delocalisation of the odd electron and the different cases are considered below:

(a) Complete delocalisation (Class III): When the electron has equal probability of being found near the two nuclei, i.e., $\psi_{\text{HOMO}} = \frac{1}{\sqrt{2}}(\phi_{\text{Mn1}} + \phi_{\text{Mn2}})$, equal hyperfine coupling with the two nuclei results in a set of 11 lines with intensity ratio 1:2:3:4:5:6:5:4:3:2:1. The

coupling pattern is not expected to be temperature dependent.

(b) Localised (Class II): Maximum of $6 \times 6 = 36$ lines are expected due to coupling with the two nuclei. For the ground doublet state the individual couplings A_1 and A_2 are related to the hyperfine splittings of the isolated Mn^{3+} and Mn^{4+} ions as discussed in sub-section 3.3.1. We have,

$$A_1 = 2A_1'$$

$$A_2 = -A_2'$$

Since $A_1' \sim A_2'$, we have the special case $A_1 = 2A_2$ which give rise to a 16 line pattern with intensity ratio 1:1:2:2:3:3:3:3:3:3:2:2:1:1. This is the usual spectrum observed for many Mn(III, IV) complexes at low temperatures for frozen samples.

(c) Localised (Class II) with fast exchange (hopping) of the electron between the two centres: Here again 11 lines are expected as in (a), and the spacing between them can be related to the hyperfine splitting A_1' and A_2' of the individual ions, Mn^{3+} and Mn^{4+} .

$$A = (A_1 + A_2)/2 = (2A_1' - A_2')/2 \quad \dots 33.$$

The spectrum is expected to be temperature dependent because the electron exchange rate is temperature dependent. Averaging to give 11 lines will result when the rate of exchange is much faster than $|A_1| - |A_2|$, when A_1 and A_2 are expressed in Hz. With rates close to the critical rate, broadening of the individual lines will be observed and much below the critical rate the spectrum will be same as that expected for the case (b) above.

E.s.r spectra of powder Mn(III, IV) complexes:-

E.s.r spectra of the polycrystalline samples are shown in figures 26-37. The PF_6^- salts of bpy and phen complexes show some resolution of the hyperfine structure (figures 27, 30) while most of the ClO_4^- and BF_4^- salts (figures 26, 28, 29, 32, 34) show only a broad line. This implies that in the former salts the larger PF_6^- ion acts as a diamagnetic diluent and reduces the dipolar broadening. However, the PF_6^- salt of the dmf substituted complex (figure 33) does not show any resolution. The ClO_4^- salt of $(\text{Mn}_2\text{O}_2\text{bpy}_3\text{phen})^{3+}$ (figure 35) does give partial resolution while the $(\text{Mn}_2\text{O}_2\text{phen}_3\text{bpy})(\text{ClO}_4)_3$ (figure 36) gives only a single broad line. Many of the powder sample spectra show weak absorption in the low field region as well, which from their reduction in intensity at lower temperatures can be assigned to thermally populated quartet excited state.

There are several mechanisms which contribute to line broadening⁸³ in the solid samples, viz., (i) dipolar interaction, (ii) magnetic exchange between the different molecules in the lattice (iii) thermal population of excited states and (iv) electron exchange between the two centres. Of these (i) and (ii) are intermolecular processes which are present in magnetically concentrated systems while (iii) and (iv) are intramolecular processes peculiar to the mixed valent Mn(III, IV) systems. While dipolar interaction is expected to broaden all the hyperfine lines resulting in a broad envelope, intermolecular exchange coupling, in the fast limit, is expected to give a single narrow line. Population of thermally accessible excited states will increase the number of transitions and may eventually contribute to broadening. Intramolecular

electron transfer as discussed in sub-section 3.3.3 will lead to line broadening and in the fast limit will give a set of 11 hyperfine split lines. Since the two hyperfine couplings are opposite in sign (sub-section 3.3.3, assuming same sign for A_1' and A_2'), the broadening is supposed to set in on the outer lines and thereby reduce the spread of the spectrum in the fast limit.

The following compounds give exchange narrowed lines (Table X): $(\text{Mn}_2\text{O}_2\text{phen}_3\text{dmf}_2)(\text{PF}_6)_3$ (figure 33), $(\text{Mn}_2\text{O}_2\text{phen}_3\text{dmf}_2)(\text{ClO}_4)_3$ (figure 32), $(\text{Mn}_2\text{O}_2\text{phen}_4)(\text{BF}_4)_3$ (figure 29), $(\text{Mn}_2\text{O}_2\text{phen}_4)(\text{ClO}_4)_3$ (figure 28), $(\text{Mn}_2\text{O}_2\text{bpy}_4)(\text{ClO}_4)_3$ (figure 26) and $(\text{Mn}_2\text{O}_2\text{phen}_3\text{bpy})(\text{ClO}_4)_3$ (figure 36). The two pyridine substituted complexes, $(\text{Mn}_2\text{O}_2\text{phen}_3\text{py}_2)(\text{ClO}_4)_3$ and $(\text{Mn}_2\text{O}_2\text{bpy}_3\text{py}_2)(\text{ClO}_4)_3$ (figure 34) have line widths of 1300G which is more than the hyperfine spread expected for these complexes based on frozen solution data (sub-section 3.5). Therefore, these cases correspond to dipolar broadening.

The PF_6^- salts, $(\text{Mn}_2\text{O}_2\text{phen}_4)(\text{PF}_6)_3$ (figure 30), $(\text{Mn}_2\text{O}_2\text{bpy}_4)(\text{PF}_6)_3$ (figure 27), $(\text{Mn}_2\text{O}_25,5\text{-dmbp}_4)(\text{PF}_6)_3$ (figure 37), $(\text{Mn}_2\text{O}_24,4\text{-dmbp}_4)(\text{PF}_6)_3$ (figure 37) as well as the ClO_4^- salt $(\text{Mn}_2\text{O}_2\text{bpy}_3\text{phen})(\text{ClO}_4)_3$ (figure 35) show resolution of the hyperfine splitting to varying extents. We have attempted to simulate the spectrum of $(\text{Mn}_2\text{O}_2\text{phen}_4)(\text{PF}_6)_3$ (figure 31) using the following parameters $g_{||} = 2.07$, $g_{\perp} = 1.99$, $A_{||1} = A_{\perp1} = 0.00145 \text{ cm}^{-1}$, $A_{||2} = A_{\perp2} = 0.0073 \text{ cm}^{-1}$ and with an isotropic linewidth of 65G. Qualitative features are well represented by computer simulation. A good fit is not expected here because dipolar effects are not included in the simulation. The calculated spectrum for a width of 50G is included for comparison and it shows

Table X E.s.r spectra of powder samples of manganese (III, IV) complexes

Complex	RT (g)	L T (g)	Peak to Peak width (G)	A_1 ($\times 10^{-4} \text{ cm}^{-1}$)	A_2 ($\times 10^{-4} \text{ cm}^{-1}$)
$(\text{Mn}_2\text{O}_2\text{bpy}_4)(\text{ClO}_4)_3$	4.1	5.3	750		
	2.06	2.99			
	1.98	2.01			
	1.5	1.4			
$(\text{Mn}_2\text{O}_2\text{bpy}_4)(\text{PF}_6)_3$	4.5	4.6			~ 170
	2.00	2.00			
$(\text{Mn}_2\text{O}_2\text{bpy}_3\text{py}_2)(\text{ClO}_4)_3$		2.16	1300		
$(\text{Mn}_2\text{O}_2\text{bpy}_3\text{phen})(\text{ClO}_4)_3$	4.4	2.00 (g_{\parallel})			81
	1.95	1.97 (g_{\perp})		154	
$(\text{Mn}_2\text{O}_2\text{phen}_4)(\text{ClO}_4)_3$	5.48	5.26	750		
	2.02	2.65			
		2.02			
		1.3			
$(\text{Mn}_2\text{O}_2\text{phen}_4)(\text{BF}_4)_3$	4.4		500		
	1.96				
$(\text{Mn}_2\text{O}_2\text{phen}_4)(\text{PF}_6)_3$	2.01	2.07 (g_{\parallel})			72.5
		1.99 (g_{\perp})		145	
$(\text{Mn}_2\text{O}_2\text{phen}_3\text{dmf}_2)(\text{PF}_6)_3$	4.3	4.8	300		
	1.99	3.0			
		1.99			

Contd...

Complex	RT (g)	LT (g)	Peak to Peak width (G)	A_1 ($\times 10^{-4} \text{ cm}^{-1}$)	A_2 ($\times 10^{-4} \text{ cm}^{-1}$)
$(\text{Mn}_2\text{O}_2\text{phen}_3\text{dmf}_2)(\text{ClO}_4)_3$	5.0	4.9	750		
	1.98	3.0			
		1.98			
$(\text{Mn}_2\text{O}_2\text{phen}_3\text{py}_2)(\text{ClO}_4)_3$		5.3	1300		
		3.5			
		2.11			
$(\text{Mn}_2\text{O}_2\text{phen}_3\text{bpy})(\text{ClO}_4)_3$	5.8	4.6	750		
	3.8	2.8			
	2.7	2.03			
	2.00	1.5			
	1.3				

RT = room temperature

LT = low temperature. These temperatures are given in λ_{th} respective figures.

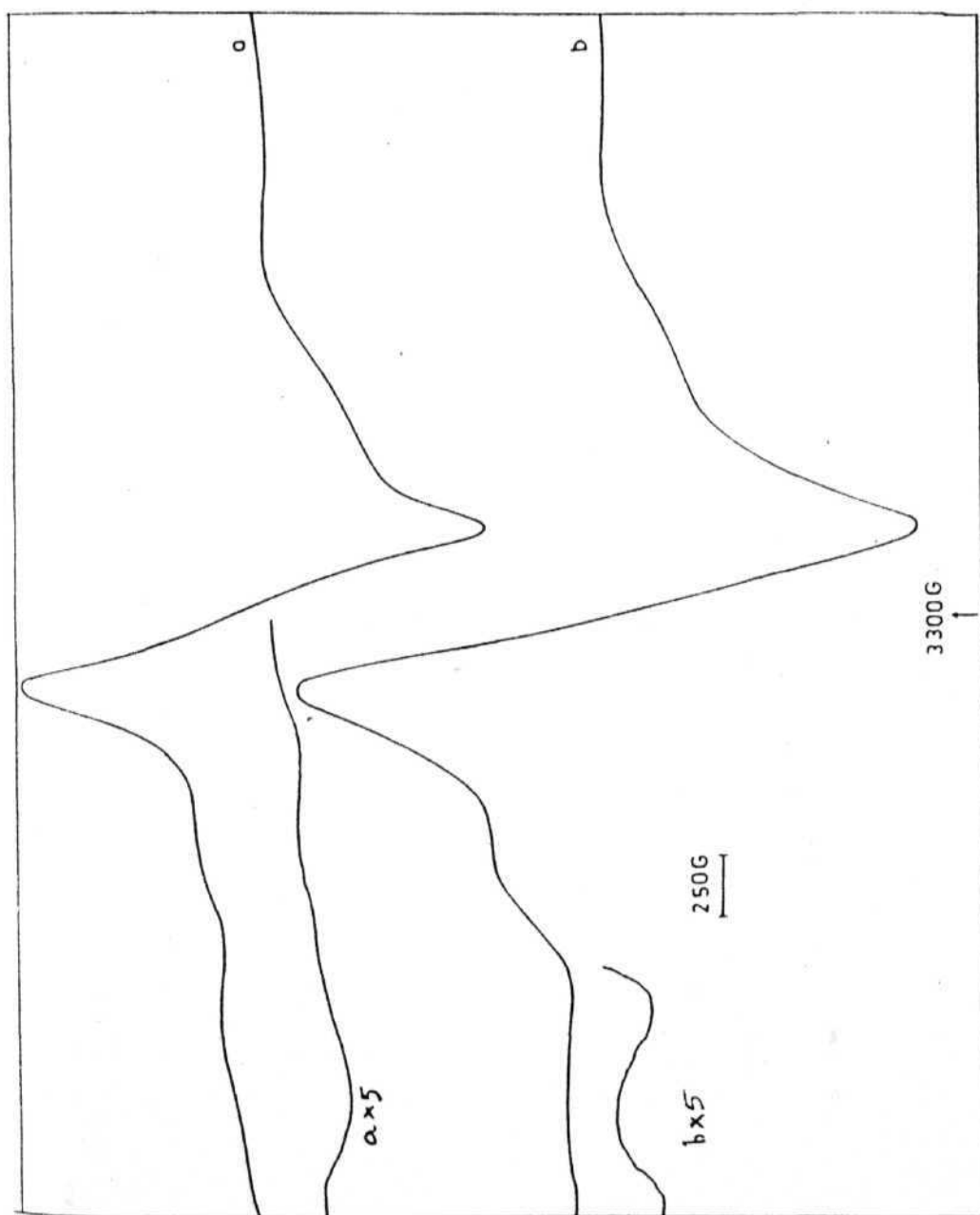


Figure 26: E.s.r spectra of powder $(\text{Mn}_2\text{O}_2\text{bpy}_4)(\text{ClO}_4)_3$ sample at (a) 300K and (b) 143K.

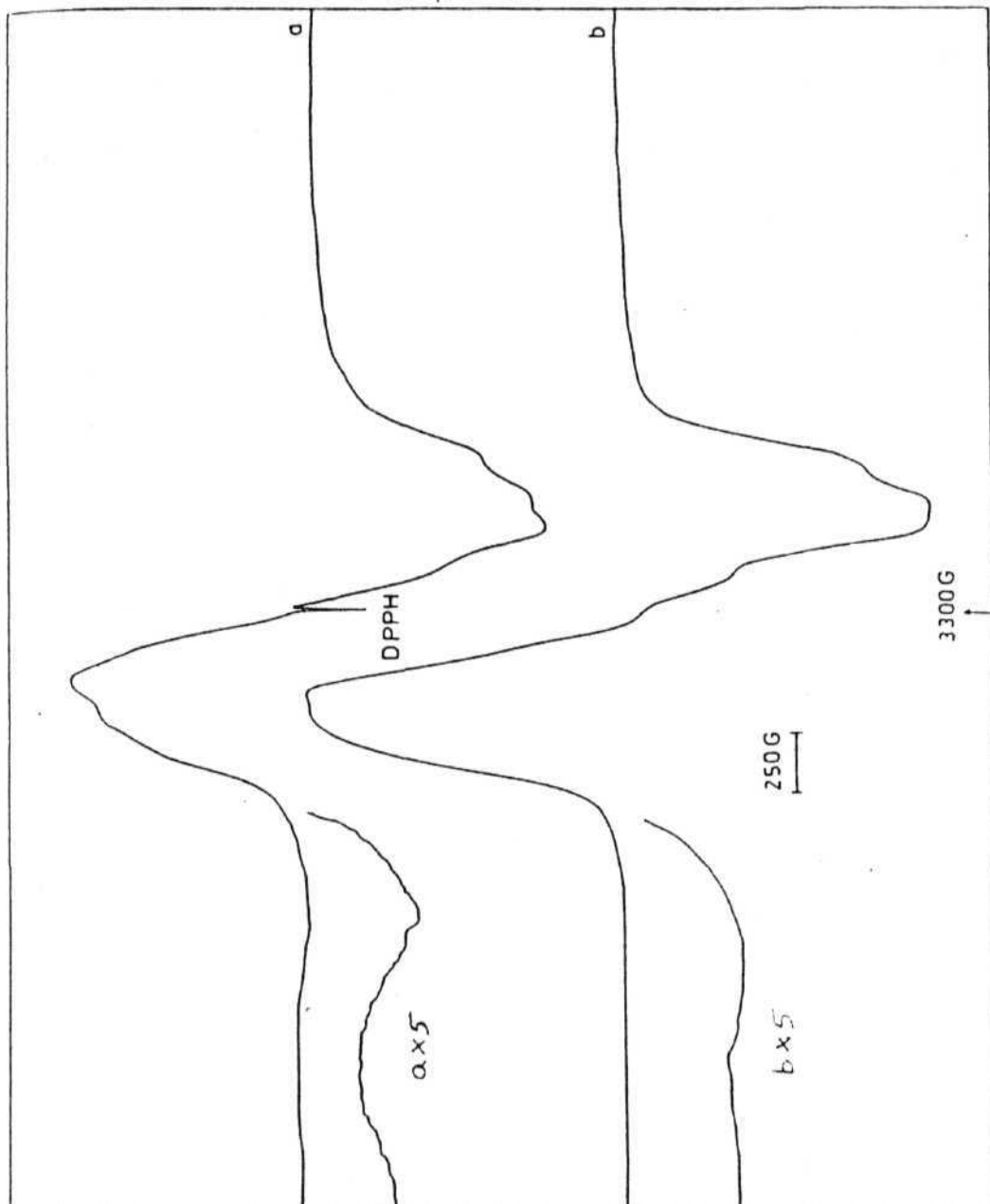


Figure 27: E.s.r spectra of powder $(\text{Mn}_2\text{O}_2\text{bpy}_4)(\text{PF}_6)_3$ sample at (a) 300K and (b) 121K.

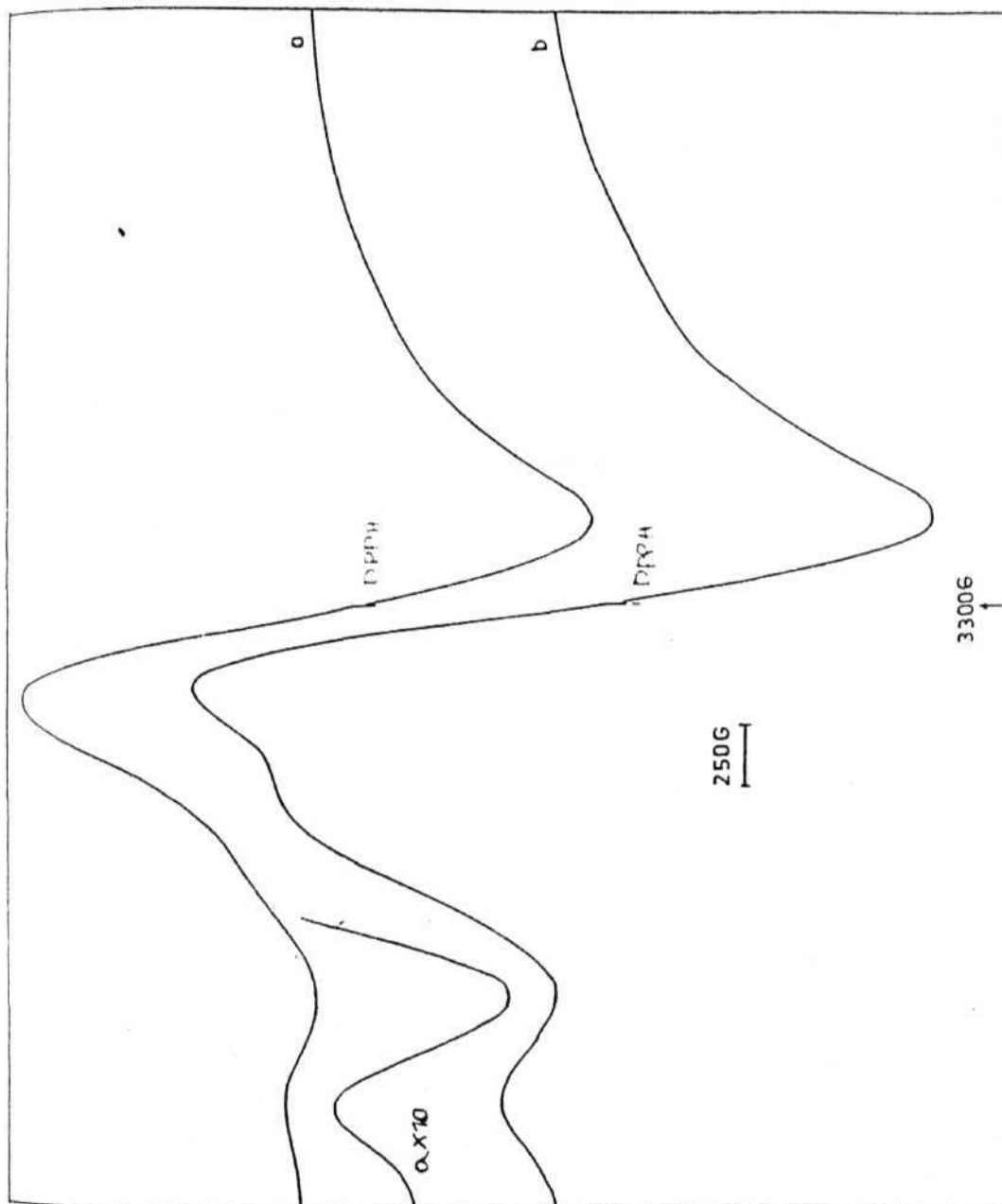


Figure 28: E.s.r spectra of powder $(\text{Mn}_2\text{O}_2\text{phen})_4(\text{ClO}_4)_3$ sample at (a) 300K and (b) 133K.

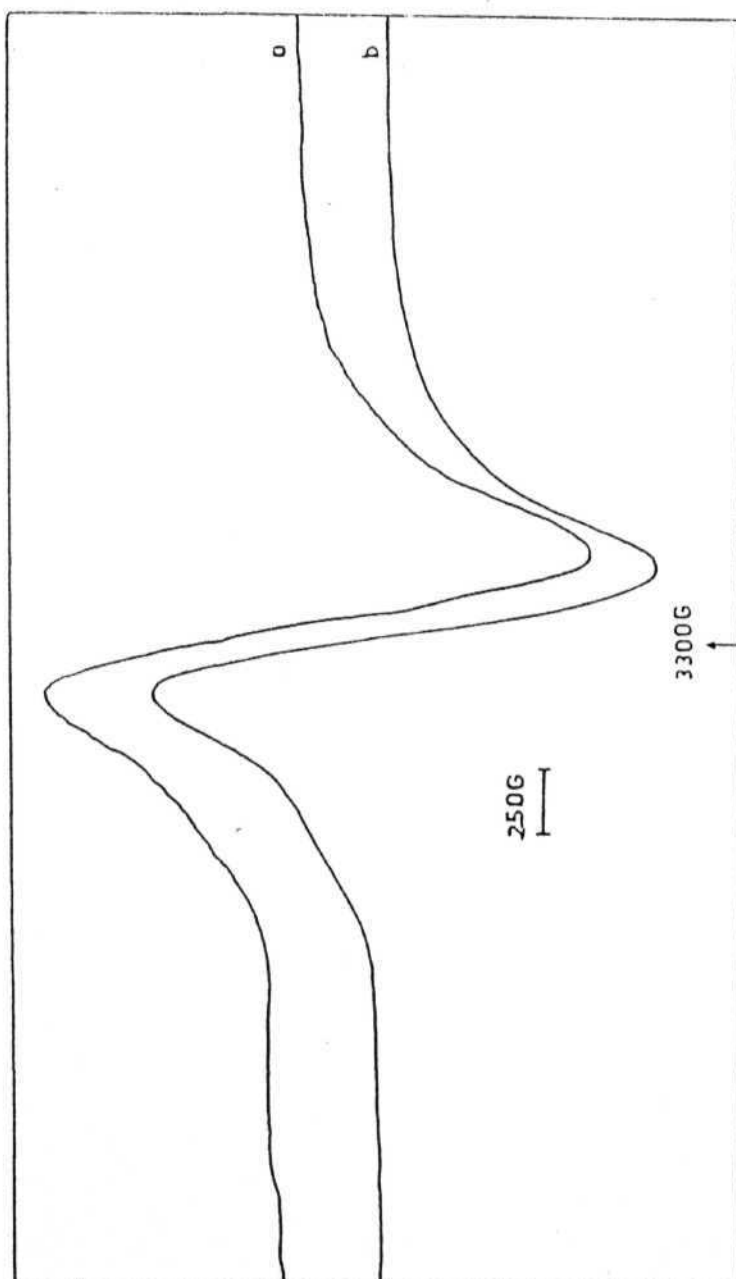


Figure 29: E.s.r spectra of powder (a) $(\text{Mn}_2\text{O}_2\text{phen}_4)(\text{BF}_4)_3$ sample at 300K and (b) $(\text{Mn}_2\text{O}_2\text{phen}_3\text{dmf}_2)(\text{BF}_4)_3$ at 300K.

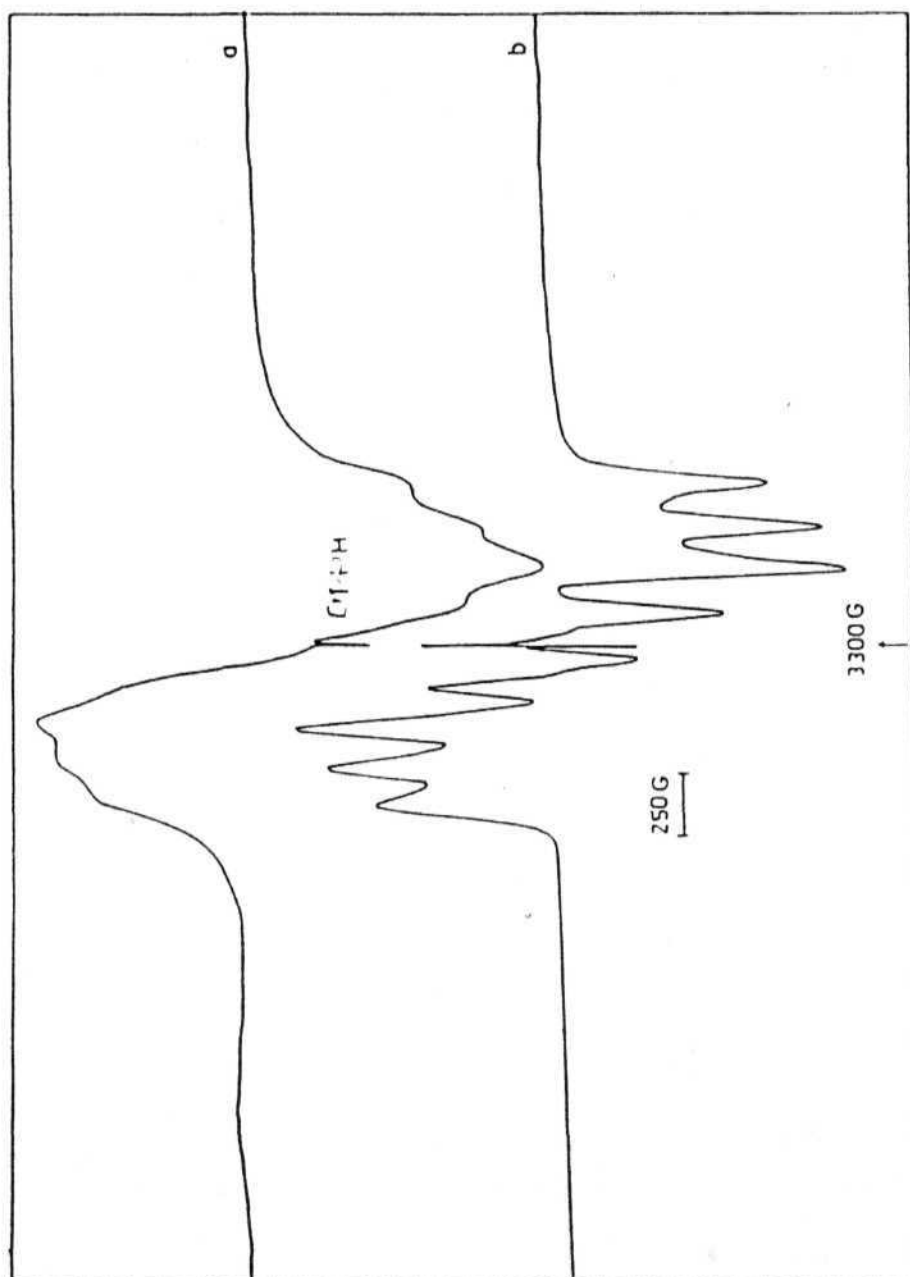


Figure 30: E.s.r spectra of powder $(\text{Mn}_2\text{O}_2\text{phen}_4)(\text{PF}_6)_3$ sample at
 (a) 300K and (b) 128K.

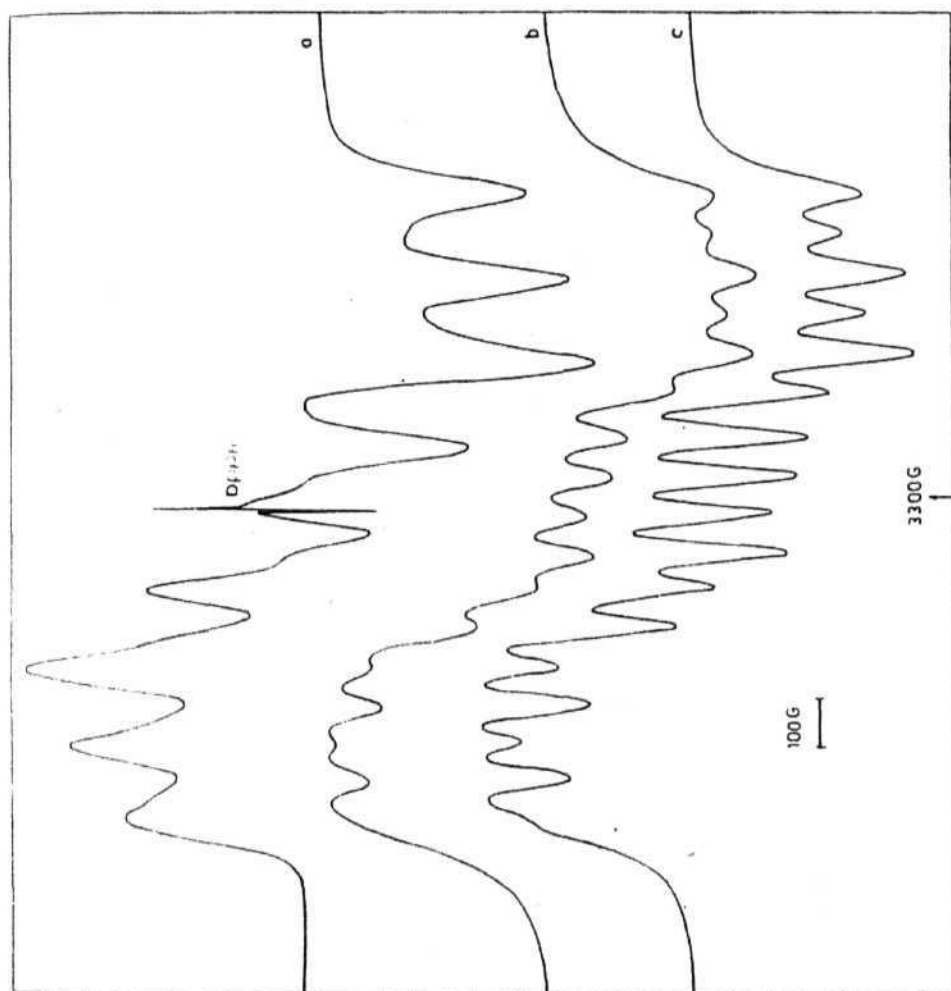


Figure 31: E.s.r spectra of powder (a) $(\text{Mn}_2\text{O}_2\text{phen}_4)(\text{PF}_6)_3$ sample at 117K (b) computer simulation with 65G line-width and (c) simulated spectrum with 50G line-width for comparison.

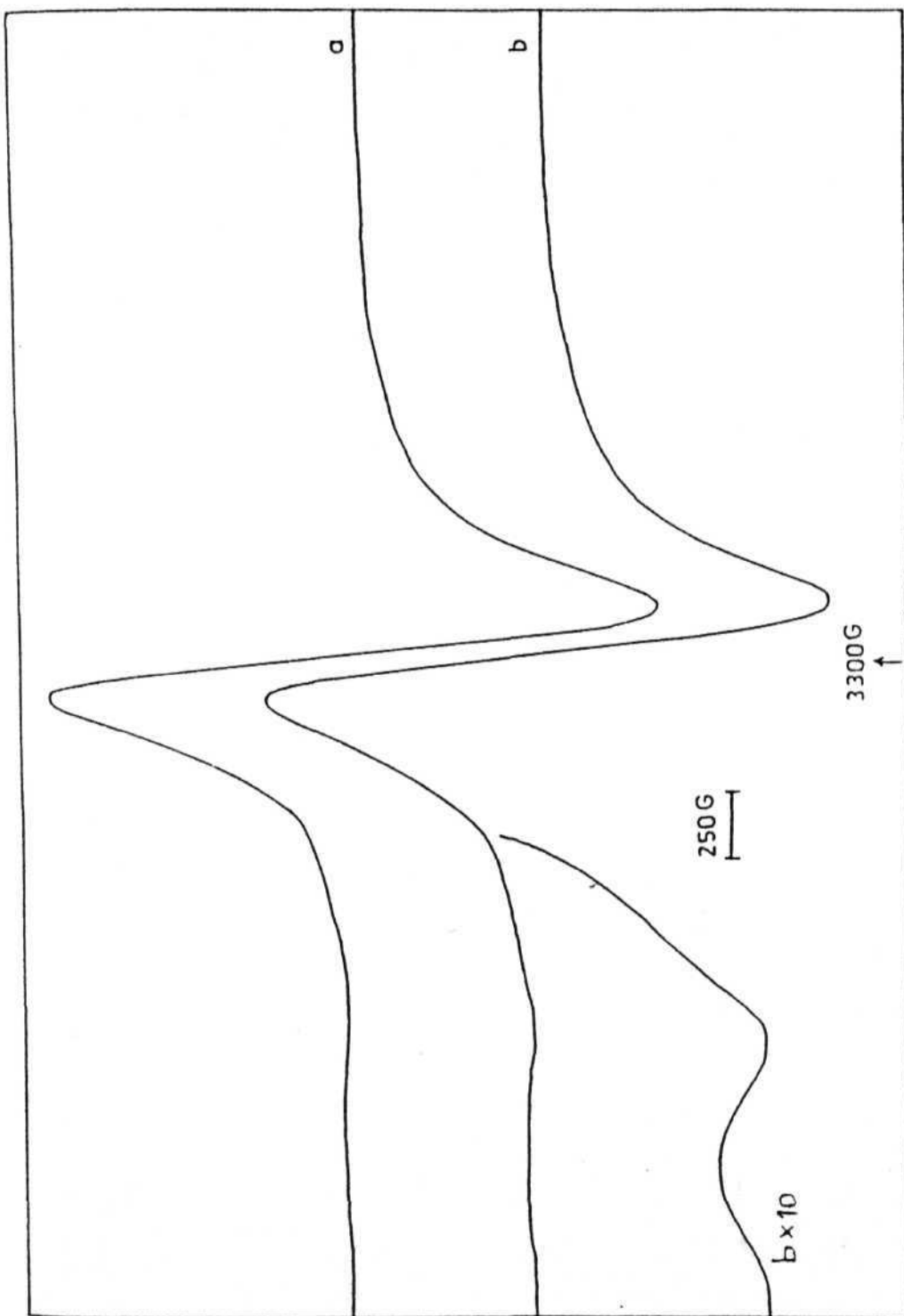


Figure 32: E.s.r spectra of powder $(\text{Mn}_2\text{O}_2\text{phen}_3\text{dmf}_2)(\text{ClO}_4)_3$ at (a) 300K, and (b) 139K.

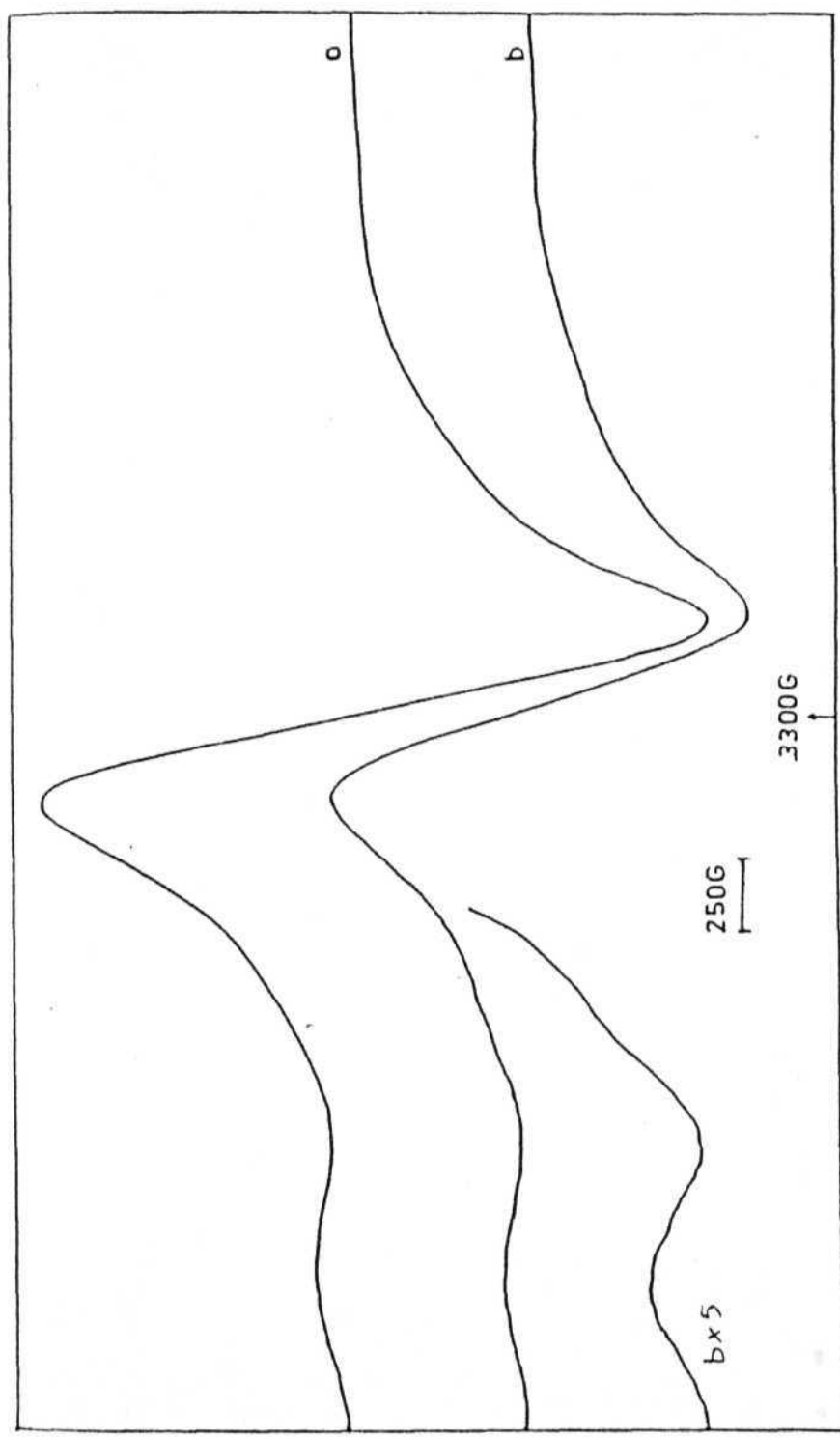


Figure 33: E.s.r spectra of powder $(\text{Mn}_2\text{O}_2\text{phen}_3\text{dmf}_2)(\text{PF}_6)_3$ at (a) 300K and (b) 121K.

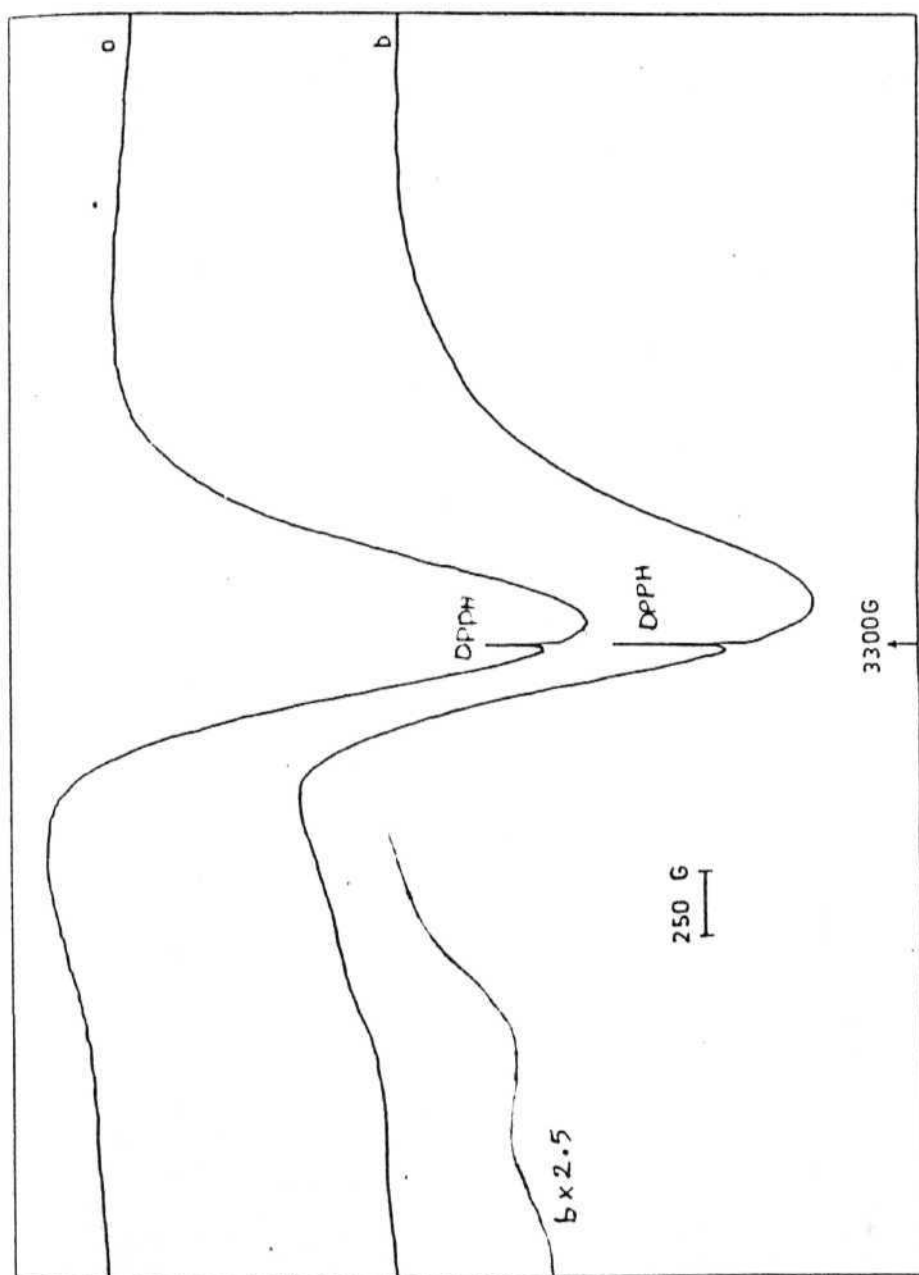


Figure 34: E.s.r spectra of powder (a) $(\text{Mn}_2\text{O}_2\text{bpy}_3\text{py}_2)(\text{ClO}_4)_3$ at 159K and (b) $(\text{Mn}_2\text{O}_2\text{phen}_3\text{py}_2)(\text{ClO}_4)_3$ at 159K.

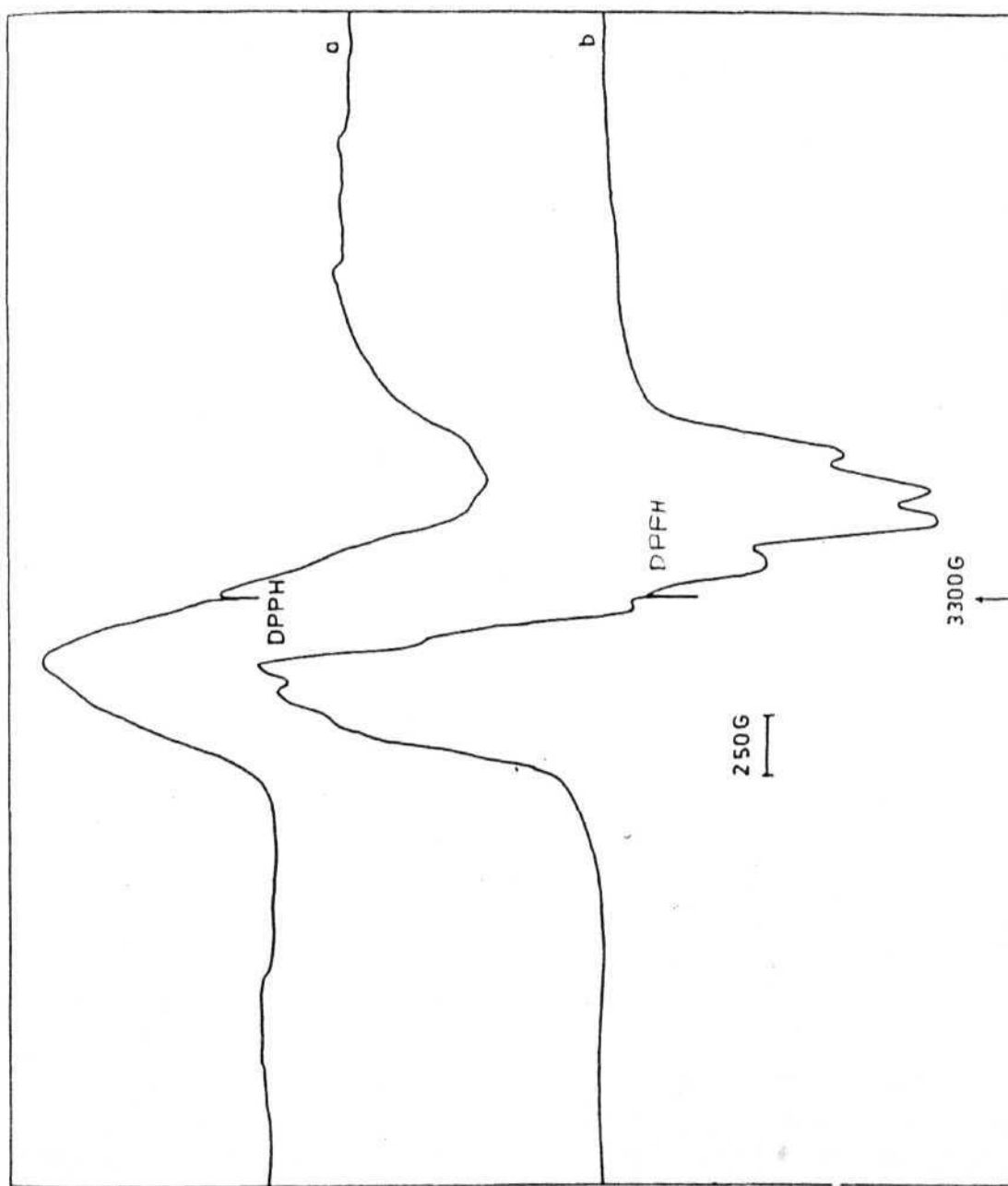


Figure 35: E.s.r. spectra of powder $(\text{Mn}_2\text{O}_2\text{bpy}_3\text{phen})(\text{ClO}_4)_3$ at (a) 300K and (b) 121K.

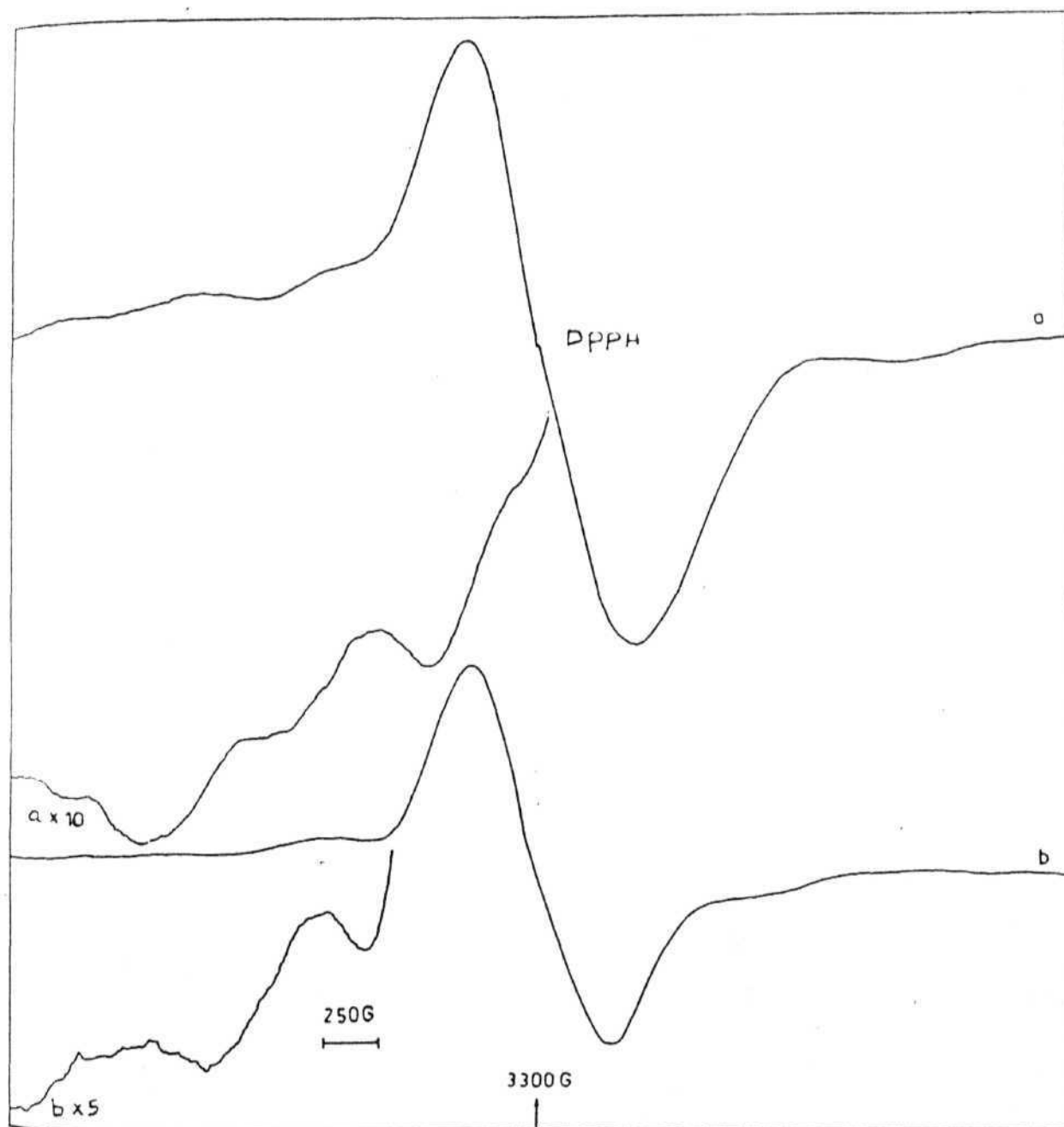


Figure 36: E.s.r spectra of powder $(\text{Mn}_2\text{O}_2\text{phen}_3\text{bpy})(\text{ClO}_4)_3$ at (a) 300K and (b) 131K.

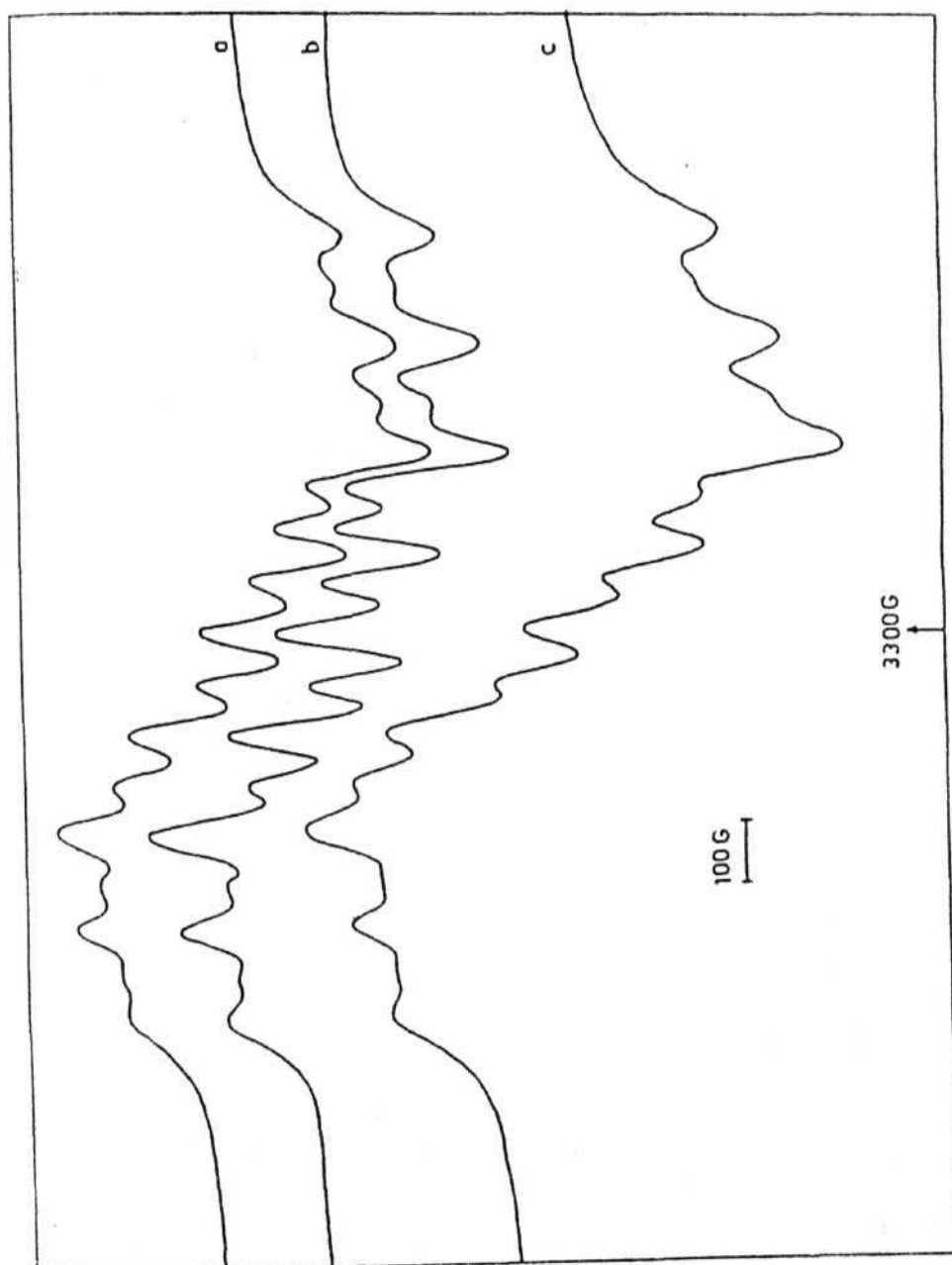


Figure 37: E.s.r spectra of powder (a) $(\text{Mn}_2\text{O}_24,4'\text{dmbp}_4)(\text{PF}_6)_3$ at 121K and $(\text{Mn}_2\text{O}_25,5'\text{dmbp}_4)(\text{PF}_6)_3$ at (b) 120K and (c) at 300K.

further splittings towards an eventual resolution of 16 lines. The complexes of 4,4'-dmbp (figure 37) and 5,5'-dmbp (figure 37) show slightly better resolution. The line narrowing observed upon cooling the samples is most likely due to reduction in the intensity of the signals from excited spin states. In no cases did we observe a narrowing effect with reduction in hyperfine spacing which could be attributed to fast electron transfer between the two manganese centres. Since the difference between $|A_1|$ and $|A_2|$ is 0.0070 cm^{-1} we conclude that the intramolecular electron transfer rate in the solid samples to be much less than $2 \times 10^8 \text{ Hz}$.

3.5

E.s.r spectra of frozen solutions:-

The frozen solution spectra of the Mn(III, IV) complexes in different solvents (CH_3CN , dmf, py) are shown in figure 38, 41, 42. We have attempted to simulate two typical spectra and best fit spectra using the program described in Chapter 2 are shown in figures 39, 40. Since $A_1 \sim 2A_2$, 16 lines are readily resolved in all cases, while in some cases, mostly for dmf solution further splittings are resolved. The g and A values are tabulated in Table XI.

Most of the previous computer simulations of Mn(III, IV) spectra^{9,59,61} were done assuming isotropic g and A values. Our spectra were fit to axial Hamiltonian (sub-section 3.3.1) and it is clear that significant anisotropy is present in these compounds. The fitting is not exact due to the constraints in the simulation procedure viz., isotropic line width, treatment of one of the ^{55}Mn hyperfine coupling (the smaller value, A_2) only to first order and also neglect of the small amount of Mn^{2+} impurity and also the small contribution from the quartet excited state.

Table XI g and A values from frozen solution e.s.r spectra of manganese (III, IV) complexes

Complex	Solvent	T (K)	g	g _⊥	A ₁ ($\times 10^{-4} \text{ cm}^{-1}$)	A ₂ ($\times 10^{-4} \text{ cm}^{-1}$)
(Mn ₂ O ₂ bpy ₄)(ClO ₄) ₃	CH ₃ CN	143	2.05	1.96	139	65
"	dmf	123	2.07	1.97	137	66
" (BF ₄) ₃	CH ₃ CN	127	2.06	1.96	137	65
"	dmf	118	2.06	1.96	135	65
" (PF ₆) ₃	CH ₃ CN	143	2.05	1.94	138	64
"	(Simulated)	143	2.090	1.970	137.0 (A)	131.0 68.5 (A _⊥) (A)
"	dmf	143	2.05	1.95	139	65 (A _⊥)
(Mn ₂ O ₂ bpy ₃ phen)(ClO ₄) ₃	CH ₃ CN	159	2.05	1.95	139	65
"	dmf	143	2.05	1.95	139	65
(Mn ₂ O ₂ phen ₄)(ClO ₄) ₃	CH ₃ CN	119	2.06	1.96	138	64
"	dmf	143	2.05	1.95	139	65
"	py	143	2.05	1.96	135	65

Contd.....

$(\text{Mn}_2\text{O}_2\text{phen}_4)(\text{BF}_4)_3$	dmf	124	2.06	1.96	135	68
" $(\text{PF}_6)_3$	CH_3CN	143	2.05	1.95	138	65
" "	dmf	115	2.06	1.96	135	65
" "	(Simulated)	115	2.098	1.980	137.8 (A)	64.7 (A _I)
$(\text{Mn}_2\text{O}_2\text{phen}_3\text{dmf}_2)(\text{ClO}_4)_3$	CH_3CN	126	2.06	1.96	130.0 (A _I)	64
" "	dmf	122	2.06	1.96	135	65
" $(\text{PF}_6)_3$	CH_3CN	128	2.05	1.96	137	64
" "	dmf	115	2.06	1.96	135	66
$(\text{Mn}_2\text{O}_2\text{phen}_3\text{py}_2)(\text{ClO}_4)_3$	CH_3CN	143	2.06	1.96	137	65
$(\text{Mn}_2\text{O}_2\text{phen}_3\text{bpy})(\text{ClO}_4)_3$	CH_3CN	143	2.05	1.95	138	65
" "	dmf	143	2.05	1.96	139	65
$(\text{Mn}_2\text{O}_24,4'\text{dmbp}_4)(\text{PF}_6)_3$	CH_3CN	125	2.06	1.96	139	65
$(\text{Mn}_2\text{O}_25,5'\text{dmbp}_4)(\text{PF}_6)_3$	CH_3CN	124	2.06	1.96	139	65
" "	dmf	106	2.06	1.96	138	64
$(\text{X}^{\text{IV}}\text{TPP})\text{-O-Mn}^{\text{III}}\text{TPP})^{\text{a}}$	CH_3CN		2.0		139	69
$[\text{Mn}_2\text{O}_2(\text{N}_4\text{-py})_2](\text{ClO}_4)_3\cdot\text{H}_2\text{O}^{\text{b}}$ (Simulated)	CH_3CN		2.002		151G	75G

a = Ref.53; b = Ref.59; G = Gauss.

The striking feature of the spectra of the various compounds and the data in Table XI is that the parameters are not very sensitive to the type of ligands around the two manganese ions. The parameters in solution and solid, whenever resolution was possible, are also very similar. As pointed out in sub section 3.3 the major contribution to hyperfine splitting arise from core-polarisation. Covalent delocalisation is expected to reduce the A values. Since t_{2g} electrons are not delocalised to any great extent the A values are not very sensitive to the type of ligands. The porphyrin complex in Table XI does show a reduced coupling constant which may be attributed to increased covalency⁵³. The g anisotropy is also very small in these compounds due to the small ($\lambda/\Delta \sim 360/18000 = 0.02$ for Mn^{3+} and $\sim 390/39000 = 0.013$ for Mn^{4+}) contribution from spin-orbit interaction. From the first order equations, g-shifts of nearly 0.1 are expected for $Mn^{3+}(g_1)$. The actual shift is found to be less than this value showing that first order interpretation using a single free-ion spin-orbit parameter is not sufficient to account for such small variation of g from free-spin value.

Finally it may be mentioned that recently Nishida⁸⁷ has reported a multiline spectrum very similar to that of Mn(III, IV) complex and attributed the same to a Mn(III, III) complex with very small antiferromagnetic coupling ($J \sim -0.88 \text{ cm}^{-1}$), without a detailed interpretation of the spectrum. We are at a loss to understand this result because exchange between identical spins ($S_1 = S_2 = 2$) should give rise to 11 line pattern with hyperfine splitting equal to half that of the individual centres. The 16-line pattern with a spacing of $\sim 77G$ is not compatible with this description. The author has not considered a possible dispropor-

tionation of Mn(III) with eventual formation of (Mn III, IV) complex in solution, and has also not reported solution magnetic susceptibility data. We tend to maintain that the multiline spectra of the type shown in this thesis for solid and solution samples are typical for dinuclear Mn(III, IV) complexes and that spectral parameters are not very sensitive to the coordination environment of the manganese ions.

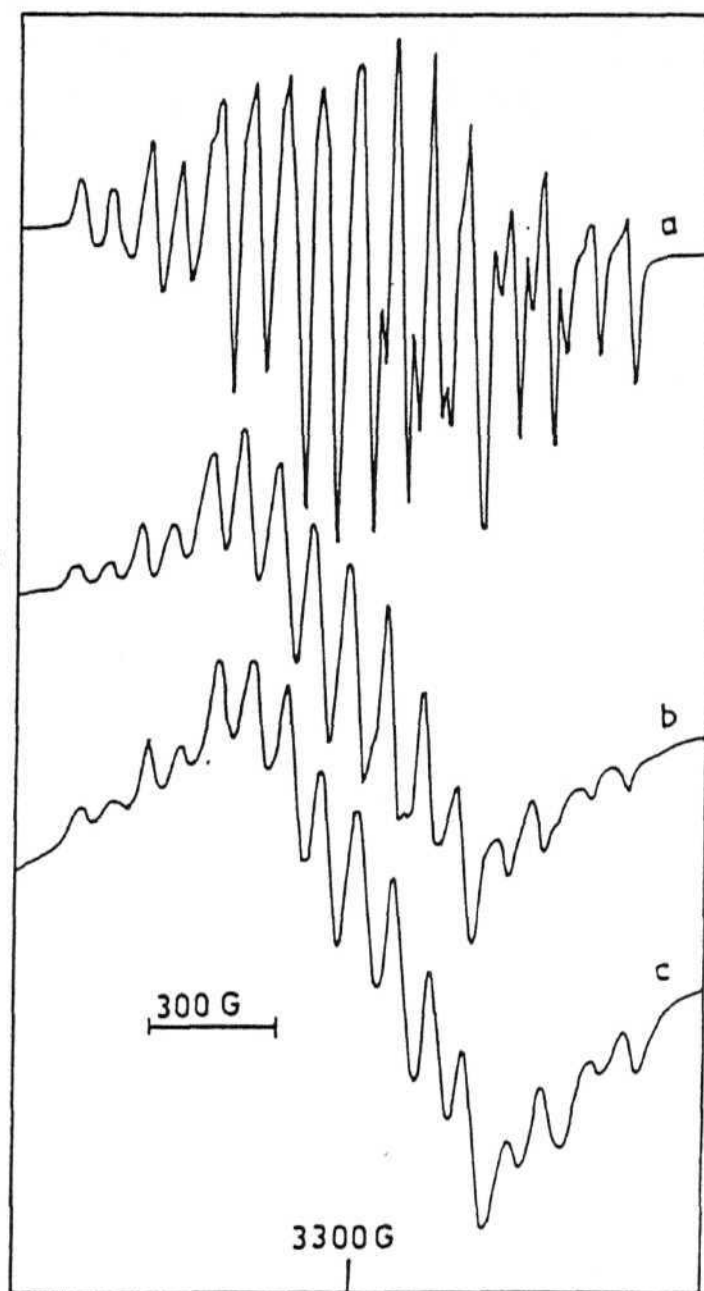


Figure 38: E.s.r spectra of frozen solutions (120K) of (a) $(\text{Mn}_2\text{O}_2\text{phen}_4)(\text{PF}_6)_3$ in dmf, (b) $(\text{Mn}_2\text{O}_2\text{phen}_4)(\text{ClO}_4)_3$ in py and (c) $(\text{Mn}_2\text{O}_2\text{phen}_4)(\text{ClO}_4)_3$ in CH_3CN .

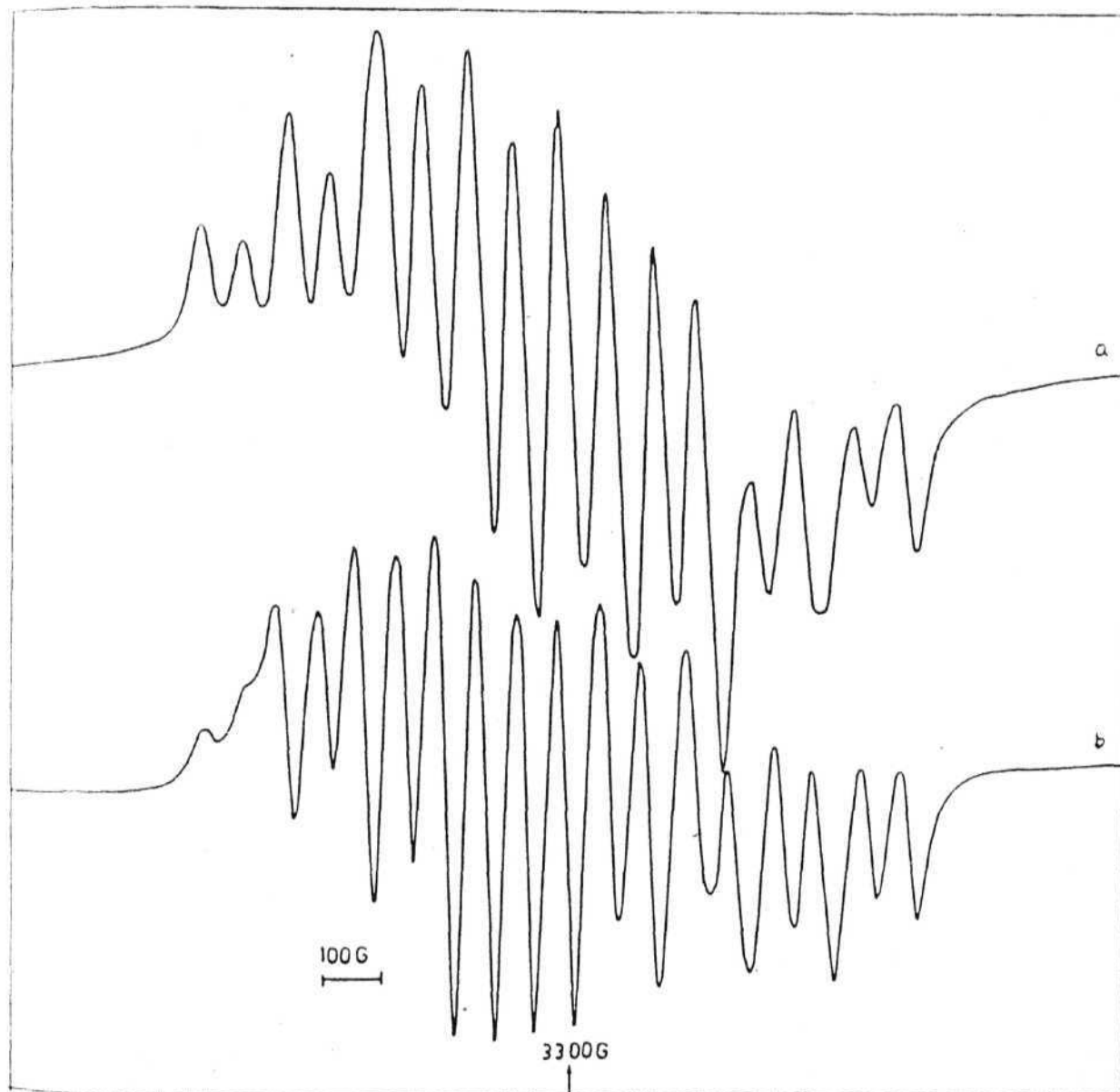


Figure 39: E.s.r. spectrum of frozen solution (125K) of (a) $(\text{Mn}_2\text{O}_2\text{bpy}_4)\text{PF}_6/3$ in CH_3CN and (b) computer simulated spectrum of the same.

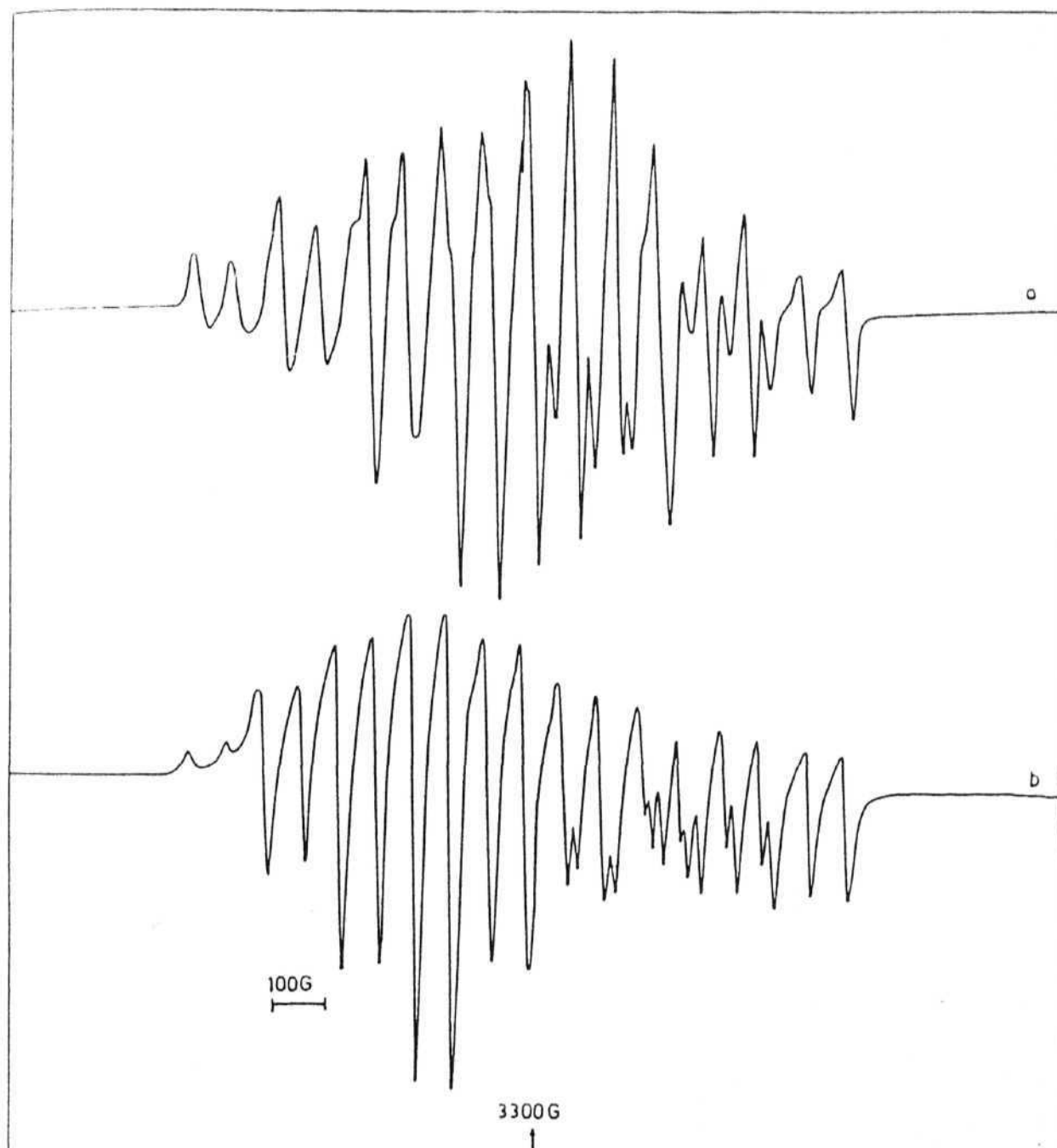


Figure 40: E.s.r. spectrum of frozen solution (120K) of (a) $(\text{Mn}_2\text{O}_2\text{phen}_4)(\text{PF}_6)_3$ in dmf and (b) computer simulated spectrum of the same.

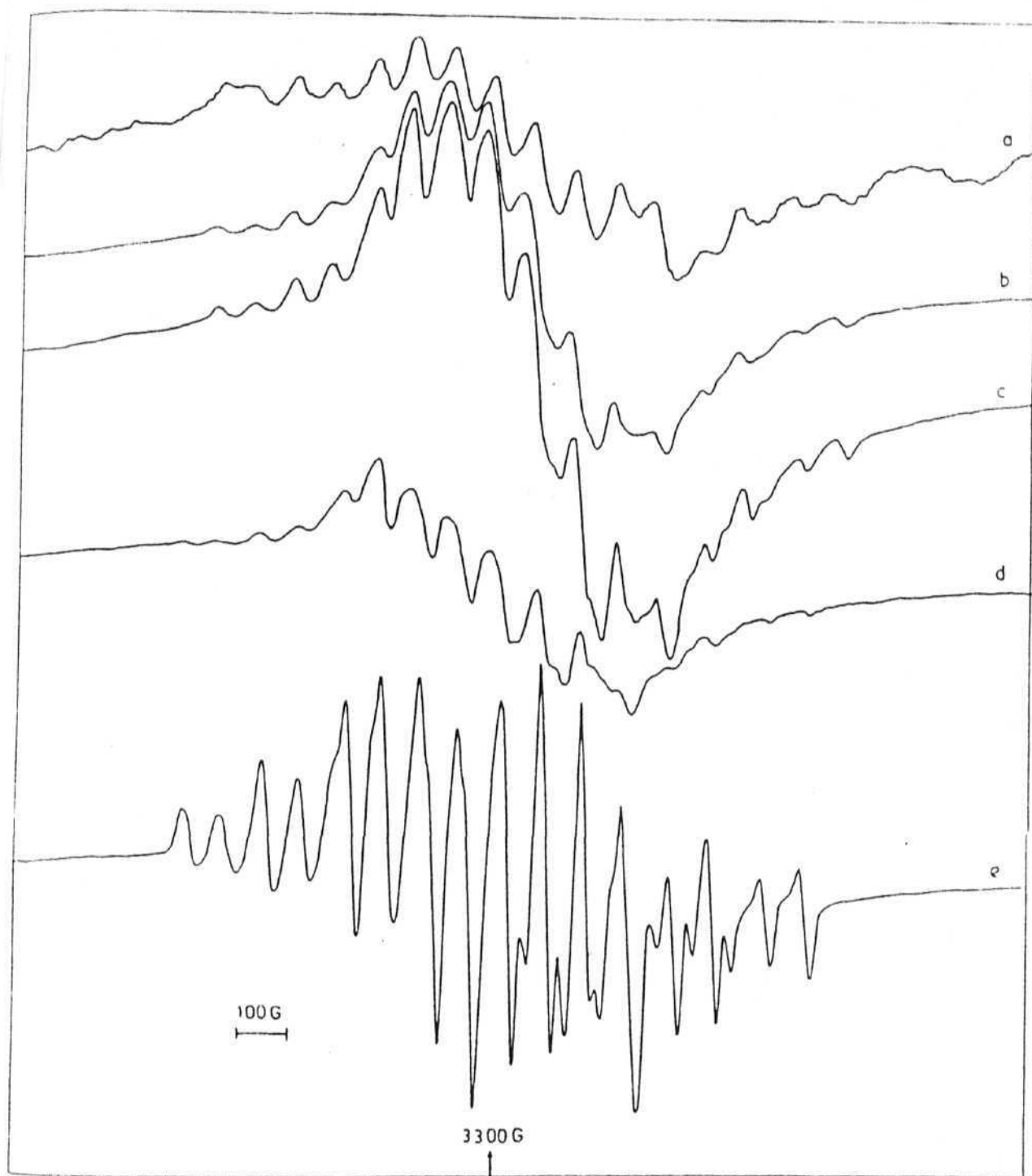


Figure 41: E.s.r spectra of $(\text{Mn}_2\text{O}_2\text{phen}_3\text{dmf}_2)(\text{ClO}_4)_3$ in dmf at various temperatures (a) 212K (b) 186K, (c) 168K, (d) 149K and (e) 122K.

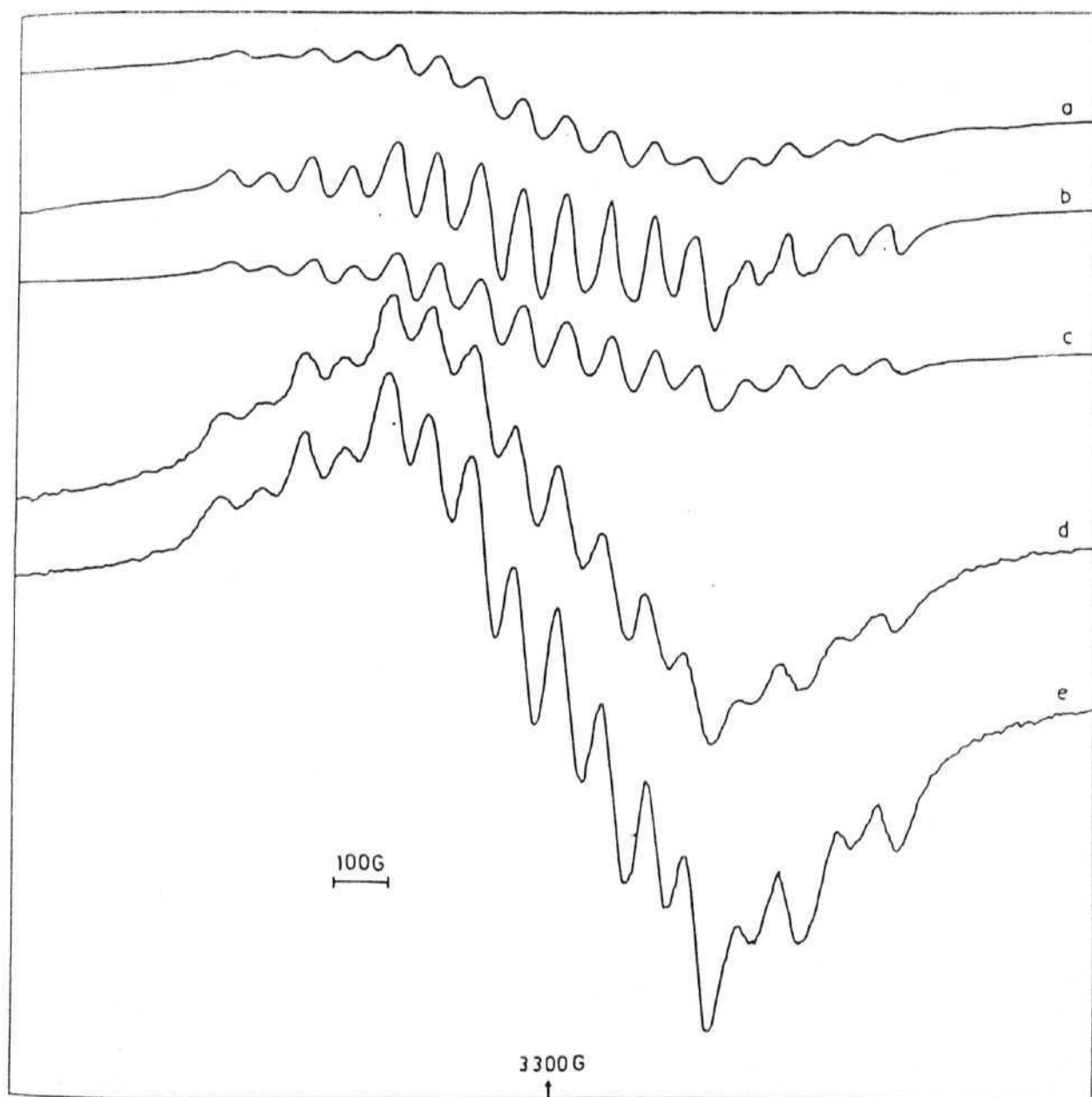


Figure 42: E.s.r spectra of $(\text{Mn}_2\text{O}_2\text{phen}_4)(\text{ClO}_4)_3$ in CH_3CN at various temperatures (a) 216K, (b) 193K, (c) 200K, (d) 150K and (e) 119K.

Oxygen evolution studies on the manganese(III, IV) complexes:-

Recently Ramaraj et al⁴⁵ have reported Oxygen evolution in a heterogeneous system containing solid $(Mn_2O_2bpy_4)(ClO_4)_3$ in contact with an aqueous solution of $(NH_4)_2Ce(NO_3)_6$. The phen complex was reported to behave in an analogous, though less efficient, manner. In this section we report our results from the similar studies on the unsymmetrically ligated complexes.

The gas evolution experiment described below is of a preliminary nature and no detailed kinetic studies were undertaken. The manganese complex was added to a strong (40%) aqueous solution of $(NH_4)_2Ce(NO_3)_6$. Gas bubbles were immediately seen to evolve from the surface of the undissolved portion of the complex. In the absence of the solid phase no gas evolution occurred. Also no gas evolved in the absence of Ceric salt. In fact, all the manganese complexes discussed here are decomposed by water at neutral pH, the substituted ones being more susceptible to reduction in neutral water. The volume of the evolved gas was measured using a gas burette and the results are given in Table XII. The rate is rapid in the initial stages but it slows with time till after about 30 hrs the gas evolution becomes imperceptibly slow. The average rate is reproducible for a given amount of sample within about 25%. The turnover number, defined as the total number of moles of O_2 evolved (till the system became inactive) for every four moles of the Mn(III, IV) complex, clearly shows that the process is catalytic rather than stoichiometric. Since the solubilities and grain size are not exactly same, only qualitative comparison is possible between the different compounds. It is seen that the

Table XII Data on oxygen evolution studies with Mn(III, IV) complexes in the presence of Ce^{4+} .

Complex	Amount of solid phase (m moles)	Time observed (hrs)	Amount of O_2 evolved ^a (ml)	Turnover number ^b
$(\text{Mn}_2\text{O}_2\text{bpy}_4)(\text{ClO}_4)_3$	0.18	19	2.9	3
$(\text{Mn}_2\text{O}_2\text{bpy}_3\text{py}_2)(\text{ClO}_4)_3$	0.18	32	7.5	7
$(\text{Mn}_2\text{O}_2\text{phen}_4)(\text{PF}_6)_3$	0.24	24	1.9	1
$(\text{Mn}_2\text{O}_2\text{phen}_3\text{py}_2)(\text{ClO}_4)_3$	0.18	39	7.1	7
$(\text{Mn}_2\text{O}_2\text{phen}_3\text{dmf}_2)(\text{PF}_6)_3$	0.02	20	1.2	10

^a at ambient conditions

^b defined as the number of moles of O_2 for four moles of the complex.

unsymmetrical complexes are more active. Interestingly, the dmf complex which is the most active, is also the most unstable towards water, being instantaneously reduced at neutral pH (in the absence of Ce^{4+}).

3. 6. 2

Electronic spectra of the $(\text{Mn}_2\text{O}_2\text{bpy}_4)(\text{ClO}_4)_3$ complex in presence of Ce^{4+} :-

The electronic spectrum of the bpy complex in water at neutral pH in presence of Ce^{4+} is shown in figure 43. It has at least six bands in the region 17.8 to 20.8kK and the IVTA band is almost completely absent. This means that the solution contains only mononuclear species and no dinuclear ions. The intensity of the higher energy bands slowly increases with time. Our observation that the dioxo-bridged species are not stable in neutral water is in agreement with the earlier observations of Cooper et al³⁶ but in disagreement with the report of Ramaraj et al⁴⁵.

The bands in the figure 43d can be assigned to MnO_4^- ion⁷⁷. The same bands with similar time evolution were also observed when manganese perchlorate was dissolved in $(50\%)(\text{NH}_4)_2\text{Ce}(\text{NO}_3)_6$ but not in $(\text{NH}_4)_2\text{Ce}(\text{SO}_4)_3$ ⁸⁸. The latter solution develops these bands when the sulphate is replaced by nitrate by adding barium nitrate showing that in the presence of nitrate the $\text{Ce}^{4+}/\text{Ce}^{3+}$ potential is sufficiently high to oxidise Mn^{2+} to MnO_4^- . The formation of permanganate ion in the oxygen evolving solution complicates the picture because MnO_4^- in acidic medium can also oxidise water slowly. However, this alone cannot account for the copious evolution of oxygen bubbles from the solid manganese complex in the heterogeneous solution. While detailed mechanistic conclusions are not warranted from these prelimi-

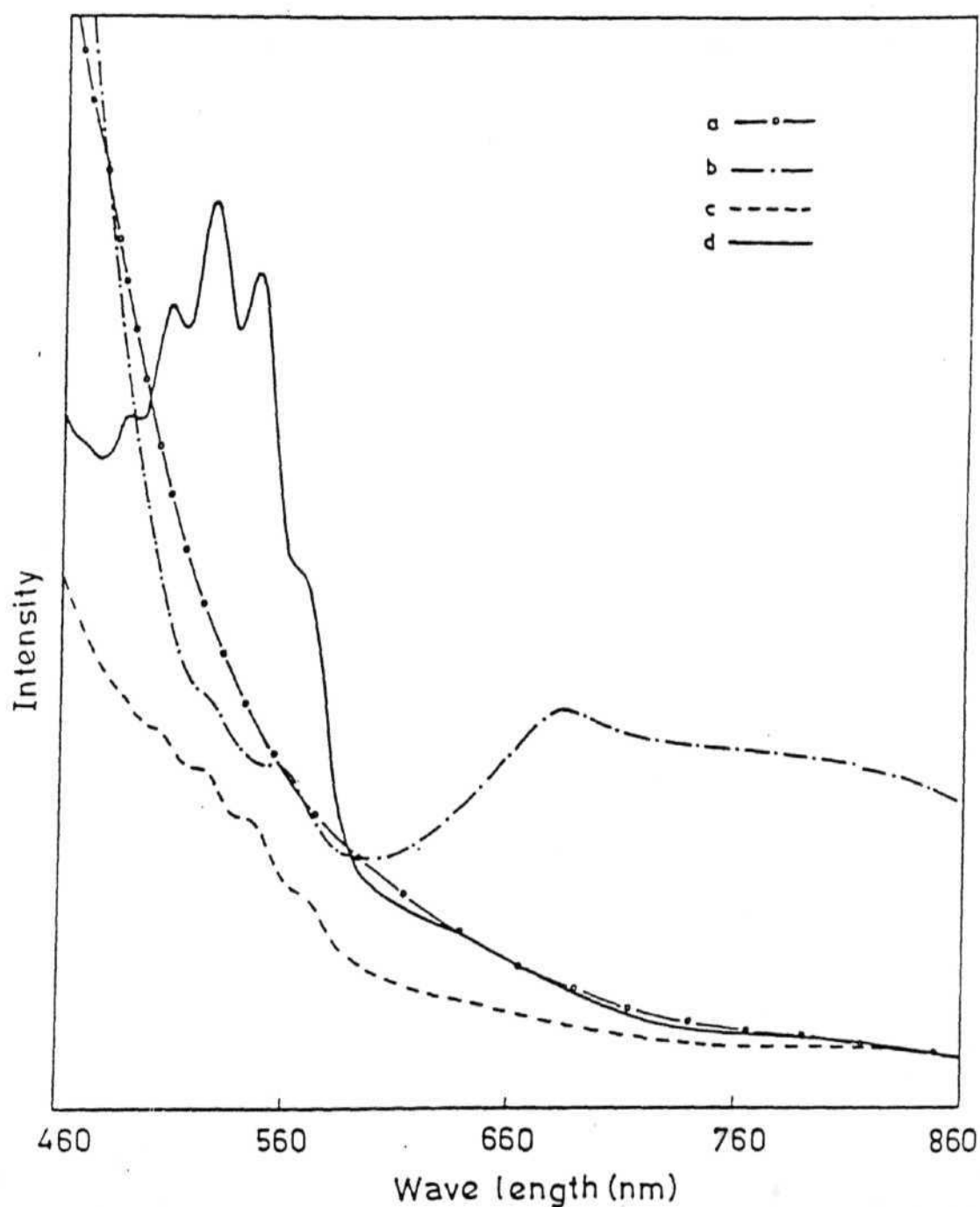


Figure 43: Electronic spectra of aqueous solutions of $(\text{Mn}_2\text{O}_2\text{bpy}_4)(\text{ClO}_4)_3$ (a) at neutral pH, (b) at pH 4.5, (c) at neutral pH in presence of Ce^{4+} and (d) after aging solution (c) for a day.

nary experiments, it is interesting to note that the unsymmetrically ligated complexes have significantly larger turnover numbers than the parent bpy and phen complexes. This is what one would expect if the $\text{Mn(IV)} \rightarrow \text{Mn(III)}$ reduction is the slow step in the water oxidation process, because the unsymmetrical complexes will have more deeply trapped valencies, and therefore the Mn(IV) centre will be more susceptible to reduction.

REFERENCES

1. "Miscellanea Berolinensia incrementum scientiarum", Berlin, (1710),p.377, quoted in ref 5, Chapter 2.
2. A. Werner, Z. anorg. Chem., 12(1896)46, quoted in ref.5, Chapter 1.
3. (a) G.C. Allen and N.S.Hush, Prog. Inorg. Chem., 8(1967)357.
(b) P. Day, Endeavour, 29(1970)45.
(c) N.S. Hush, Prog. Inorg. Chem., 8(1967)391.
(d) N.S. Hush, Electrochim. Acta., 13(1968)1005.
(e) M.B. Robin and P.Day , Adv. Inorg. Radiochem., 10(1967)247.
4. (a) E.J.W. Verwey, P.J. Haayman, F.C.Romaeijh and G.W. van Oosterhout, Philips. Res., 5(1950)173.
(b) E.J.W. Verwey, P.J. Haayman and F.C. Romaeijh , J.Chem. Phys., 15(1947)181.
5. D.B.Brown, "Mixed-Valence Compounds", D. Reidel, Holland, (1979).
6. J.M. Williams, M.A.Beno, K.D.Carlson, U. Geiser, H.C. Iyvkao, A.M.Kini, L.C. Porter, A.J. Schultz, R.J.Thorn and H.H. Wang and M.H. Whangbo and M.Evain, Acc. Chem. Res., 21(1988)1.
7. A.G. Sharpe, "The Chemistry of Cyano Complexes of the Transition Metals", Academic Press, New York, (1976)p.99 and references therein.
8. A.Y. Aleksandrov, S.P. Ionov, D.A. Baltrunas and E.F. Makarov, J.E.T.P. Letters, 16(1972)147.
9. S.R. Cooper, G.C. Dismukes, M.P. Klein and M.Calvin , J.Am. Chem. Soc., 100(1978)7248.
10. F.A. Cotton and T.E. Haas , Inorg. Chem., 3(1964)10.
11. Ref. 3 (e).
12. H.R. Zeller, Festkorperprobleme, 13(1973)31, quoted in ref.5.

13. (a) S.B. Piepho, E.R. Krausz and P.N. Schatz, J. Am. Chem. Soc., 100(1978)2996.
(b) K.Y. Wong and P.N. Schatz, Prog. Inorg. Chem., 28(1981)369.
14. N.S. Hush, Trans. Faraday. Soc., 57(1961)557., and ref. 3(d).
15. (a) R.J.H. Clark and B. Stewart, Struct. Bond., 36(1979)1 and references therein.
(b) R.J.H. Clark and P.C. Turtle, Inorg. Chem., 17(1978)2526.
16. U. Furholz, H.B. Burgi, F.W. Wagner, A. Stebler, J.H. Ammeter, E. Krausz, R.J.H. Clark, M.J. Stead and A. Ludi, J. Am. Chem. Soc., 106(1984)121.
17. M.J. Ondrechen, J. Ko and L.T. Zhang, Int. J. Quant. Chem. Sym., 19(1986)393.
18. L. Dubicki, J. Ferguson and E.R. Krausz, J. Am. Chem. Soc., 107(1985)179.
19. (a) C. Creutz, H. Taube, J. Am. Chem. Soc., 91(1969)3988; 95(1973)1086.
(b) C. Creutz, Prog. Inorg. Chem., 30(1983)1 and references therein.
20. C. Creutz, M.L. Good and S. Chandra, Inorg. Nucl. Chem. Lett., 9(1973)171.
21. P.H. Citrin, J. Am. Chem. Soc., 95(1973)6472.
22. (a) J.K. Beattie, N.S. Hush and P.R. Taylor, Inorg. Chem., 15(1976)992.
(b) N.S. Hush, Chem. Phys., 10(1975)361.
23. T.C. Strekas and T.G. Spiro, Inorg. Chem., 15(1976)974.
24. B.C. Bunker, R.S. Drago, D.N. Hendrickson, R.M. Richman and S.L. Kessel, J. Am. Chem. Soc., 100(1978)3805.

25. N.S. Hush, A. Edgar and J.K. Beattie, *Chem. Phys. Lett.*, 69(1980) 128.
26. J.K. Beattie, N.S. Hush, P.R. Taylor, C.L. Raston and A.H. White, *J.Chem. Soc. Dalt. Trans.*, (1977)1121.
27. J.F. Keggin and F.D. Miles, *Nature*, 137(1936)577.
28. P.Day, *Comments. Inorg. Chem.*, 1(1981)155.
29. H.J. Buser, D.Schwarzenbach, W.Petter and A. Ludi, *Inorg. Chem.*, 16(1977)2704.
30. M.B. Robin, *Inorg. Chem.*, 1(1962)337.
31. B.Mayoh and P.Day, *J.Chem. Soc. Dalt. Trans.*, 1974(1974)846.
32. D.Davidson and L.A. Welo, *J.Phys. Chem.*, 32(1928)1191, quoted in ref.5.
33. (a) K.Maer Jr., M.L.Beasley, R.L. Collins, and W.O. Milligan, *J.Am.Chem.Soc.*, 90(1968)3201.
(b) A.K.Bonnette Jr. and J.F. Allen, *Inorg. Chem.*, 10(1971)1613.
(c) A. Ito, M. Suenaga and K.Ono, *J.Chem. Phys.*, 48(1968) 3597.
34. R.S. Nyholm and A. Turco, *Chem & Ind.*, (1960)74.
35. R.C.Stoufer, P.M. Plaksin, M.Mathew and G.J. Palenik, *J.Am. Chem. Soc.*, 94(1972)2121.
36. S.R. Cooper and M. Calvin, *J.Am. Chem. Soc.*, 99(1977)6623.
37. R.W. Callahan and T.J. Meyer, *Chem. Phys. Lett.*, 39(1976)82.
38. R.W. Callahan, G.M. Brown and T.J. Meyer, *Inorg. Chem.*, 14 (1975)1443.
39. M. Inoue, *Bull. Chem. Soc. Jpn.*, 51(1978)1400.
40. M.M. Morrison and D.T. Sawyer, *Inorg. Chem.*, 17(1978)333.
41. M.M. Morrison and D.T. Sawyer, *Inorg. Chem.*, 17(1978)338.

42. M. Stebler, A. Ludi and H.B. Burgi, *Inorg. Chem.*, 25(1986)4743.
43. P.S. Pavacik, J.K. Huffman and G.Christan, *J.Chem. Soc. Chem. Comm.*, (1986)43.
44. D.F. Evans, *J.Chem. Soc.*, (1959)2003.
45. R.Ramaraj, A.Kira and M.Kaneko, *Angew. Chem. Int. Ed. Engl.*, 25(1986)825.
46. (a) B.D. Sarma, K.R. Ray, R.E. Sievers and J.C.Bailar Jr., *J.Am. Chem. Soc.*, 86(1964)14.
(b) B.C. Sharma and C.C. Patel, *Ind. J.Chem.*, 8(1970)747.
(c) K.Dey, *J.Ind. Chem. Soc.*, 48(7)(1971)641.
(d) L.J. Boucher and M.O. Farrell, *J. Inorg. Nucl. Chem.*, 35 (1973)3731.
47. H.S.Maslen and T.W. Waters, *J.Chem. Soc. Chem. Comm.* (1973) 760.
48. J.D. Miller and F.D. Oliver, *J. Inorg. Nucl. Chem.*, 34(1972)1873.
49. T.Matsushita, T. Yarino, I Masuda, T.Shono and K.Shinra, *Bull. Chem. Soc. Jpn.*, 46(1973)1712.
50. L.J.Boucher and C.G. Coe, *Inorg. Chem.*, 14(1975)1289.
51. L.J.Boucher and C.G.Coe, *Inorg. Chem.*, 15(1976)1334.
52. B.C.Schardt, F.J.Hollander and C.L. Hill, *J.Am.Chem.Soc.*, 104 (1982)3964.
53. M.J. Camenzind, B.C. Schardt and C.L.Hill, *Inorg. Chem.*, 23 (1984)1984.
54. K. Wieghardt, U. Bossek, J.Bonvoisin, P.Beavillain, J. Girerd, B. Nuber, J.Weiss and J. Heinze, *Angew. Chem. Int. Ed. Engl.*, 25(1986) 1030.

55. K.Wieghardt, U.Bosseck, D.Ventur and J. Weiss, J.Chem. Soc. Chem. Comm. (1985)347.
56. W.F.Beyer Jr and I. Fridovich, Biochem., 24(1985)6460.
57. B.U.Nair and G.C. Dismukes, J.Am. Chem. Soc., 105(1983)124.
58. T.Matsushita, L.Spencer and D.T. Sawyer, Inorg. Chem., 27(1988) 1167.
59. M.Suzuki, S.Tokura, M. Suhara and A.Uehara, Chem. Lett. (1988) 477.
60. B.Kok, B. Forbush and M. Mc Gloin, Photochem. Photobiol., 11 (1970)157.
61. G.C. Dismukes and Y. Siderer, Proc. Natl. Acad. Sci. U.S.A., 78(1981)274.
62. D.B. Goodin, V.K. Yachandra, R.D. Britt, K. Sauer and M.P. Klein, Biochim. et Biophysica Acta., 767(1984)209.
63. J.C. de Paula and G.W. Brudvig, J.Am. Chem. Soc., 107(1985) 2643.
64. G.C. Dismukes, K. Ferris and P. Watnick, Photobiochem. Photobiophys., 31(1982)243.
65. (a) O. Hansson and L.E. Andreasson, Biochem. Biophys. Acta., 679(1982)261.
(b) O. Hansson, L.E. Andreasson and T. Vanngard, Adv. Phosyn. Research ,1 (1984)307.
66. "Vogel's Text book of Practical Organic Chemistry", B.S. Furniss, A.J.Hannaford, V.Rogers, P.W.G.Smith and A.R.Tatchell Ed., ELBS, (1978).
67. W.H.F. Sasse and C.P. Whittle, J.Chem. Soc., (1961)1347.
68. G.R. Newkome, D.C. Pantaleo, W.E.Puckett, P.L. Ziefle and W.A. Deutsch, J.Inorg. Nucl. Chem., 43(1981)1529.

69. R.H. Fabian, D.M.Klassen and R.W. Sonntag, *Inorg. Chem.*, 19 (1980)1977.
70. (a) J.E.Dickson and L.A. Summers, *Aust. J. Chem.*, 23(1970) 1023.
(b) G.E. Inglett and G.F. Smith, *J.Am. Chem. Soc.*, 72(1950) 842.
(c) J. Druey and P.Schmidt, *Helv. Chem. Acta.*, 33(1950)1080.
71. R.H.Linnell, *J.Org. Chem.*, 22(1957)1691.
72. M.V.Rajasekharan and P.T. Manoharan, *Mol. Phys.*, 44(1981)1145.
73. B.J. Hathaway, D.G. Holah and M.Hudson, *J.Chem. Soc.*, (1963) 4586.
74. A.S. Quist, J.B. Bates and G.E. Boyd, *J.Chem. Phys.*, 54(1971) 4896.
75. H.G. Mayfield jun. and W.E. Bull, *J. Chem. Soc. A* (1971)2279.
76. F.A. Cotton and G. Wilkinson, "Advanced Inorganic Chemistry", 4th edition, Interscience New York (1980),p.744.
77. A.B.P.Lever, "Inorganic Electronic Spectroscopy", Elsevier, New York (1984) pp.430, 435.
78. H.A. Goodwin and R.A. Sylva, *Aust J. Chem.*, 20(1967)629.
79. J.F. Gibson, D.O. Hall, J.M. Thonly, and F.R. Whately, "Magnetic Resonance in Biological systems", A. Ehrenberg, B. Malstrom and T. Vanngard Ed., Pergamon Press, New York, 18 quoted in Ref.80.
80. G.F. Kokoszka and R.W. Duerst, *Coord. Chem. Revs.*, 5(1970)209.
81. W.B. Euler, *Inorg. Chem.*, 25(1986)1871.
82. B.A. Goodman and J.B. Raynor, "Adv. Inorg. Chem. Radiochem.", 13(1970)136.

83. A. Abragam and B. Bleaney, "Electron paramagnetic resonance of transition ions", Clarendon Press, Oxford (1970).
84. J.R. Hartman, B.M. Foxman and S.R. Cooper, *Inorg. Chem.*, 23(1984)1381.
85. D.T. Richens and D.T. Sawyer, *J. Am. Chem. Soc.*, 101(1979)3681.
86. M.J. Camenzind, F.J. Hollander and C.L. Hill, *Inorg. Chem.*, 22(1983)3776.
87. Y. Nishida, *Inorg. Chim. Acta.*, 151(B22)(1988)177.
88. N.Venkatalakshmi, G.Swarnabala and M.V. Rajasekharan, unpublished results.

SECTION - II

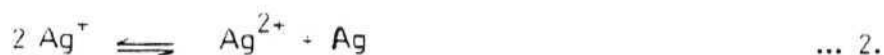
CHEMISTRY OF BIVALENT SILVER COMPLEXES WITH
STERICALLY HINDERED HETEROAROMATIC LIGANDS

CHAPTER -1

INTRODUCTION TO BIVALENT SILVER CHEMISTRY

A general introduction to bivalent silver chemistry:-

The sub-group of coinage metals is unique among transition metal groups in that each member has a different stable oxidation state in water.



Cu^+ and Au^+ disproportionate readily (equations (1) and (3), K for copper is $5 \times 10^5 \text{ m}^{-1}$ l at 25°C) while for silver, the disproportionation (equation 2) is not detectable. The major factors that decide the stability of the oxidation states are the difference in the size of the ions in different oxidation states and the differences in the ionization energies of the atoms^{1,2}. Thus the Cu^{2+} ion, being much smaller than Cu^+ ion, has a much larger hydration energy and this is responsible for the ready disproportionation of Cu^+ in water. Silver on the other hand has a much larger second ionization energy while the heats of hydration are not very different. For silver the stable oxidation state in water is +1. The difference between silver and gold is mainly due to the lesser value for the third ionization energy of gold and the crystal field stabilisation of d^8 configuration in square-planar geometry.

The redox potentials are profoundly influenced by ligands. Thus, Ag^+ undergoes disproportionation according to equation (2) in the presence of porphyrins. Complexes are known for most of the +1, +2 and +3 ions. However Au(II) complexes have been rather elusive^{1,3}.

Numerous Ag(II) complexes are known. Some of them are isolable in the solid state like $\text{Ag}(\text{bpy})_2 \text{S}_2\text{O}_8$ while some are obtained only in solution or in mixed crystals, for example, $\text{Ag}(\text{dedtc})_2$. Silver salts catalyse several oxidation reactions and they are believed to involve Ag^{2+} as the electron transfer intermediary. In the following sub-sections the silver(II) chemistry involving heteroaromatic ligands is reviewed so as to provide the necessary background for the novel complexes and electron transfer reaction to be presented in the subsequent chapters.

1.2

Survey of bivalent silver complexes with heteroaromatic ligands:-

Several reviews in the past⁴ as well as in the recent past⁵ have highlighted the synthetic and structural aspects of Ag(II) chemistry. The salient features of the complexes with pyridyl, bipyridyl and related ligands only are discussed in this sub-section.

The $\text{Agpy}_4\text{S}_2\text{O}_8$ was originally prepared by Barbieri⁶. This has been reexamined by several workers⁷ and e.s.r. was studied⁸. Evidence for more than four pyridines coordinating with bivalent silver was not seen even in neat pyridine solution. In frozen nitric acid solution, formation of $\text{Agpy}_2(\text{NO}_3)_2$ was suggested⁷ which was not confirmed by recent authors⁸. E.s.r. of this complex as polycrystalline solid solution at 1% concentration in $\text{Cdpy}_4\text{S}_2\text{O}_8$ showed hyperfine structure corresponding to an axial symmetry. All the pyridine complexes are reported⁹ to be magnetically dilute except polymeric $\text{Agpz}_2\text{S}_2\text{O}_8$, which is antiferromagnetic¹⁰. The electronic spectrum¹¹ of Agpy_4^{2+} suggests square-planar configuration with much larger energy compared to 10-12 kK expected for a tetrahedral

complex. The silver hyperfine and nitrogen superhyperfine structures were observed³⁷ for $\text{Agpy}_2(\text{NO}_3)_2$ in frozen nitric acid solution at 77 K. Number of substituted pyridine complexes were also studied¹³.

Perhaps the most popularly studied complex is $\text{Ag}(\text{bpy})_2^{2+}$ which was isolated¹⁴ with $\text{S}_2\text{O}_8^{2-}$, ClO_4^- , HSO_4^- , NO_3^- , ClO_3^- , CF_3SO_3^- and SO_3F^- anions. Tris(bipyridine)silver (II) reported¹⁵ earlier was shown not to exist¹⁶ but the presence of this bivalent silver species was suggested as an intermediate in the electrochemical studies of the $\text{Ag}^+/\text{Ag}^{2+}$ system in propylene carbonate containing excess of bipyridine¹⁷. X-ray structure of $\text{Ag}(\text{bpy})_2(\text{NO}_3)_2 \cdot \text{H}_2\text{O}$ was determined¹⁸ which showed a distortion of $\sim 28^\circ$ from square-planar AgN_4 unit with a weak axial interaction with two bridging nitrates to form a chain structure. In neutral solution $\text{Ag}(\text{bpy})_2^{2+}$ is present but in nitric acid $\text{Ag}(\text{bpy})(\text{NO}_3)_2$ is produced¹⁹ which was also structurally characterised²⁰. It has a distorted square-planar structure with a chelating bipyridine ligand and two cis-monodentate nitrate groups with long axial contacts to two farther nitrate groups.

Similar complexes with phen as ligand are also known²¹. They are found less soluble compared to bipyridine complexes and in nitric acid solution $[\text{Ag}(\text{phen})(\text{NO}_3)]^+$ was expected²² to form. With 2, 2', 2''-terpyridine the 1:1 complexes are prepared²³ easily and probably are four-coordinate. Dark brown $\text{Ag}(\text{terpy})_2\text{S}_2\text{O}_8 \cdot 3\text{H}_2\text{O}$ was obtained from AgNO_3 , $\text{K}_2\text{S}_2\text{O}_8$ and excess terpyridine. Based on p.a.s and electronic spectra which show absorption at much lower energy than $\text{Ag}(\text{terpy})\text{X}_2$, it was suggested to be six-coordinate.

Secondary-ion mass spectra of bivalent silver complexes have been reported²⁴ recently. Bivalent silver pyridine, bipyridine and pyrazine complexes have been analysed.

Very recently, AgTPP^{2+} , was structurally characterised²⁵ by x-ray data confirming the planar geometry.

Another class of nitrogen donor ligands which form Ag(II) complexes readily are pyridine carboxylic acids²⁶. They are all expected to form 2:1 planar complexes analogous to their Cu(II) complexes. However no x-ray data is available. Most of the complexes are expected to be magnetically dilute except $\text{Ag}(\text{nicotin})_2$ being antiferromagnetic^{26a}.

1.3

Survey on copper and silver complexes of sterically hindered ligands:-

Structural studies of $\text{Cu}(\text{dmp})_2\text{NO}_3 \cdot 2\text{H}_2\text{O}$, $\text{Cu}(\text{dmp})_2\text{NO}_3$ and $\text{Cu}(\text{dmp})_2\text{ClO}_4$ and also $\text{Cu}(\text{tmbp})_2\text{ClO}_4$ and $\text{Cu}(\text{dmbp})_2\text{BF}_4$ were reported²⁷. Unlike other copper(I) complexes which are air-sensitive and are synthesised in inert atmosphere, these complexes were reported to have formed in organic solvents. In these complexes Cu-N distances showed considerable variations, ranging from 2.02-2.08 Å for dmp complexes and 2.018-2.076 Å for the substituted bipyridine complexes suggesting that for some ligands Cu-N bond lengths are significantly different. They were found to exhibit pseudotetrahedral geometry which prefers Cu(I) to Cu(II). The metal to ligand charge transfer band for $\text{Cu}(\text{dmbp})_2^+$ was found at a lower energy than in $\text{Cu}(\text{bpy})_2^+$ and the former complex will have a greater preference for tetrahedral geometry because the Cu-N bond length is expected to increase due

to the presence of methyl groups.

Compared to the Cu(II) complexes of the unsubstituted ligand which are quite stable in organic solvents, Cu(II) complexes of 6, 6'-substituted bipyridine ligands are observed²⁸ to undergo autoreduction in non-aqueous solvents, without the need of reducing agents. Cu(dmbp)_2^{2+} was found to undergo reduction in ethanol and a reduction in the intensity of the metal to ligand charge transfer band with time was observed.

Ag(dmp)NO_3 complex was prepared and its i.r. data reported²⁹. Recently x-ray structure for $\text{Ag(tmbp)}_2\text{BF}_4$ was reported³⁰. This was found to be isomorphous and isostructural with $\text{Cu(tmbp)}_2\text{ClO}_4$. A twist angle of 70° for silver compound was obtained compared to 75° for the copper analogue. The characteristic flattening distortion from tetrahedral geometry was ascribed to lattice effect of the stacking interactions involving the heteroaromatic ligands, rather than due to the participation of the Jahn-Teller active charge transfer excited state.

CHAPTER 2
EXPERIMENTAL SECTION

2. 1 Preparation of ligands:-

Ligands were prepared as per the literature procedures given in Chapter 2 of Section I.

2. 2 Preparation of silver (I) complexes of various ligands:-

2. 2. 1 Preparation of Ag(dmbp)NO_3

To a warm solution of 540 mg (2.94 mmols) of dmbp in 0.1N HNO_3 , 500 mg (2.93 mmols) AgNO_3 in water was added dropwise. The solution on cooling precipitated a white crystalline material. It was filtered, washed with water and dried in vacuum. The yield based on AgNO_3 was 80%, mpt. 222°C . Analytical data with theoretical values in parenthesis for Ag, 3N, 12C, 12H and 3O was C=40.49 (40.70), H=3.42 (3.42) and N=11.56 (11.87)%. Dmbp estimated by spectrophotometry, 52.04 (52.03)%. Long needle-like crystals were grown over concentrated H_2SO_4 in a desicator.

2. 2. 2 Preparation of Ag(dmp)NO_3 :-

To a warm solution of 320 mg(1.50 mmols) of dmp in 0.1 N HNO_3 , 250 mg AgNO_3 (1.47 mmols) in water was added dropwise. The solution on cooling precipitated white fine crystalline material. It was filtered, washed with water and dried in vacuum. The yield based on AgNO_3 was 90%. Analytical data for Ag, 3N, 14C, 12H and 3O was C 43.60 (44.47), H 3.20 (3.70) and N 11.00 (11.11)%.

2. 2. 3 Preparation of $\text{Ag(tmbp)}_2\text{NO}_3$:-

To a warm solution of 1.26 g (5.94 mmols) of tmbp in 0.1 N HNO_3 , 500 mg AgNO_3 (2.93 mmols) in water was added dropwise. The solution on cooling precipitated a white compound which was filtered, washed

with water and dried in vacuum. The yield based on AgNO_3 was 70%. Analytical data for Ag, 5N, 28C, 32H and 3O was C=55.05 (56.60), H=5.16 (5.42) and N=11.86 (11.78)%.

2. 2. 4 Preparation of Ag(daf)NO_3 :-

To a warm solution of 200 mg (1.19 mmols) of daf in 0.1N HNO_3 , 163 mg of AgNO_3 (1.2 mmols) in water was added dropwise. The solution on cooling precipitated a white compound which was filtered, washed with water and dried in vacuum. The yield based on AgNO_3 was 70%.

2. 2. 5 Preparation of Ag(daf-one)NO_3 :-

To a warm solution of 250 mg (1.37 mmols) of daf-one in 0.1N HNO_3 , 200 mg (1.18 mmols) AgNO_3 in water was added dropwise. On leaving the turbid solution at 6°C a white precipitate settled. It was filtered, washed with water and dried in vacuum. Based on AgNO_3 the yield was 80%.

2. 2. 6 Preparation of Ag(mmbp)NO_3 :-

To a warm solution of 100 mg (0.587 mmols) of mmbp in 0.1N HNO_3 , 100 mg AgNO_3 (0.588 mmols) in water was added slowly. The clear solution formed was cooled at 0°C . The white precipitate formed after a few hours was filtered, washed with water and dried in vacuum. The yield based on AgNO_3 was 70%.

2. 3 Oxidation of Ag(I) complexes:-

2. 3. 1 Oxidation of Ag(dmbp)NO_3 :-

To a concentrated aqueous solution of $(\text{NH}_4)_2\text{S}_2\text{O}_8$ at -20°C solid

Ag(dmbp)NO_3 was added. The solid turned brown in colour. It was centrifuged and the dark brown precipitate (I) was washed with ice-cold water and dried in vacuum. Reliable analysis could not be obtained due to its instability. However, it is believed to be $\text{Ag(dmbp)(NO}_3)_2$.

The dark brown mother liquor was precipitated with cold concentrated aqueous solution of NH_4PF_6 . A light brown precipitate (II) obtained was washed thrice with cold water and dried in vacuum. It was formulated as $[\text{Ag(dmbp)NO}_3]\text{PF}_6 \cdot \text{NH}_4\text{PF}_6$. Analytical data for Ag, 4N, 12C, 16H, 2P, 12F, 3O was C=22.63 (21.77), H=3.41 (2.44) and N=9.04 (8.46); Ag^{2+} (iodometry) 16.8 (16.3), Ag(gravimetry) 16.2 (16.3) and dmbp (spectrophotometry) 32.0 (27.8)%.

Samples I and II were sealed into quartz tubes in nitrogen atmosphere for e.s.r. measurement.

2. 3. 2 Oxidation of Ag(dmp)NO_3 :-

To a concentrated aqueous solution of $(\text{NH}_4)_2\text{S}_2\text{O}_8$ at room temperature solid Ag(dmp)NO_3 was added. The solid turned brown. It was separated by centrifugation, washed with cold water and dried in vacuum (III). The bright yellow solution was cooled to 0°C and was precipitated by cold concentrated aqueous solution of NH_4PF_6 to obtain a light brown precipitate. It was washed with ice-cold water and dried in vacuum (IV). Samples III and IV were sealed in e.s.r. tubes in nitrogen atmosphere. They were unstable over a period of time even in sealed tubes. No analysis was attempted but the similarity of the e.s.r. spectra for the freshly prepared complexes indicate that they are analogous to the dmbp complexes, I and II.

2. 3. 3 Oxidation of $\text{Ag}(\text{tmbp})_2\text{NO}_3$:-

Solid $\text{Ag}(\text{tmbp})_2\text{NO}_3$ was added to a concentrated aqueous solution of $(\text{NH}_4)_2\text{S}_2\text{O}_8$ at room temperature. The solid dissolved to give a pink solution. However, it could not be precipitated by the addition of NH_4PF_6 at room temperature or even below 0°C .

2. 3. 4 Oxidation of $\text{Ag}(\text{daf})\text{NO}_3$:-

To the concentrated aqueous solution of $(\text{NH}_4)_2\text{S}_2\text{O}_8$ solid $\text{Ag}(\text{daf})\text{NO}_3$ was added at room temperature. The solution turned yellow in colour. It was precipitated with concentrated aqueous solution of NH_4PF_6 to obtain a pale yellow precipitate which was separated by centrifugation, washed with water and dried in vacuum. However, no e.s.r. spectrum was observed probably because of very low concentration of $\text{Ag}(\text{II})$ in the sample. No analysis was therefore attempted.

2. 3. 5 Oxidation of $\text{Ag}(\text{daf-one})\text{NO}_3$:-

To the concentrated aqueous solution of $(\text{NH}_4)_2\text{S}_2\text{O}_8$ at room temperature solid $\text{Ag}(\text{daf-one})\text{NO}_3$ was added. The solid dissolved and the brown coloured solution was precipitated by concentrated aqueous solution of NH_4PF_6 . The light yellow coloured precipitate was washed with water and dried in vacuum. The sample was unstable over a period of days.

2. 3. 6 Oxidation of $\text{Ag}(\text{mmbp})\text{NO}_3$:-

To the concentrated aqueous solution of $(\text{NH}_4)_2\text{S}_2\text{O}_8$, solid $\text{Ag}(\text{mmbp})\text{NO}_3$ was added at room temperature. The solution turned dark brown in colour and was precipitated by concentrated aqueous solution of NH_4PF_6 . The dark brown precipitate was separated by centrifugation, washed with water and dried in vacuum.

2. 4 Analytical procedures employed:-

The details of the analytical procedures and the instruments employed are given in Section 1, Chapter 2. For the estimation of dmbp by spectrophotometry, we used $\epsilon_{(288 \text{ nm})} = 0.248 \times 10^{-5} \text{ m}^{-1} \text{ cm}^{-1} \text{ l}$ measured for the free ligand in methanol.

2.5 Computer simulation of e.s.r spectra.

Polycrystalline spectra of the magnetically dilute double salts were simulated using the computer program described in Section 1, Chapter 2.

The Hamiltonian employed was

$$H = \beta_e \vec{H} \cdot \underline{g} \cdot \vec{S} + \vec{I} \cdot \underline{A} \cdot \vec{S} - g_n \beta_n \vec{H} \cdot \vec{I} + \vec{I}_{N1} \cdot \underline{A}_{N1} \cdot \vec{S} + \vec{I}_{N2} \cdot \underline{A}_{N2} \cdot \vec{S} \quad \dots 4.$$

For the present compounds \underline{g} and \underline{A} turned out to be axially symmetric. The nitrogen hyperfine tensors were assumed to be equivalent and axial with the Ag-N bond direction as the symmetry axis. For planar coordination, this would mean that $A_{||}$ for silver is in the (x, y) planes of the nitrogen tensors. The resultant hyperfine constants A and B are related to $A_{||}(N)$ and $A_{\perp}(N)$ as $A_{||}(N) = B$ and $A_{\perp}(N) = \frac{1}{\sqrt{2}}(A^2 + B^2)^{1/2}$ for square planar configuration. The program has provision for any arbitrary orientation of the principal axis of the ^{14}N tensor, but the results are not sensitive to moderate distortions due to the small hyperfine anisotropy. The calculations were performed on an IBM compatible WIPRO Machines personal computer. A typical simulation (with a grid spacing of 1° in θ and 90° in ϕ) needed one hour of computer time.

CHAPTER 3

RESULTS AND DISCUSSION

3. 1 Nature of the solid Ag(I) and Ag(II) complexes:-

3. 1. 1 I.r. spectra of Ag(I) complexes:-

In the absence of crystal structures, a clue to the coordination mode of the nitrate ligand may be sought from the i.r. spectral data which are collected in Table I. Of the three stretching vibrations expected for coordinated NO_3^- , the two higher frequency ones are known³¹ to have a separation of about 150 cm^{-1} or more when the NO_3^- binds in the bidentate chelating mode. For monodentate NO_3^- , the separation is usually much less. For the present complexes, the nitrate bands, in most cases, could be readily identified by comparing the spectra of the complex with that of the free aromatic ligand and their frequencies are underlined in Table I. The dmbp and dmp complexes have a separation of 160 cm^{-1} and 150 cm^{-1} respectively for the nitrate bands indicating chelation. Figure 1 shows the i.r. spectrum of the dmbp complexes.

$\text{Ag}(\text{tmbp})_2\text{NO}_3$ on the other hand has only two bands at 1320 and 815 cm^{-1} which are clearly distinct from the bands in the ligand and may be assigned to NO_3^- vibrations. In this complex the NO_3^- is not expected to coordinate. The molecular structure is expected to be analogous to that in the BF_4^- salt³⁰. The complexes of mmbp, daf and daf-one also have only one band $1360\text{--}1370\text{ cm}^{-1}$. While a firm conclusion about the coordination mode of the NO_3^- is not warranted from these data, it is likely that these complexes do not have a bidentate nitrate. Since a trigonal geometry will be coordinatively unsaturated a polymeric structure with NO_3^- acting as bridging ligand is proposed for these compounds. Attempts to grow

TABLE I I. r data (cm^{-1}) for Ag(I) Complexes^a.

dmbp	AgLNO ₃	dmp	AgLNO ₃	tmbp	AgL ₂ NO ₃	mmbp	AgLNO ₃	daf-one	AgLNO ₃	daf	AgLNO ₃
2930	3080	3030	3055	2900(b)	3040	3050	3040	3030	3030	3040	3030(w)
1580	1590	1605	1615	1580(b)		2960	2905	1715	1715	2920	2920(w)
1440(s)	<u>1440(b)</u>	1580	1585	1530(b)	2940	2930	1580	1585	1595	1550	1550
1370	1380	1538	1545	1420(b)	2920	2870	1550	1550	1550	1400	1400
1250	<u>1280</u>	1485	1498	1380(b)	1600	1575	<u>1360(b)</u>	1460	1460	1285	<u>1370</u>
1150	1250	1418	<u>1425(b)</u>	1260	1550	1448	1280(b)	1400	1398	1275	1290
1110	1170	1345	<u>1350</u>	1170	1440	1442	<u>1160(w)</u>	1250	<u>1370</u>	1160	1260
1080	1125	1290(w)	<u>1275(s)</u>	1020	1370	1361(w)	1145	1140	1250	1100	1165
1025	<u>1028(s)</u>	1210(w)	1215(w)	970	<u>1320</u>	1250	1080	1090	1140	1085	1150
990	1000	1200	1200	925	1240	1140	1040	1070	1090	970	1098
900	900	1128	1135	880	1160	1080	1020	1010	1020	850	1085
810	820	1095	1090	840	1020	1038	995	910	900	780	970
780	780	1010	<u>1020</u>	740	990	1000	800	820	830	760	<u>890</u>
710	720	840	850	710	940	880(w)	760	750	740	730	840
620	690	800	800		920	760(s)	630	700	<u>718</u>	720	810
	620	770	755		845		610	670	700	620	760
		720	720		<u>815</u>			600			725
		660	660		740						705
		620	635		710						610

^aNitrate bands are underlined, b:broad, s:sharp and intense, w:weak.

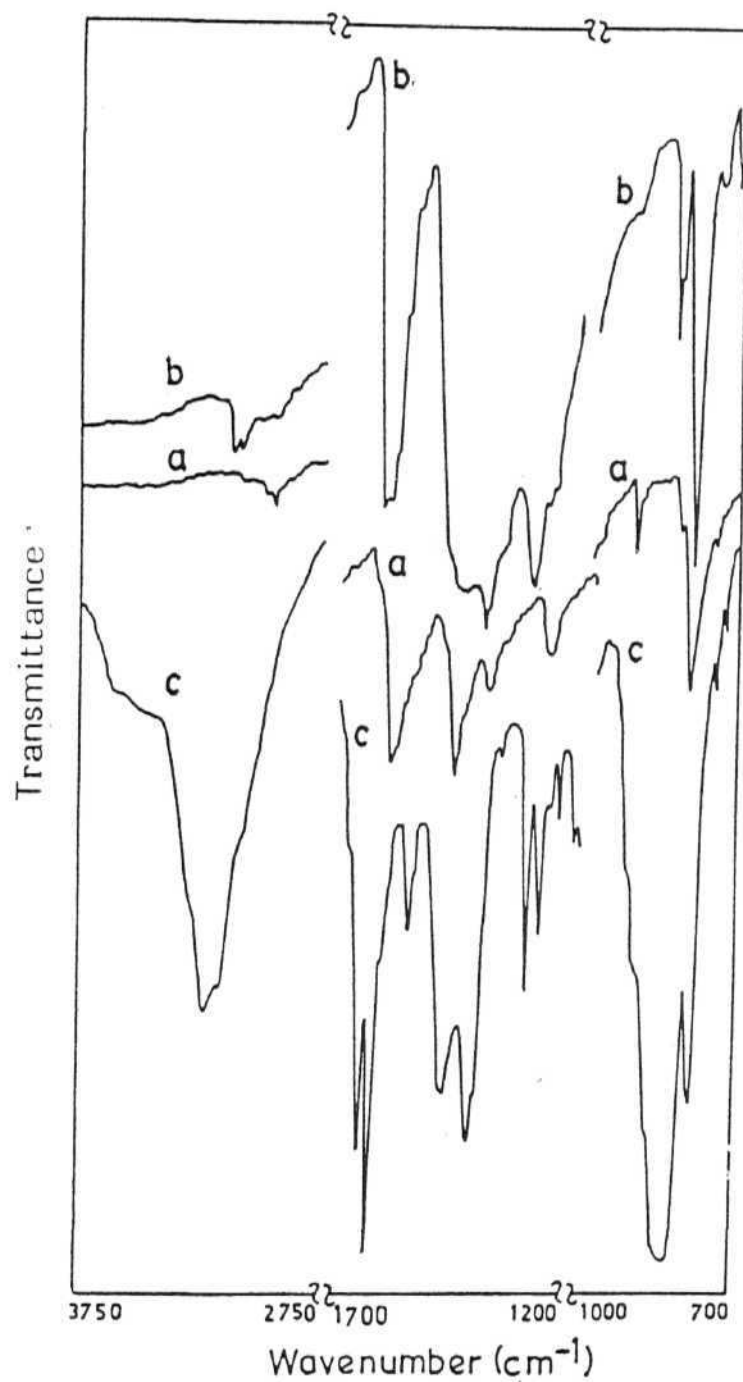


Figure 1: I.r spectra to show chelating nitrate (a) dmbp (b) Ag(dmbp)NO_3 and (c) $(\text{AgdmbpNO}_3)\text{PF}_6 \cdot \text{NH}_4\text{PF}_6$.

single crystals have not been successful.

3. 1. 2 I .r . spectra of Ag(II) complexes:-

Three types of solid complexes were obtained upon persulfate oxidation of Ag(I) compounds. With dmp and dmbp a brown solid separated initially when the AgLNO_3 was added to $(\text{NH}_4)_2\text{S}_2\text{O}_8$ solution. These solids were extremely unstable and analysis was not attempted. They gave e.s.r. spectra (sub-section 3.5) typical of magnetically concentrated samples. They are believed to be either $\text{AgL}(\text{NO}_3)_2$ or $[\text{AgLNO}_3]\text{NO}_3$.

From the mother liquor, a pale yellow compound was precipitated by the addition of NH_4PF_6 . The i.r spectra (Table II) shows bands corresponding to chelating NO_3^- and PF_6^- . They also contain a broad absorption around 3300 cm^{-1} suggesting the presence of NH_4^+ ion (Figure 1). These compounds were therefore formulated as the double salts $[\text{AgLNO}_3]\text{PF}_6 \cdot \text{NH}_4\text{PF}_6$. In the case of dmbp this stoichiometry was confirmed by C,H,N,Ag,Ag²⁺ and ligand estimations (sub-section 2.3). The Photoacoustic spectrum of this sample showed a broad asymmetric band centered at 530 nm (Figure 2), very similar to that observed in solution (sub-section 3.2 and Figure 3) indicating that the Ag(II) centre in the double salt is similar to that obtained in solution. This type of double salts are unprecedented in Ag(II) chemistry and the e.s.r investigations on them have been particularly rewarding (sub-section 3.4 and Figures 8 and 9).

In the case of daf, daf-one and mmbp (unstable) solid complexes were obtained only upon the addition of NH_4PF_6 to the solution

Table II. I.r. data (cm^{-1}) for Ag(II) Complexes^a.

$[\text{Ag}(\text{dmbp})\text{NO}_3]\text{PF}_6 \cdot \text{NH}_4\text{PF}_6$	$[\text{Ag}(\text{dmp})\text{NO}_3]\text{PF}_6 \cdot \text{NH}_4\text{PF}_6$	$[\text{Ag}(\text{mmbp})\text{NO}_3]\text{PF}_6^c$	$[\text{Ag}(\text{daf-one})\text{NO}_3]\text{PF}_6$	$[\text{Ag}(\text{daf})\text{NO}_3]\text{PF}_6$
3300	3380 (b)	3250	3105	3130
3210	3180 (s)	1620	1715	1620
3130 (w)	1600	1610	1575	1550
3060 (w)	1550 (w)	1590	1545	1520
1620	1520	1540	1400	1410
1600	1500 (w)	1460	1155 (b)*	1320
1510	1450	1330	810 (b)*	1210
1455	<u>1375</u>	<u>1320</u>	730	1190
<u>1390</u>	1340	1280	700	1060
1380	1315	1180	645	860 (b)
1320	1260	<u>1120</u>		760
1275	<u>1240</u>	1020		670
<u>1240</u>	1200	1000		620
1200	1140	840 (b)*		
1100	1100	760		
1030	1020	620		
980	980			
820 (b)*	910			
760	840 (b)*			
710	700			
610	660			
	620			

^aNitrate bands are underlined, PF_6 bands are marked by an asterisk, ^c tentative formulation, see text.

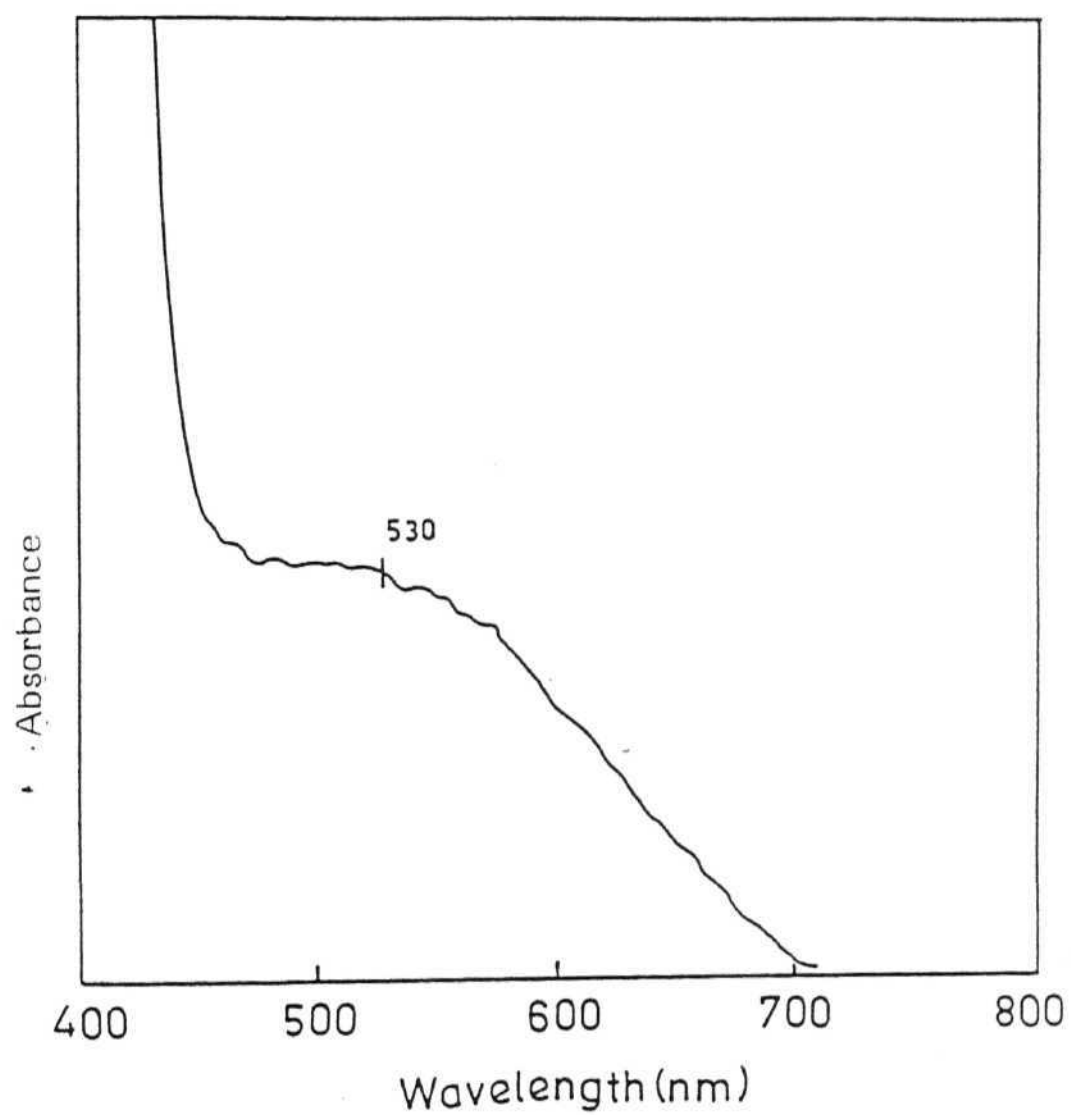


Figure 2: P.l.s spectrum of $(\text{AgdmbpNO}_3)\text{PF}_6 \cdot \text{NH}_4\text{PF}_6$.

containing the oxidised species. However, these precipitates were not double salts. The i.r. spectra (Table II) shows evidence for PF_6^- . Nitrate band can be assigned with confidence only for the mmbp complex. All the compounds gave e.s.r. corresponding to magnetically concentrated systems with no resolution of hyperfine splitting. It is not clear whether these complexes are $[\text{AgLNO}_3]\text{PF}_6$ or $\text{AgL}_2(\text{PF}_6)_2$.

2

Electronic spectra of silver (II) complexes:-

The electronic spectra of the persulfate oxidised solutions of $\text{Ag}(\text{dmbp})\text{NO}_3$ and $\text{Ag}(\text{dmp})\text{NO}_3$ are shown in Figure 3, $\text{Ag}(\text{tmbp})_2\text{NO}_3$ and $\text{Ag}(\text{daf})\text{NO}_3$ in Figure 4 and $\text{Ag}(\text{mmbp})\text{NO}_3$ in Figure 5.

In all cases three bands are observed, a broad one in the visible and two sharp bands in the UV. The highest energy UV band corresponds to a transition mainly localised on the ligands.

The visible bands are assigned to d-d transitions and the first UV band to a ligand to metal charge transfer (LMCT) transition. It is possible that under each band there is more than one transition. The ν_{max} values are collected in (Table III) which also includes values for the Ag (II) complexes of bpy and phen for comparison.

Since hexacoordinate Ag(II) has not been detected even with py as ligand, it is reasonable to assume that the electronic transition arises from four-coordinate species in solution. In view of the 1:1 complexes formed by dmbp, dmp, mmbp and daf ligands with AgNO_3 and also anticipating the discussion on the double salts containing Ag(II) (sub-section 3.4) we suggest that in the case of these ligands the predominant species in solution is $\text{AgL}(\text{NO}_3)^+$ with chelating NO_3^- ligand.

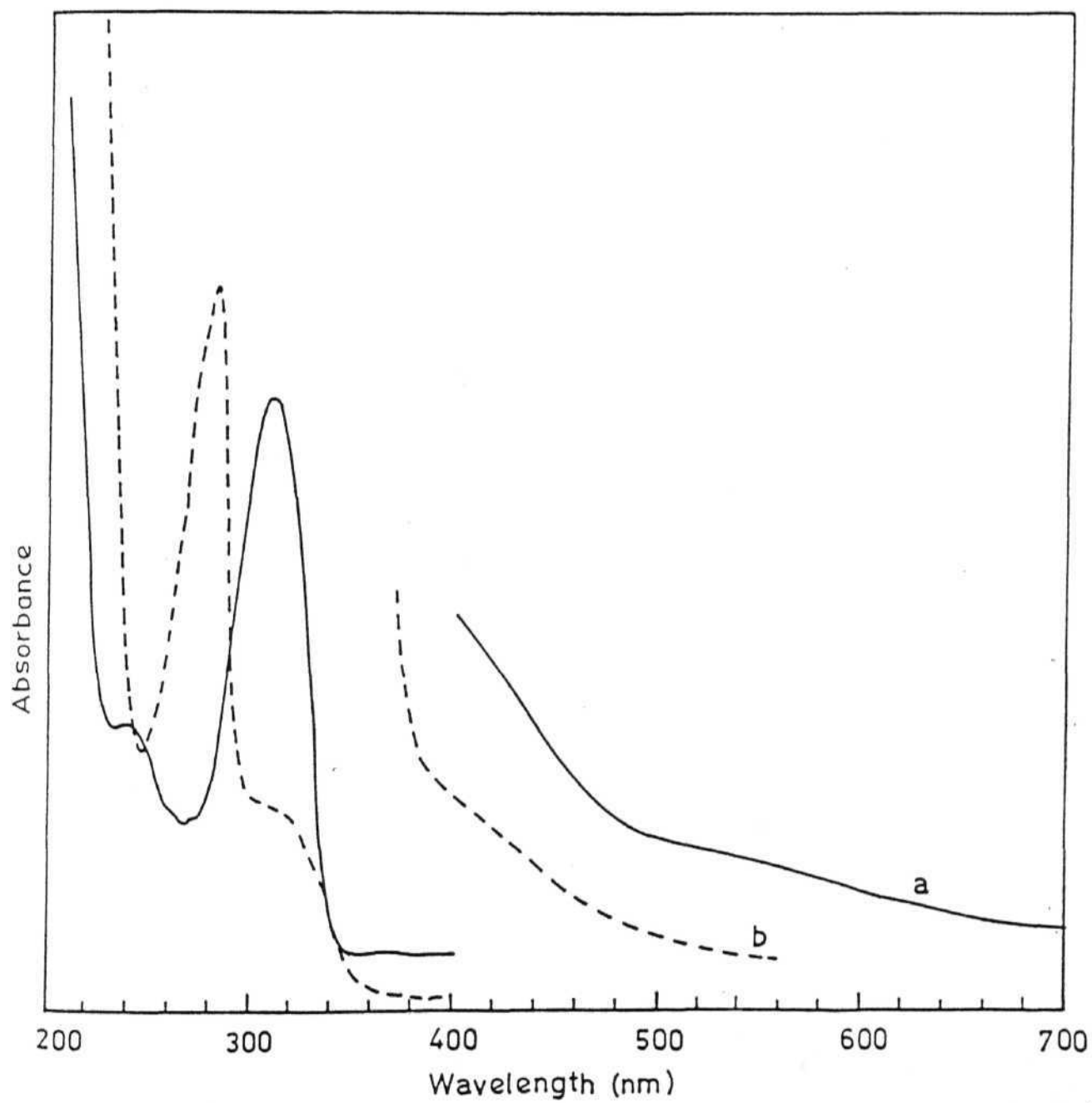


Figure 3: Electronic spectra of persulphate oxidised solutions of (a) Ag(dmbp)NO_3 , (b) Ag(dmp)NO_3 .

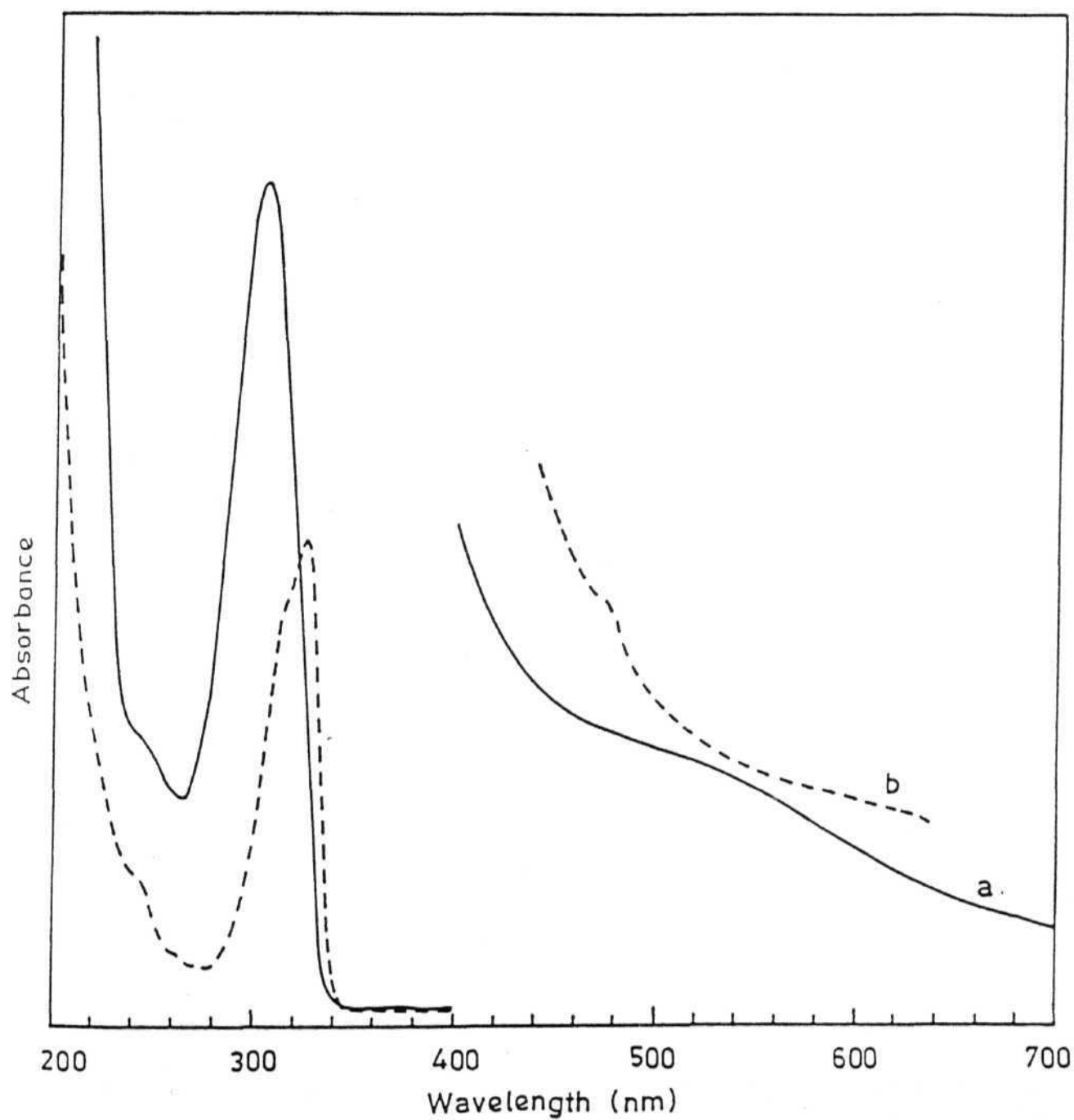


Figure 4: Electronic spectra of oxidised solutions of (a) $\text{Ag}(\text{tmbp})_2\text{NO}_3$, (b) $\text{Ag}(\text{daf})\text{NO}_3$.

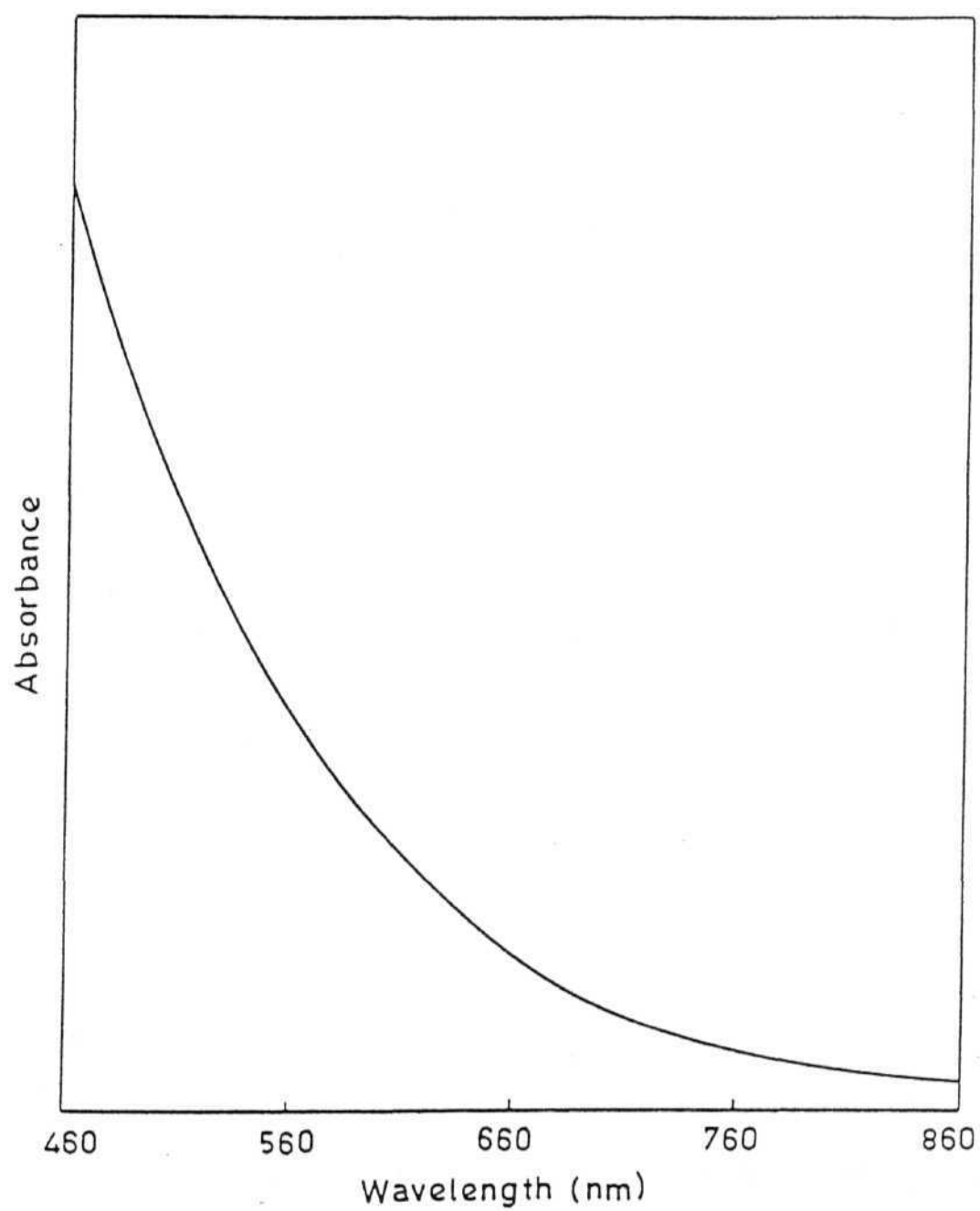


Figure 5: Electronic spectrum of oxidised solution of Ag(mmbp)NO_3 .

TABLE III ν_{\max} values (kK) for Ag(II) Complexes.

Complex	visible band	u.v. band
Ag(bpy) ₂ S ₂ O ₈ /HNO ₃ ^{a,c}	22.0	34.1
Ag(phen) ₂ S ₂ O ₈ /HNO ₃ ^{b,c}	25.56	31.1
Ag(dmbp)NO ₃ ⁺	18.9	31.6
Ag(dmp)NO ₃ ⁺	23.5	31.0
Ag(tmbp) ₂ ²⁺	19.1	32.8
Ag(daf)NO ₃ ⁺	22.9	30.8
Ag(mmbp)NO ₃ ⁺	~19	31.2

^aRef. 12, ^bRef. 9b, ^cIn these the dominant species are Ag(bpy)(NO₃)₂ and [Ag(phen)(NO₃)₂]⁺(Ref.8).

The four-coordinate species will have either planar, or more likely flattened tetrahedral structure. The distortion from planarity is expected to lower the energies of both the d-d band as well as the LMCT band. All the new complexes listed in (Table III) have considerably red-shifted LMCT band. For similar ligands the position of this band is a measure of the energy of the HOMO. Lowering of the HOMO energy is consistent with our observation that all these new species are much more unstable towards reduction. The redox potential of the stable $\text{Ag}(\text{bpy})_2^{2+}$ is $E^\circ = 1.453\text{V}^5$, whereas the present complexes are all rapidly reduced in solution implying a potential in the range 1.7 to 2.0 V.

Coming to the d-d bands, in square-planar or pseudotetrahedral geometry the highest orbital will be d_{xy} . The position of the remaining levels depends on the extent of the tetrahedral distortions as well as the amount of π -interactions involved. Since the degeneracy is completely removed (effective symmetry C_{2v} or D_{2h}) four d-d transitions are expected. When the distortion is small and there is considerable π -interaction involving d_{xz} and d_{yz} orbitals, the lowest energy band will correspond to d_{xz} or $d_{yz} \rightarrow d_{xy}$ excitation. Since we observe only one broad maximum in the visible region we assign it to this transition. The d_{z^2} and $d_{x^2-y^2} \rightarrow d_{xy}$ transition are most likely buried under the charge transfer band in the uv.

The d-d bands for dmbp, tmbp and mmbp complexes have considerably lower energies ($\sim 19\text{kK}$) compared to 22.0kK for the bpy complex. The red shift could be due to increased tetrahedral distortions as

well as due to the reduced ligand field provided by these ligands. The higher values of the d-d maximum for the dmp and daf complexes imply greater planarity of the coordination with these ligands. It may be noted that unlike the substituted bipyridyls the two rings in dmp and daf are constrained to remain coplanar or nearly coplanar thereby facilitating greater $d_{\pi} - p_{\pi}$ interaction. The difference in bonding involving dmbp and dmp are further discussed in sub-section 3.4 after presenting the e.s.r results.

3.3

E.s.r spectra of Ag(II) complex ions in frozen aqueous solution:-

Spectra of Ag(dmbp)NO_3 complex oxidised to give brown coloured aqueous solutions were measured at 124 K. The first derivative spectrum (Figure 6a) shows an axial character with 6 lines in the perpendicular region and unresolved signals in the parallel region. The six line pattern suggests the presence of two equivalent nitrogen atoms coordinated to the metal. Thus there is no evidence for the formation of a bis bidentate complex with four nitrogens coordinating. The parallel region clearly shows the presence, of at least three Ag(II) sites in the aqueous glass with g_{\parallel} values 2.34 (site I), 2.22 (site II) and 2.15 (site III). The site I with $g = 2.34$ corresponds to Ag^{2+} aquo ion⁸.

Figure 6b shows a spectrum of the above solution after aging the glass for a day at 77 K. The Ag^{2+} aquo ion had gained in intensity. Further, two weak signals were observed at higher g values at 2.46 (site IV) and 2.58 (site V). The different sites probably involve mixed ligand complex ions like $\text{AgL(H}_2\text{O)}_2^{2+}$, $\text{Ag(H}_2\text{O)}_2\text{NO}_3^+$ and $\text{Ag(NO}_3)_2\text{H}_2\text{O}$.

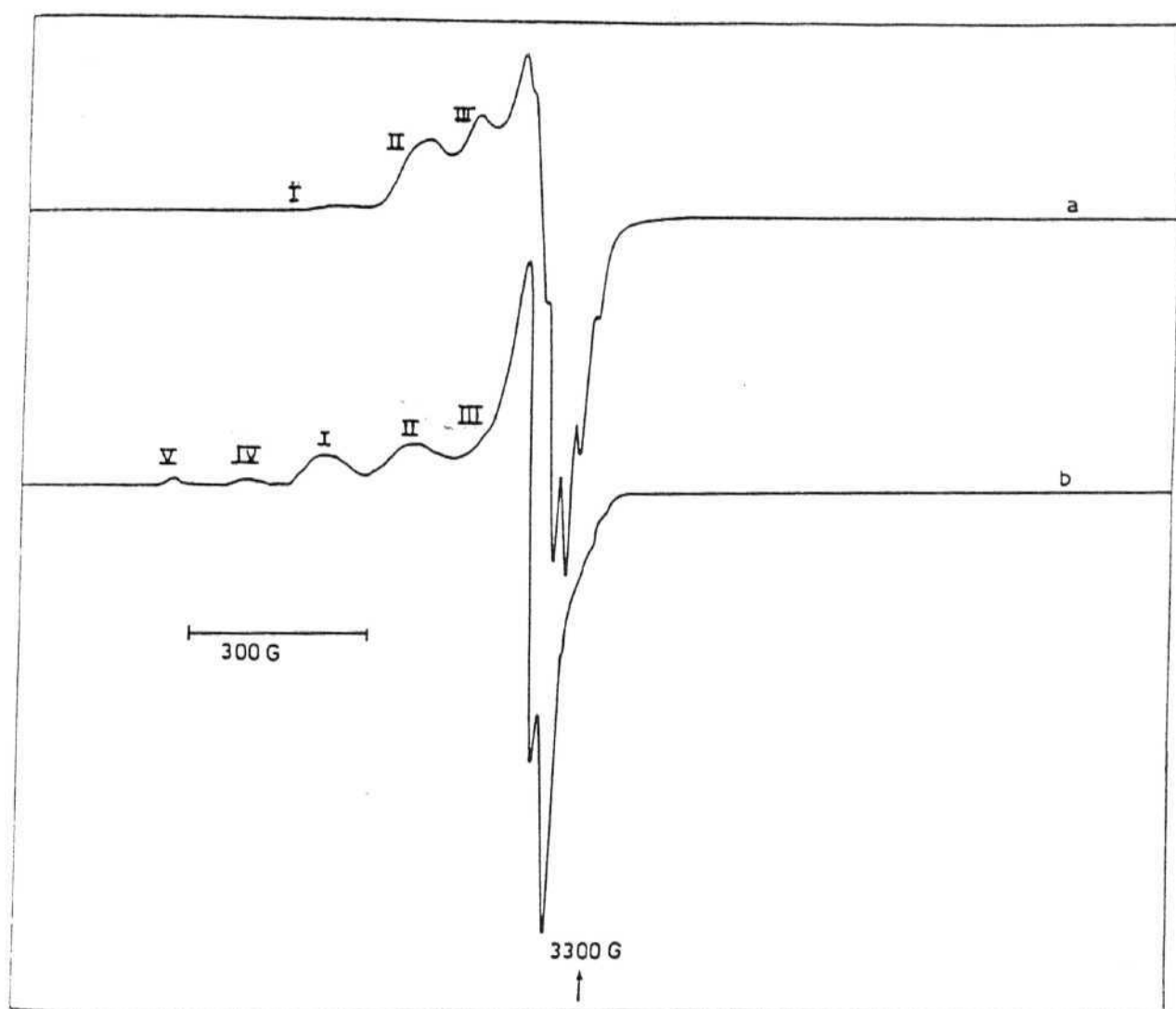


Figure 6: Frozen solution e.s.r spectra of the oxidised Ag(dmbp)NO_3 complex (a) freshly prepared solution (b) on aging the glass at 77K for a day.

The high g_{\perp} values of the weakly populated sites (IV and V) imply large orbital angular momentum induced by spin-orbit coupling which could result from greater distortion towards tetrahedron or from weak axial coordination by water or nitrate ion on an essentially planar complex.

Figure 7a shows a spectrum at 159 K for a pink aqueous solution obtained from $\text{Ag}(\text{tmbp})_2\text{NO}_3$. The signals were weak because of the low concentration obtained in this case. The line pattern at g_{\perp} is not fully resolved and g_{\parallel} is observed at 2.24 similar to the above complexes. An approximately six line pattern about g_{\perp} can be observed suggesting the formation of $\text{Ag}(\text{tmbp})\text{NO}_3^+$ or $\text{Ag}(\text{tmbp})(\text{NO}_3)_2$ species in solution with only two equivalent nitrogens coordinating.

Figure 7b shows a spectrum of brown coloured aqueous solution of $\text{Ag}(\text{mmbp})\text{NO}_3^+$ at 183 K. The solution shows a clear six line pattern about g_{\perp} and a broad signal at $g_{\parallel} = 2.24$ again suggesting two equivalent nitrogens coordinating to the metal ion.

Thus it can be concluded that in all cases the complex species contain only one aromatic ligand. The e.s.r. spectrum for oxidised solution of the daf complex could not be recorded as the signals were too weak.

3. 4

E.s.r. spectra of $[\text{Ag}(\text{dmbp})\text{NO}_3]\text{PF}_6 \cdot \text{NH}_4\text{PF}_6$ and $[\text{Ag}(\text{dmp})\text{NO}_3]\text{PF}_6 \cdot \text{NH}_4\text{PF}_6$:-

Solid $[\text{Ag}(\text{dmbp})\text{NO}_3]\text{PF}_6 \cdot \text{NH}_4\text{PF}_6$ and $[\text{Ag}(\text{dmp})\text{NO}_3]\text{PF}_6 \cdot \text{NH}_4\text{PF}_6$ complexes show highly resolved e.s.r. spectra at room temperature.

The light brown coloured complexes exhibit 8 lines

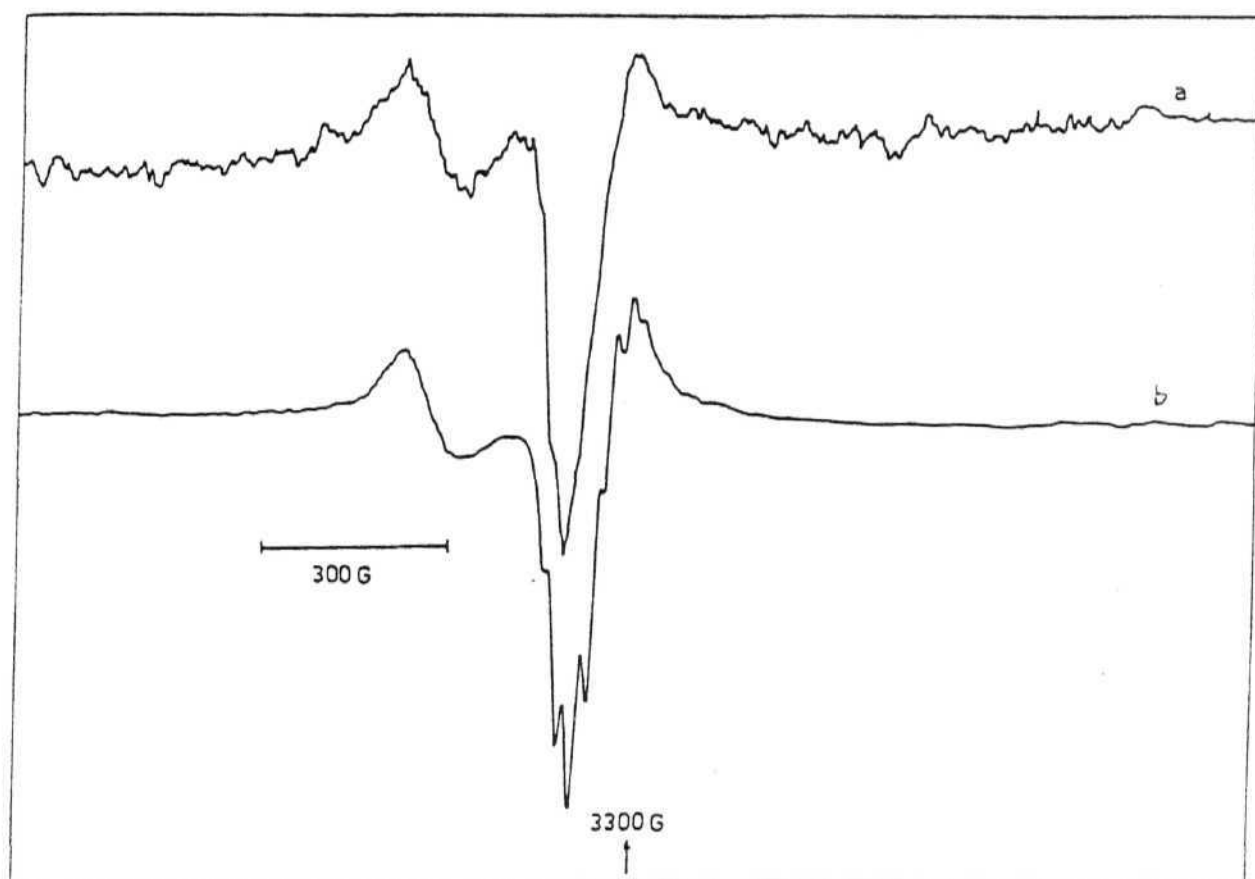


Figure 7: E.s.r spectra of the oxidised aqueous solution of (a) $\text{Ag}(\text{tmbp})_2\text{NO}_3$ at 159K, (b) $[\text{Ag}(\text{mmbp})\text{NO}_3]^+$ at 183K.

about $g_{||}$ and 7 lines about g_{\perp} for the dmbp complex and 8 lines about $g_{||}$ and 6 lines about g_{\perp} in the case of dmp complex. The resolution is slightly improved when the temperature is lowered (Figures 8 and 9). The former spectrum implies

$$A_{||}(\text{Ag}) \cong 3A_{||}(\text{N})$$

and

$$A_{\perp}(\text{Ag}) \cong 2 A_{\perp}(\text{N}) \quad \dots 5.$$

while for the latter we have

$$A_{||}(\text{Ag}) \cong 3A_{||}(\text{N})$$

and

$$A_{\perp}(\text{Ag}) \cong A_{\perp}(\text{N}) \quad \dots 6.$$

As discussed in sub-section 2.5, the $A_{||}(\text{N})$ and $A_{\perp}(\text{N})$ are related to the A and B components of nitrogen hyperfine tensor, where A is along the Ag-N bond directions, by the following relation

$$A_{||}(\text{N}) = B \text{ and } A_{\perp}(\text{N}) = \frac{1}{\sqrt{2}}(A^2 + B^2)^{1/2} \quad \dots 7.$$

The spin Hamiltonian parameters obtained by computer simulation are given in Table IV.

3. 4. 1

Theoretical analysis of e.s.r. spectra:-

While the symmetry of the AgN_2O_2 moiety cannot be higher than $C_{2v}(x)$, as is often the case, the electronic structure may be described in terms of $D_{2h}(\text{planar})$ or $C_{2v}(z)$ (pseudotetrahedral) point groups. The higher values of the transition energies and greater delocalisation of the odd electron are responsible for the reduced

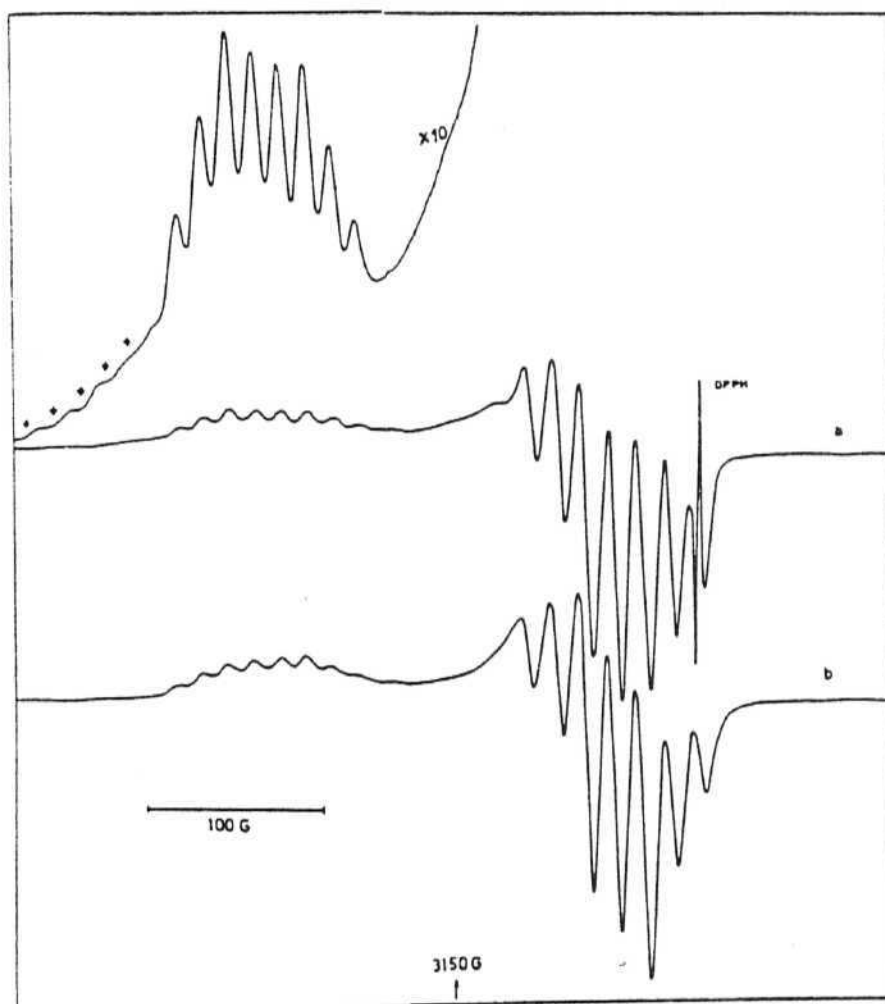


Figure 8: E.s.r spectra of the double salt
 (a) $(\text{AgdmbpNO}_3)\text{PF}_6 \cdot \text{NH}_4\text{PF}_6$ at 112K.

The weak signals, shown by the asterisk, on the low field side of the amplified portion are probably due to a weakly populated chemically inequivalent Ag(II) site (b) Computer simulated spectrum.

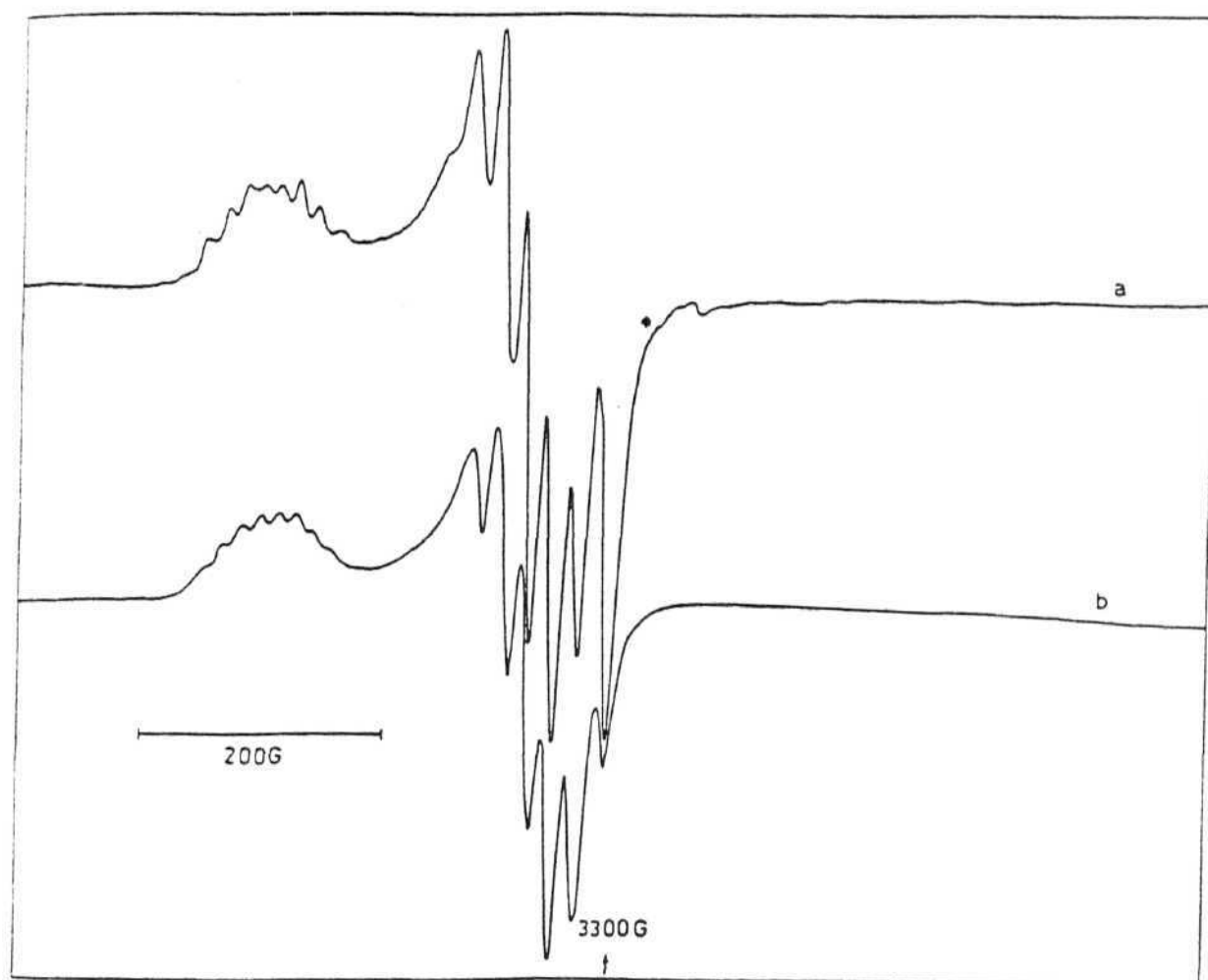


Figure 9: E.s.r spectra of the double salt (a) $(\text{AgdmpNO}_3)\text{PF}_6 \cdot \text{NH}_4\text{PF}_6$ at 149K, asterisk shows an unidentified organic radical which was present in the free ligand, dmp, superimposed on the highest-field line of the experimental spectrum. (b) Computer simulated spectrum.

Table IV. E.s.r. parameters from computer fit spectra.

Complex	$g_{ }$	g_{\perp}	$10^4 A_{ } (^{107,109}Ag)$ (cm^{-1})	$10^4 A_{\perp} (^{107,109}Ag)$ (cm^{-1})	$10^4 A(^{14}N)$ (cm^{-1})	$10^4 B(^{14}N)$ (cm^{-1})
$[Ag(dmbp)NO_3]PF_6 \cdot NH_4PF_6$	2.165	2.032	45.0	30.0	16.0	14.6
$[Ag(dmp)NO_3]PF_6 \cdot NH_4PF_6$	2.194	2.037	47.5	24.0	25.0	15.8

anisotropy in the case of silver(II) complexes compared to similar complexes of copper(II). Among the silver(II) complexes of nitrogen heterocyclic ligands the dmp and dmbp complexes have the smallest g-anisotropy. On the other hand, they have rather small ^{14}N hyperfine splittings. Therefore, the extensive σ - and π - delocalisation implied by the small g-anisotropy is mainly taking place into the chelating NO_3^- ligand. The molecular orbital containing the odd electron (the HOMO) can be written as,

$$\psi_1 = \beta_1 d_{xy} - \beta_1' \phi_{L1} \quad \dots 8.$$

where $\beta_1' \phi_{L1} = C_1 \phi_{\text{NN}} + C_2 \phi_{\text{NO}_3^-}$ with $C_2^2 > C_1^2$.

The other molecular orbitals which are coupled to the HOMO via spin-orbit interaction are

$$\begin{aligned} \psi_2 &= \beta_2 d_{x^2-y^2} - \beta_2' \phi_{L2} \\ \psi_{3,4} &= \epsilon d_{xz, yz} - \epsilon' \phi_{L3, 4} \end{aligned} \quad \dots 9.$$

The experimental spin-Hamiltonian parameters can be related to the characteristics of the electronic state of the system using the Abragam-Pryce Hamiltonian.³² The following equations, based on the second-order perturbation treatment, then connect the experimental numbers to the molecular parameters.

$$\begin{aligned} g_{||} - g_e &= \Delta g_{||} \\ g_{\perp} - g_e &= \Delta g_{\perp} \\ A_{||} &= A_F + 2 A_D + A_{||}^{(1)} \\ A_{\perp} &= A_F - A_D + A_{\perp}^{(1)} \end{aligned} \quad \dots 10.$$

where $g_e = 2.0023$ is the free electron g-value. The significance of the various terms in the above equations are briefly discussed below.

(i) $\Delta g_{||}$ and Δg_{\perp} : These quantities measure the deviation of the proposed g-values from the free electron value. In an electronically non-degenerate state ($L=0$) the g-anisotropy arises due to mixing of the excited state into the ground state by spin-orbit interaction. Using perturbation theory, and retaining only terms in the first power of the interaction, these quantities are given as

$$\begin{aligned}\Delta g_{||} &= -8 E_{||} k_{||} \\ \Delta g_{\perp} &= -2 E_{\perp} k_{\perp}\end{aligned}\quad \dots 11.$$

where

$$\begin{aligned}E_{||} &= \lambda / (E_1 - E_2), \\ E_{\perp} &= \lambda / (E_1 - E_{3,4})\end{aligned}\quad \dots 12.$$

E_1 , E_2 , E_3 and E_4 are the energies of the appropriate molecular orbitals and λ is the spin-orbit coupling constant. $k_{||}$ and k_{\perp} are the covalency reduction factors which are functions of the overlap integral, S and a quantity, T which is related to the orbital angular momentum matrix elements of the ligand part of the molecular orbitals.

$$\begin{aligned}k_{||} &= \beta_1^2 \beta_2^2 \{1 - (\beta_1'/\beta_1)S_1 - (\beta_1'\beta_2'/2\beta_1\beta_2)T\} \\ k_{\perp} &= \beta_1^2 \epsilon^2 \{1 - (\beta_1'/\beta_1)S_1 - (\beta_1'\epsilon'/2\beta_1\epsilon)T\}\end{aligned}\quad \dots 13.$$

Since λ is negative for a d^9 system, equations (11) and (12) imply that $g_{||}$ and g_{\perp} will be greater than g_e . $g_{||}$ deviates from g_e due to mixing of the $|d_{x^2-y^2}\rangle$ state, and g_{\perp} deviates from g_e due to mixing of $|d_{xz}\rangle$ and $|d_{yz}\rangle$ states into the ground state derived from $|d_{xy}\rangle$. The deviation is proportional to the spin-orbit coupling constant and is inversely proportional to the energy separation between the ground state and the respective excited states connected by the spin-orbit interaction. Equation (13) implies that the anisotropy is reduced by covalent delocalisation. It may be noted that spin-orbit coupling due to ligand atoms is negligible due to the much smaller values of λ (N or O).

(ii) A_F is the Fermi contact interaction constant and it is an isotropic term contributing equally to $A_{||}$ and A_{\perp} . This interaction arises due to the presence of unpaired electron (spin) density, $\phi_{\text{spin}}^2(0)$, at the nuclei. $\phi_{\text{spin}}^2(0)$ can be either due to s contribution (5s in the case of Ag) to the HOMO via configuration interaction or, more importantly, due to core polarisation. In simple terms polarisation of the inner s-shells takes place because the unpaired electron in 4d orbital (\uparrow spin) repels one of the two electrons (the \uparrow spin electron) in the s-shell less than the other. In other words the exchange interaction between the electrons having identical spins (\uparrow or α) leaves a net β spin density at the nucleus. The contact contribution is given as,

$$A_F = \frac{8\pi}{3} g_e \beta_e g_n \beta_n \{ |\phi_{\uparrow}(0)|^2 - |\phi_{\downarrow}(0)|^2 \} \quad \dots 14,$$

Where g_e and g_n are electronic and nuclear Lande factors, and β_e and β_n are electronic and nuclear Bohr magnetons respectively.

For convenience, we define,

$$\beta_1^2 \kappa = -\left(\frac{8\pi}{3}\right) \{ |\phi_{\uparrow}(0)|^2 - |\phi_{\downarrow}(0)|^2 \} / \langle r^{-3} \rangle_{dxy} \quad \dots 15.$$

$$\text{and} \quad P = g_e \beta_e g_n \beta_n \langle r^{-3} \rangle_{dxy} \quad \dots 16.$$

so that,

$$A_F = -\beta_1^2 P \kappa \quad \dots 17.$$

It is clear that in the free atom or ion (i.e., in the absence of covalency) $A_F = -P\kappa$. Both P and κ can be obtained for atoms and ions by unrestricted Hartree-Fock calculations³³. Accurate calculations for molecules are more involved, and approximation methods like X- α have been used for this purpose with some success³⁴.

(iii) A_D is the dipolar contribution to hyperfine splitting and is primarily responsible for the anisotropy in the observed splittings. Its value depends on the d-orbital containing the unpaired electron. For the present case (d_{xy} ground state), we have

$$A_D = (-2/7) \beta_1^2 P \quad \dots 18.$$

Here again, covalency reduces the anisotropy due to the factor β_1^2 (< 1) in equation (18), and also due to the reduction in the value of P . P is reduced by covalency because the d orbital becomes more diffuse due to reduction in effective nuclear charge of the metal.

(iv) $A_{||}^{(1)}$ and $A_{\perp}^{(1)}$ are the first order corrections to hyperfine splitting due to spin-orbit interaction. These corrections are related to the g-anisotropy by the following equation,

$$A_{||}^{(1)} = (\Delta g_{||} + 3/7 \Delta g_{\perp})P = -8E_{||} P\beta_1^2 \beta_2^2 - (6/7)E_{\perp} P\beta_1^2 \epsilon^2 \quad \dots 19.$$

$$A_{\perp}^{(1)} = \frac{11}{14} \Delta g_{\perp} P = (-22/14)E_{\perp} P\beta_1^2 \epsilon^2 \quad \dots 20.$$

3. 4. 2

Interpretation of e.s.r. parameters of Ag(II) complexes of hetero-aromatic ligands:-

Using equation (10) all the bonding parameters for the Ag(II) complexes listed in Table V, have been calculated and are tabulated in Table VI. It is seen that the odd electron is delocalised to the extent of 35-50%. There is also extensive π -interaction involving d_{xz} and d_{yz} orbitals.

The lower values of the d-d transition energies for the dmbp complex imply a greater tetrahedral distortion compared to the dmp complex. This distortion as well as a possible twisting of the bipyridyl ligand about the C-C single bond will considerably relieve the steric strain in Ag(dmbp)NO_3^+ . A greater degree of metal-ligand interaction is therefore expected and it is reflected in the lesser value of β_1^2 for this compound. The Fermi contact contribution to hyperfine splitting varies from 0.0033 to 0.0041 cm^{-1} for the systems listed in Table VI. The contact interaction is very sensitive to 5s contribution which in turn is usually a strong function of metal-ligand bond length³⁴. In the absence of structural data and theoretical estimates no attempt will be made here to explain the observed variation in A_F .

Coming to the nitrogen hyperfine splitting, the two components, A and B can be written as,

$$A = f_{\sigma s} a_s + 2f_{\sigma p} a_p + 2A_D'$$

$$B = f_{\sigma s} a_s - f_{\sigma p} a_p - A_D' \quad \dots 21.$$

Table V. E.s.r. parameters for Ag(II) Complexes.

Complex	$g_{ }$	g_{\perp}	$A_{ }(Ag)$ ($\times 10^{-4} \text{ cm}^{-1}$)	$A_{\perp}(Ag)$ ($\times 10^{-4} \text{ cm}^{-1}$)	$A(N)$ ($\times 10^{-4} \text{ cm}^{-1}$)	$B(N)$ ($\times 10^{-4} \text{ cm}^{-1}$)	E_{xy} (kK)	$E_{xz,yz}$ (kK)	Ref.
$[Ag(dmbp)NO_3]PF_6 \cdot NH_4PF_6$	2.165	2.032	45.0	30.0	16.0	14.6	30.4	18.9	this work
$[Ag(dmp)NO_3]PF_6 \cdot NH_4PF_6$	2.192	2.031	47.5	24.0	25.0	15.8	31.1	23.5	this work
$Ag(bpy)_2S_2O_8$	2.210	2.047	42.2	26.0	21.1	30.1	28.0	22.0	14b, 12
$Ag(phen)(NO_3)_2$	2.214	2.048	34.0	23.5	23.5	20.5	31.1	25.6	8, 9b
$Ag(py)_4S_2O_8/Cd(py)_4S_2O_8$	(A) 2.204	2.042	18.0	34.5	21.0	19.6	22.0	20.4	8, 4a
	(B) 2.18	2.04	34.0	22.0	17.0	22.0	22.0	20.4	37, 4a

Table VI: Calculated bonding parameters^a:

Complex	$\Delta g_{ }$	Δg_{\perp}	$10^{-3}E_{xy}$ (cm^{-1})	$10^{-3}E_{xz,yz}$ (cm^{-1})	$10^4 A_F$ (cm^{-1})	$10^4 A_D$ (cm^{-1})	$10^4 A_{ }$ (cm^{-1})	$10^4 A_{\perp}^{(1)}$ (cm^{-1})	β_1^2	β_2^2	ϵ^2	κ
[Ag(dmbp)NO ₃](PF ₆) ₄	0.163	0.030	30.4	18.9	41.1	8.9	-13.9	-2.2	0.49	0.84	0.46	1.32
[Ag(dmp)NO ₃](PF ₆) ₄	0.192	0.035	31.1	23.5	38.6	12.3	-15.6	-2.2	0.68	0.71	0.42	0.896
[Ag(bpy) ₂ S ₂ O ₈] (in frozen HNO ₃)	0.208	0.045	28.0	22.0	39.0	10.1	-17.3	-2.9	0.56	0.84	0.62	1.10
Ag(phen)(NO ₃) ₂ (in frozen HNO ₃)	0.212	0.046	31.1	25.6	34.4	8.1	-14.9	-2.8	0.45	1.00	0.89	1.22
Ag(py) ₄ S ₂ O ₈ /Cd(py) ₄ S ₂ O ₈	(A)	0.202	0.040	22.0	20.4	-14.4	18.0	-14.8	-2.1	^b 0.32	0.24	-0.228
		(B)	0.178	0.038	22.0	20.4	33.0	-16.0	-2.6	0.47	0.74	1.12
Ag(TPP)/(H ₂ O)Zn(TPP) ^c		0.106	0.035	36.7	43.7	48.1	12.0	-9.6	-2.1	0.66	0.51	1.15

^aCalculated with $\lambda = -1840 \text{ cm}^{-1}$, $P = -63.0 \times 10^{-4} \text{ cm}^{-1}$, $S_1 = 0.1$, $S_2 = 0.0$, $S_{3,4} = 0.05$, $T = 0.33$. $A_{||}$, A_{\perp} were taken to be positive, except for Ag(py)₄S₂O₈/Cd(py)₄S₂O₈ (A) for which the results quoted are for $A_{||} > 0$, $A_{\perp} < 0$.

^bNot physically meaningful. Other combinations for $A_{||}$ and A_{\perp} also fail to give meaningful results.

^cRef. 35(e.s.r, ENDOR), ref. 36 (theoretical estimates of transition energies).

where $a_s = (8\pi/3)g\beta g_n \beta_n |\psi_0|^2$ and $a_p = (2/5)g\beta g_n \beta_n \langle r^{-3} \rangle_{2p}$, the atomic values being 0.05179cm^{-1} and 0.00155cm^{-1} respectively³³. The correction due to direct dipolar interaction A_D' is of the order of $1 \times 10^{-5} \text{cm}^{-1}$ and can be neglected. The quantities f_{os} and f_{op} are the 2s and $2p_o$ electron densities for the HOMO. This data has often been used in the past to estimate the s:p hybridisation ratio for the nitrogen σ orbital and even to calculate bond angles^{14b}. However, the ratio depends on the difference, $A - B$, which, due to the proximity of A and B will often be subject to large errors. Further, the appreciable difference in the energies of 2s and 2p and also any significant core polarisation in the bonded nitrogen atom can further complicate the analysis. For Ag(dmbp)NO_3^+ and Ag(dmp)NO_3^+ we get 1.0 and 0.2 respectively for the ratio f_{os}/f_{op} . The small s:p ratio for the dmp complex is evident in the unusually high anisotropy in the nitrogen hyperfine splitting. We postulate that the large p contribution relative to s is due to a much longer Ag-N bond which favours greater interaction of the silver σ -orbitals with the nitrogen $2p_o$ orbital compared to the less diffuse 2s component.

A good system to compare with the simple N-heterocyclic ligands is porphyrins, which readily induce disproportionation of silver (I) forming silver (II) complexes with square-planar N_4 coordination. Single crystal ENDOR studies on Ag(TPP) doped into $(\text{H}_2\text{O})\text{Zn(TPP)}$ yielded very accurate metal and ligand hyperfine tensors for this system³⁵. Subsequently, χ_α - calculations have also been reported³⁶. The data from our analysis of the g and ^{109}Ag hyperfine splitting are included in (Table VI). It has been pointed out that first order

perturbation treatment of g and metal hyperfine tensors gives less reliable bonding parameters than a zeroth order analysis of the ^{14}N hyperfine data, and the latter procedure is to be preferred whenever precise ^{14}N coupling parameters are available³⁵. We do find that the bonding coefficients are sensitive to transition energies. The low value of β_2^2 (0.51) implying greater in-plane π -bonding than σ - and out-of-plane π -bonding is unrealistic. β_2^2 is raised to 0.75 when E_{xy} is raised by about 50%, while the other coefficients are not significantly modified. What is clear from the comparison of data in (Table VI) is that the higher values of d-d transition energies in Ag(TPP) compared to other compounds are responsible for its lower g -anisotropy as well as the reduced magnitude of spin-orbit contribution to hyperfine splitting ($A_{||}^{(1)}$ and $A_{\perp}^{(1)}$). Since the latter contributions are negative, the experimental hyperfine splitting values are considerably higher for Ag(TPP).

Finally, it may be mentioned that the recent analysis⁸ of the Ag/Cd(py)₄S₂O₈ is likely to be in error with regard to the silver hyperfine splittings because their assignment leads to unreasonable bonding parameters and a negative A_F (Table VI). We tend to favour the earlier analysis³⁷. The difference between the two lies in counting the number of lines in the parallel region of the spectrum where 10 lines are expected if $A_{||}(\text{Ag}) = A_{||}(\text{N})$, and 11 lines if $A_{||}(\text{Ag}) = 2A_{||}(\text{N})$. However, we agree with Evans et al.⁸ that the nitrogen hyperfine splittings³⁷ have to be revised. The revised values are also included in (Table VI).

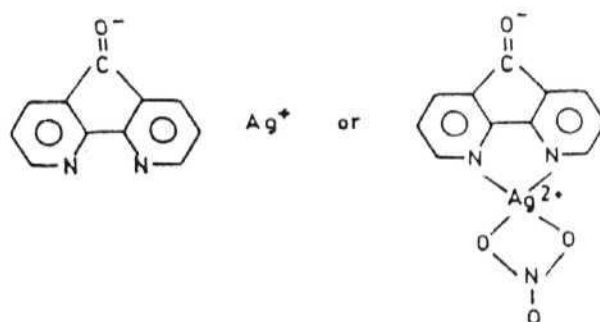
3. 5

E.s.r spectra of undiluted solid bivalent silver complexes:

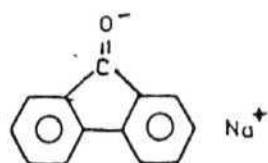
The dark brown coloured solids which precipitated on oxidation of

the $\text{Ag}(\text{NO}_3)_3$ complexes showed e.s.r. spectra corresponding to magnetically concentrated systems with rhombic g-tensor. The line widths are about 40 G implying that magnetic exchange interaction frequency is greater than $^{107,109}\text{Ag}$ hyperfine frequency ~ 150 MHz. They are shown in Figures (10) and (11). Figure 10(a) and (b) show the spectrum of $\text{Ag}(\text{dmbp})(\text{NO}_3)_2$ and $\text{Ag}(\text{dmp})(\text{NO}_3)_2$ respectively. The asterisk shows the presence of an unidentified organic radical which was seen also in the ligand. g values are $g_1=2.142$, $g_2=2.083$ and $g_3=2.047$ for the dmbp complex and $g_{||}=2.193$ and $g_{\perp}=2.048$ for dmp complex.

Figures 11a,b and c show the spectra of $(\text{AgLNO}_3)\text{PF}_6$ where L=mmbp, bpx and daf-one respectively. Figure 11c shows the spectrum of $[\text{Ag}(\text{daf-one})\text{NO}_3]\text{PF}_6$. In this spectrum an organic radical is present at $g = 2.0$. The anisotropic spectrum of $\text{Ag}(\text{II})$ was found to reduce in intensity on keeping the complex for a few days whereas the intensity of the organic radical increased. The radical is probably the anion radical



which is analogous to³⁸



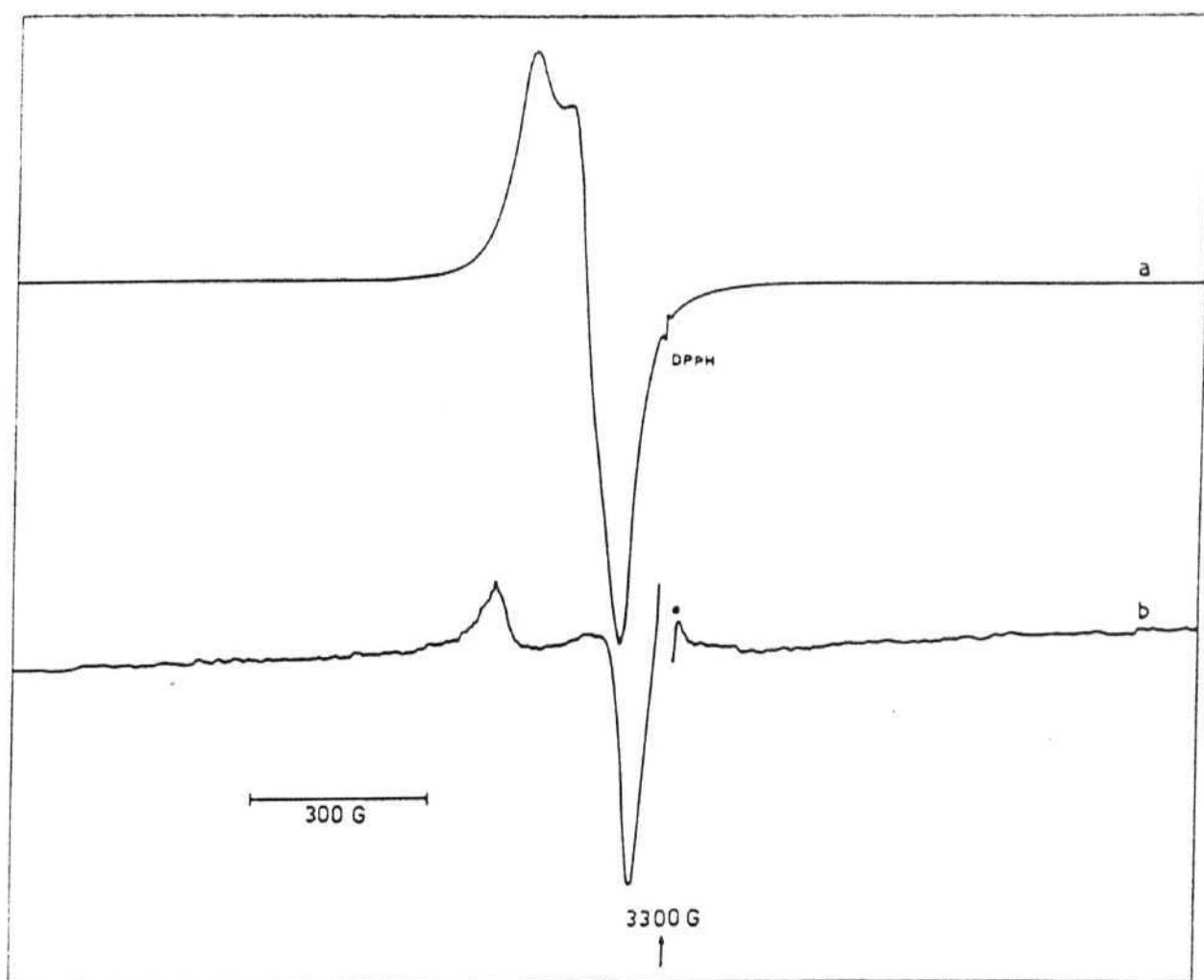


Figure 10: E.s.r spectra of solid complexes at room temperature (a) $\text{Ag(dmbp)(NO}_3)_2$ (b) $\text{Ag(dmp)(NO}_3)_2$, asterisk shows the signal from an unidentified radical.

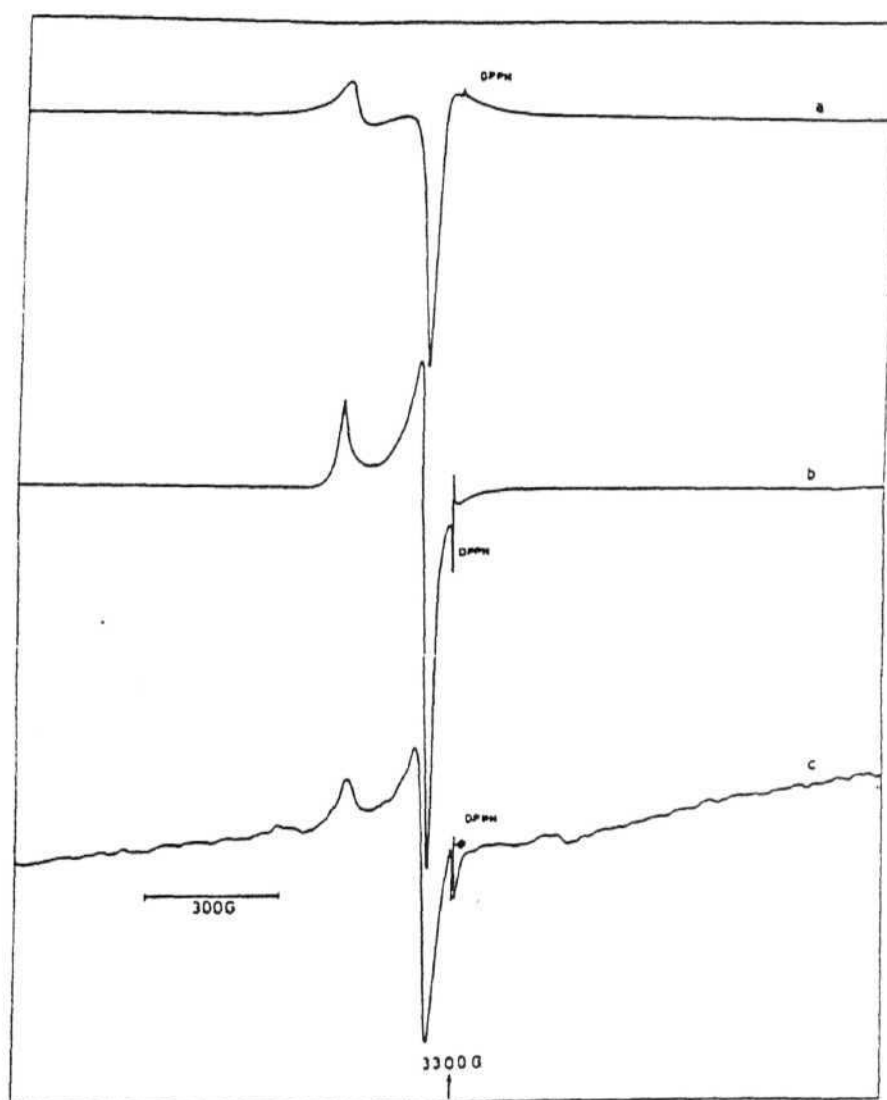


Figure 11: E.s.r spectra of solid complexes $[\text{AgLNO}_3]\text{PF}_6$ at room temperature (a) $\text{L}=\text{mmbp}$, (b) bpy (c) daf-one , the asterisk shows an unidentified organic radical.

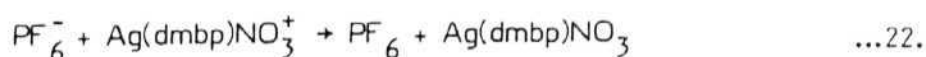
The experimental g-values for $\text{Ag(mmbp)NO}_3\text{PF}_6$ are $g_{||} = 2.18$ and $g_{\perp} = 2.049$, and for the daf-one complex $g_{||} = 2.16$ and $g_{\perp} = 2.045$.

3. 6

Observations on the solid state electron-transfer in $[\text{Ag(dmbp)NO}_3]$

$\text{PF}_6 \cdot \text{NH}_4\text{PF}_6$ -Formation of the hitherto unknown PF_6 radical (?):-

The highly resolved spectra from Ag(II) sites in the double salts shown in Figures 8 and 9 are observed only in freshly prepared samples. If the sample is exposed to the atmosphere it quickly takes up moisture and no e.s.r signal is seen after a few minutes. Even when sealed under dry nitrogen the signal intensity goes down drastically over a period of several days. In the case of $[\text{Ag(dmbp)NO}_3]\text{PF}_6 \cdot \text{NH}_4\text{PF}_6$, while the Ag(II) signal intensity decreases, a large number of new e.s.r lines are seen to appear on the wings of the Ag(II) spectrum, which continue to grow in intensity. Finally when the Ag(II) signals have completely disappeared the spectrum consists of large number of narrow (width = 8 G) lines spread over the field region 1000 G to 5800 G, as shown in Figure 12. The spectral width ($\sim 5000\text{G}$) allows us to exclude the possibility of a nitrogen containing radical or silver atom cluster as possible centres responsible for this spectrum. While the pattern in Figure 12 is uninterpretable, we propose that the signals arise from one or more radicals containing P and F atoms. The most reasonable candidate is the PF_6 radical formed by the electron transfer reaction,



This radical is unknown in the literature. The mechanism of formation viz., electron capture by a transition metal ion in an unstable oxidation

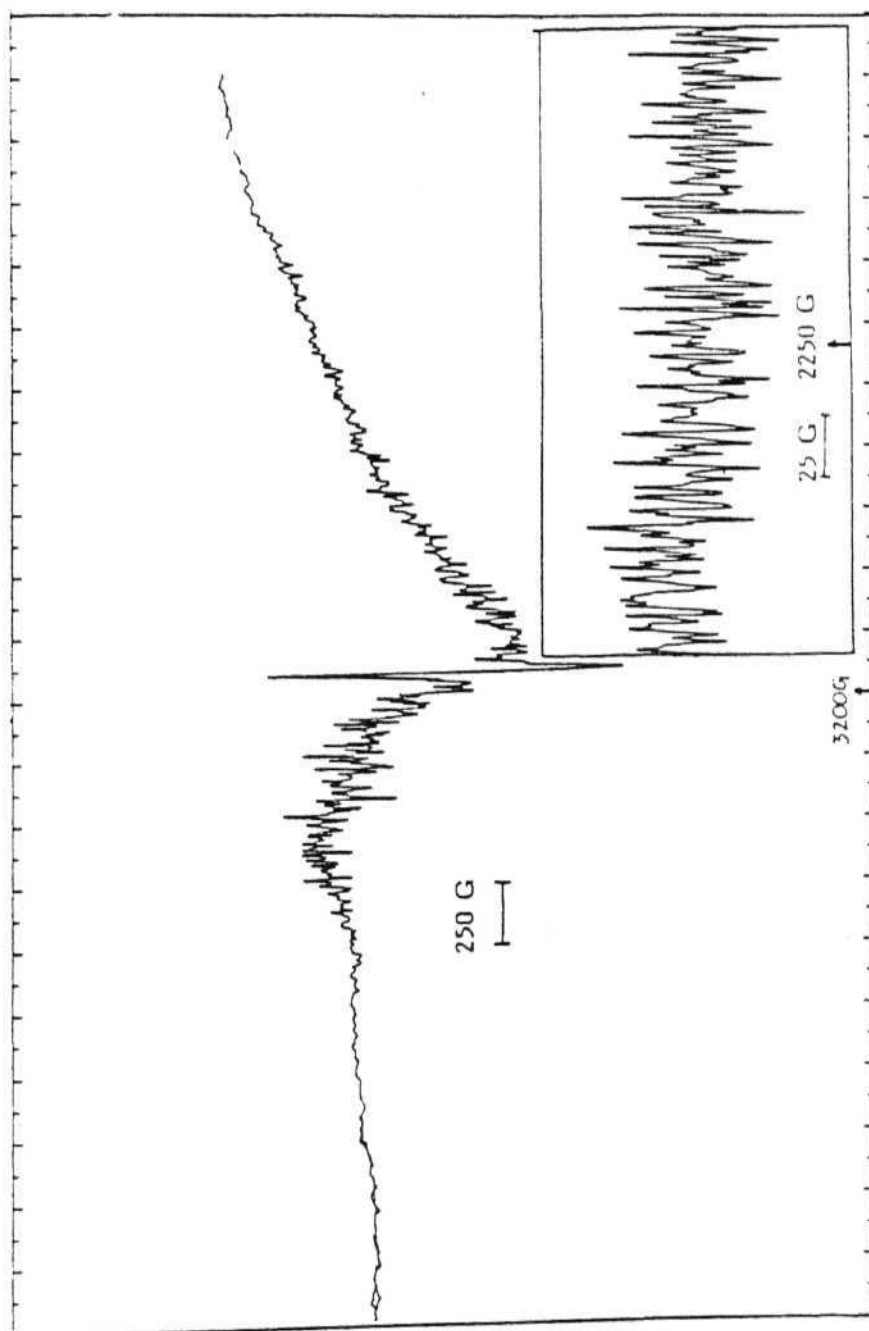


Figure 12: E.s.r spectra of radicals observed over the field region 1000G to 5800G. Insert shows enlarged field from 2000G to 2500G.

state is also unusual, if not unknown. The most popular method to prepare inorganic radicals is radiation damage of solids using uv, x-ray or γ -ray radiation. In the next sub-section the literature pertaining to radicals observed in PF_6^- salts by γ -irradiation is reviewed.

3. 6. 1

Review of the literature on radicals derived from PF_6^- salts:-

A survey of the literature suggested the formation of different radicals with the salts of PF_6^- ion. These salts are sometimes referred to as 'rotator solids' at room temperature due to the free rotation of the octahedral PF_6^- ion in the lattice³⁹. Upon γ -irradiation they give isotropic e.s.r. spectra.⁴⁰ NH_4PF_6 and KPF_6 on γ -irradiation were reported to generate FPO_2^- , PO_3^{2-} and PF_4 radicals⁴¹. The signals assigned to PF_4 were later shown to be due to PF_5^- . However the spread of the whole spectrum was only 1500 G with the lines split into interpretable spacings as shown in Figure 13. But it was stated that on γ -irradiation of single crystals of NH_4PF_6 uninterpretable spectrum was observed at low temperatures which was speculated to be due to different fragments taking up random orientations. Later the same authors have verified the formation of PF_5^- in place of PF_4 . However, there was no mention of the uninterpretable low temperature spectrum in the recent publication⁴² on γ -irradiated KPF_6 and KAsF_6 . They have reported the formation of PF_4 , PF_5^- , FPO_2^- , a geometrical isomer of PF_4 , a $\text{PF}_3\text{O}_{\text{eq}}^-$ or a possible alternative $\text{PF}_3(\text{OH})_{\text{eq}}^-$ in which hyperfine splitting due to the hydroxylic proton is unresolved. Weak spectra detected were assigned to geometrical isomers $\text{PF}_4\text{O}_{\text{ap}}^{2-}$ and $\text{PF}_4\text{O}_{\text{bs}}^{2-}$ of PF_5^- species. Another $\text{PF}_4(\text{OH})_{\text{ap}}^-$ was also thought to be isostructural to PF_5^- , where ap = apical,

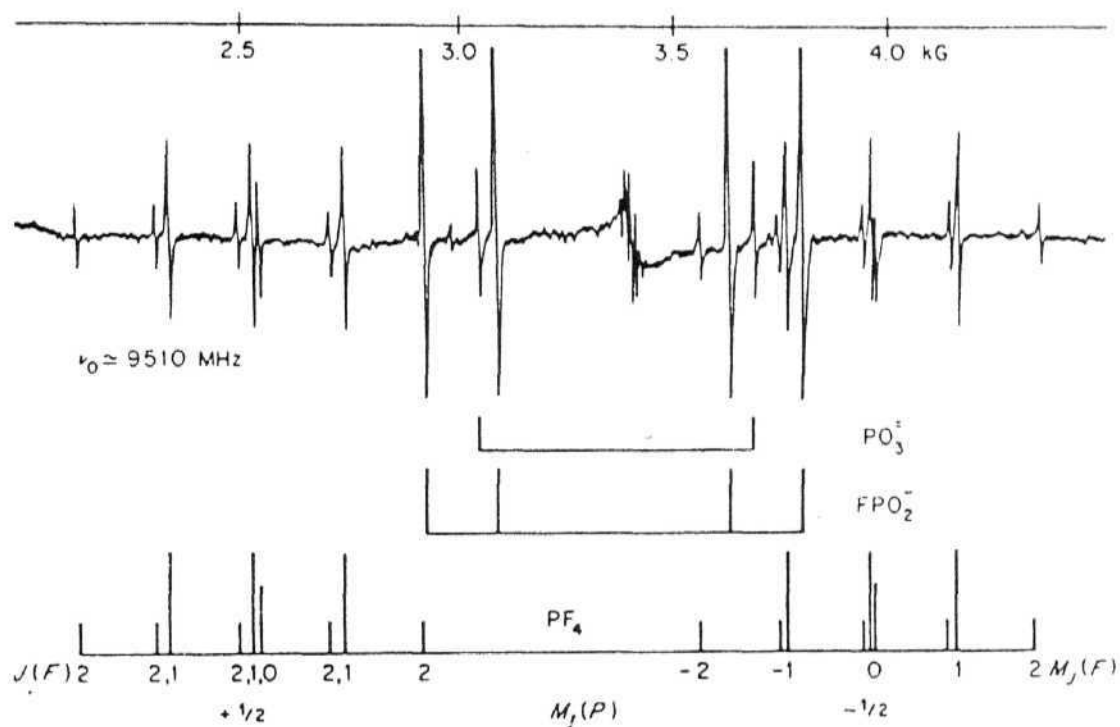


Figure 13. The e.s.r spectrum of a γ -irradiated single crystal of NH_4PF_6 . The three radicals produced have been attributed to PF_4 , FPO_2^- , and PO_3^- . The splittings of the PF_4 lines are due to second-order interactions. [Ref.41(a).] Here $J(F)$ refers to the total fluorine nuclear spin quantum number in the coupled representation.

eq = equatorial and bs = basal position.

We could not assign any of the lines in the observed spectrum to the above mentioned radicals. In the next sub-section some of the experiments performed in an attempt to simplify the spectrum are discussed.

3. 6. 2 **Attempts to simplify the spectrum:-**

In Fig.14, repetitive scan at lower modulation with different scan times are shown to check the reproducibility of the pattern. Figure 15 shows the 2900-3100 G region of the spectrum scanned at different scan times which show reproducibility of all the sharp lines. Figure 16 shows a spectrum at 2975-3025 G region with 32 mts. scan time along with an immediately repeated spectrum with almost all features reproduced.

Figure 17 shows spectra at 2000-2500 G at lower modulation with different scan times. From these studies we observed that the pattern is essentially reproducible if low modulations and long scan times (or small time constant) are employed. However, the pattern was found to change slowly as a function of time over several hours. The reason for this is not clear. One plausible explanation is modulation of the spectrum by very slow dynamics of the radical species.

The following experiments were carried out with a view to simplify the spectrum :

(a) The sample in the sealed tube was heated at about 60°C hoping to get a simpler isotropic spectrum. Eventhough there was no marked change in the clarity of the spectrum the exact details of the pattern had changed,

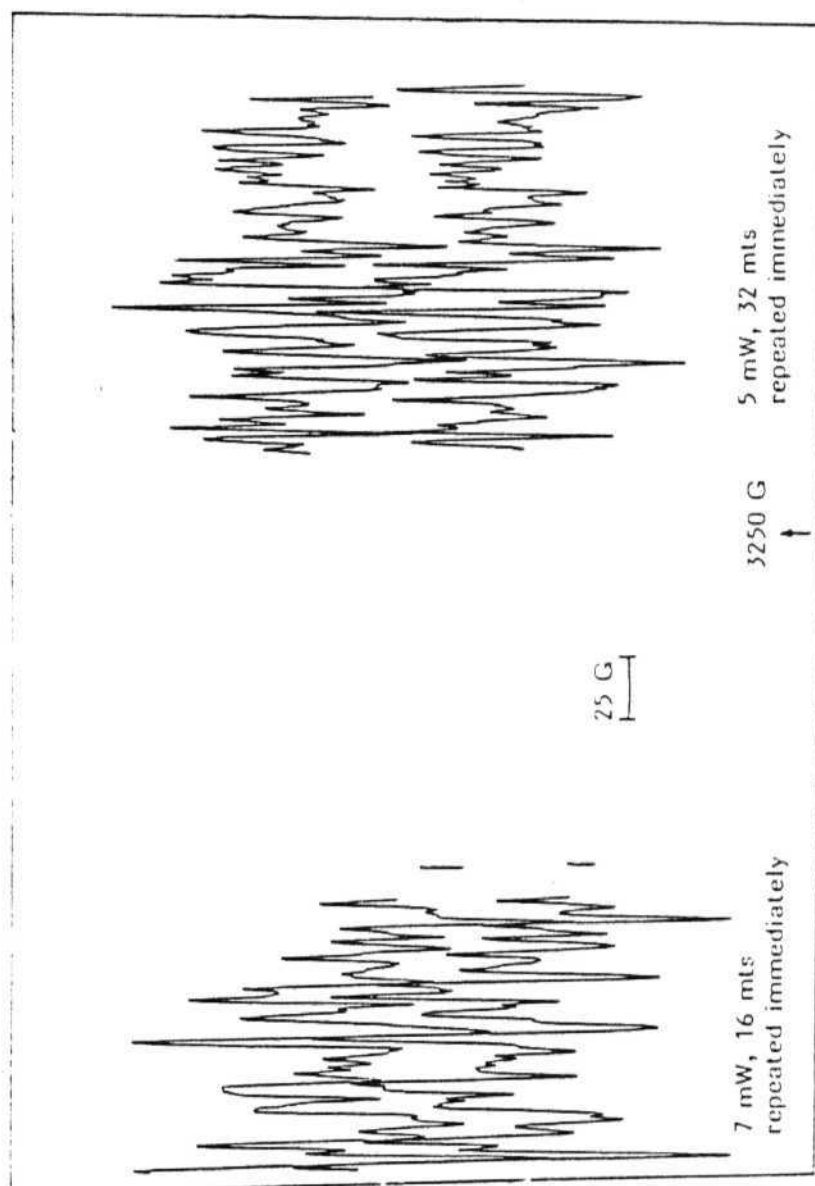


Figure 14: E.s.r spectrum of radical at lower modulation and different scan times.

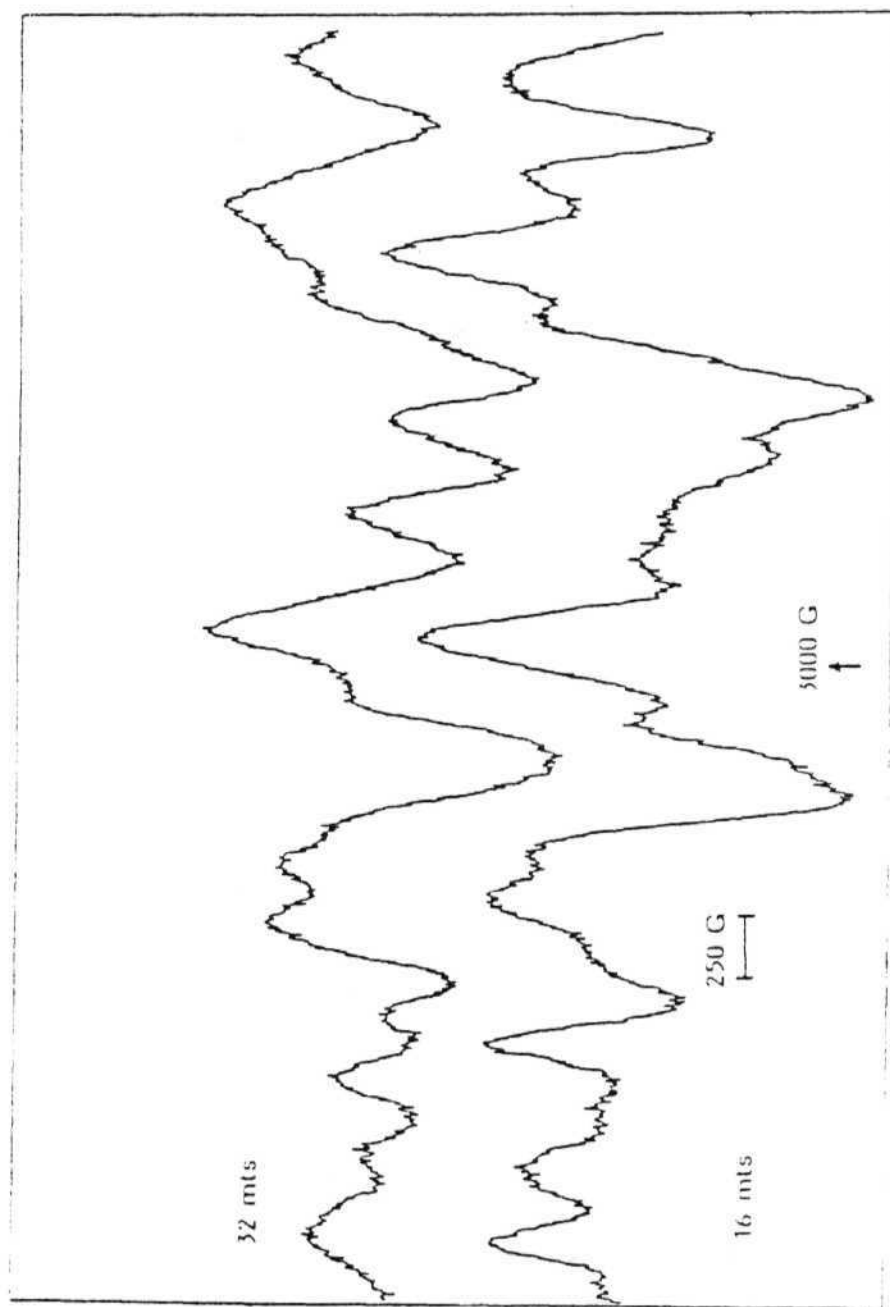


Figure 15: E.s.r spectrum of radical at 2900 - 3100G region.

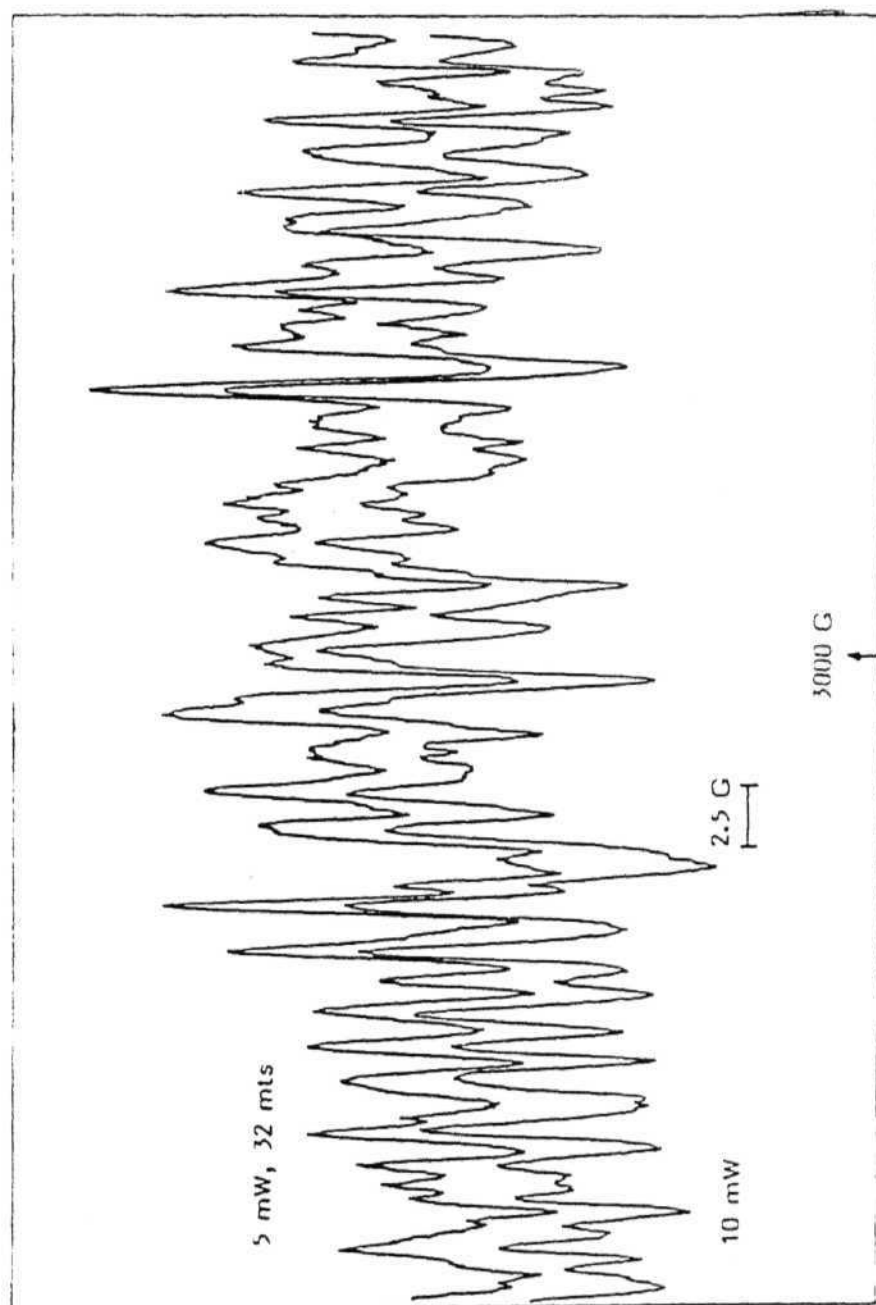


Figure 16: E.s.r spectrum of radical at 2975-3025G region.

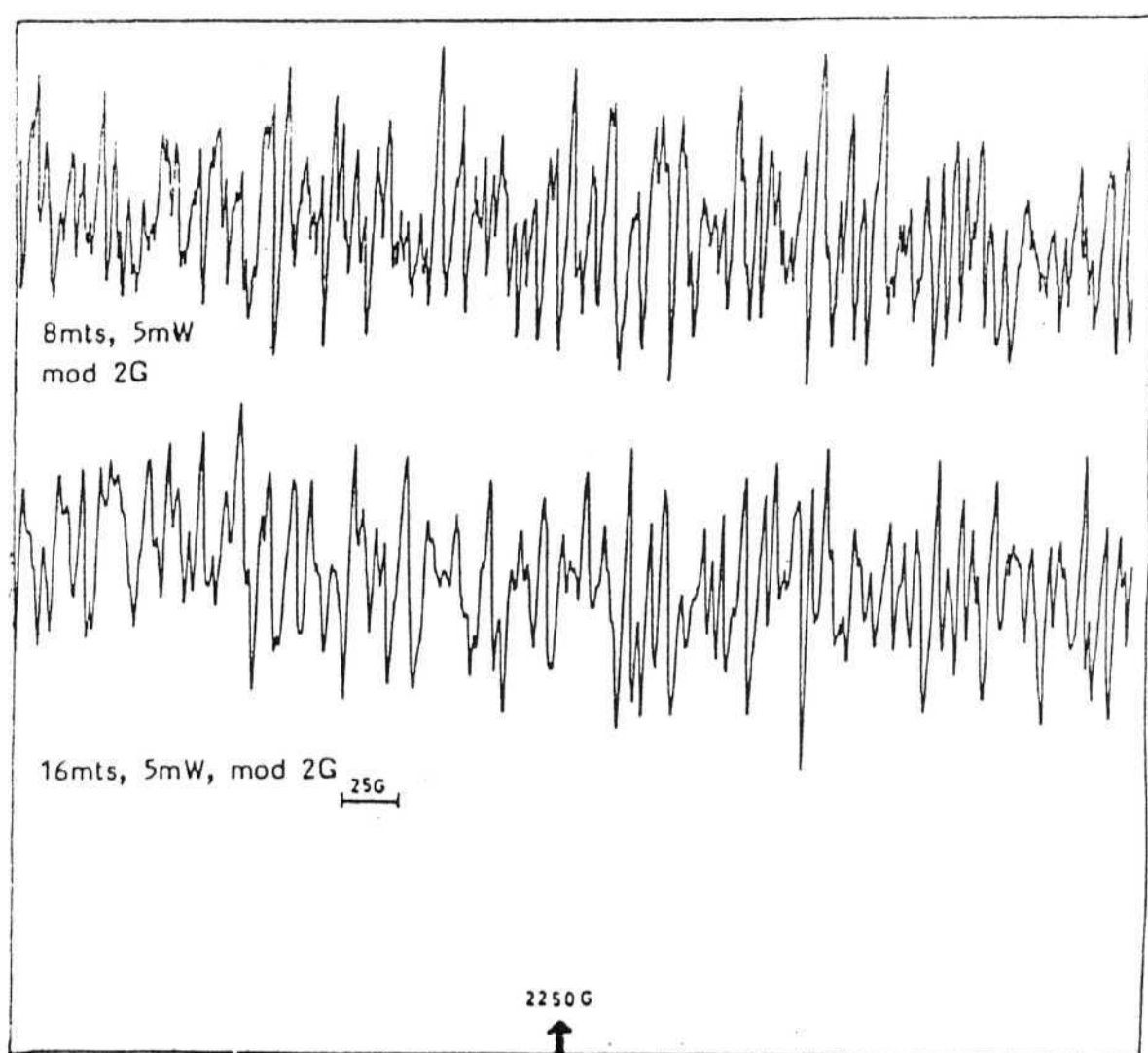


Figure 17: E.s.r spectrum of radical at 2000-2500G region.

- (b) The sample was removed from the sealed tube and powdered and was sealed back. However, there was no change in the complexity of the pattern,
- (c) high temperature e.s.r. spectra were observed at every 10°C raise in the temperature. The complex uninterpretable spectrum was observed upto about 110°C and above that no signals were observed. At 150°C the sample had already melted and no signals were recovered on cooling,
- (d) there was essentially no change upon cooling the sample to LNT,
- (e) annealing of the sample for about 6-8 hours at 100°C produced no change in the spectrum.
- (f) the sealed quartz tubes preserved in the dark at room temperature containing the sample were observed for several weeks. Eventually the radical faded and the tube was found to be etched suggesting the formation of some elemental fluorine. We have also observed etching of quartz tube on heating NH_4PF_6 on flame for a few minutes,
- (g) Analysis of the final product for PF_5 was not considered practical due to the small concentrations expected.
- (h) We attempted to prepare the PF_6 salt of the more stable $\text{Ag}(\text{bpy})_2^+$ ion. However, the solid obtained by adding NH_4PF_6 to $\text{Ag}(\text{bpy})_2\text{NO}_3$ in nitric acid in presence of $(\text{NH}_4)_2\text{S}_2\text{O}_8$ gave a magnetically concentrated e.s.r. spectrum with $g_1 = g_2 = 2.174$ and $g_3 = 2.044$ (Figure 11b) we could not observe any formation of radicals

even on heating the sample or annealing it. Nor was there any change in the bright orange colour of the sample.

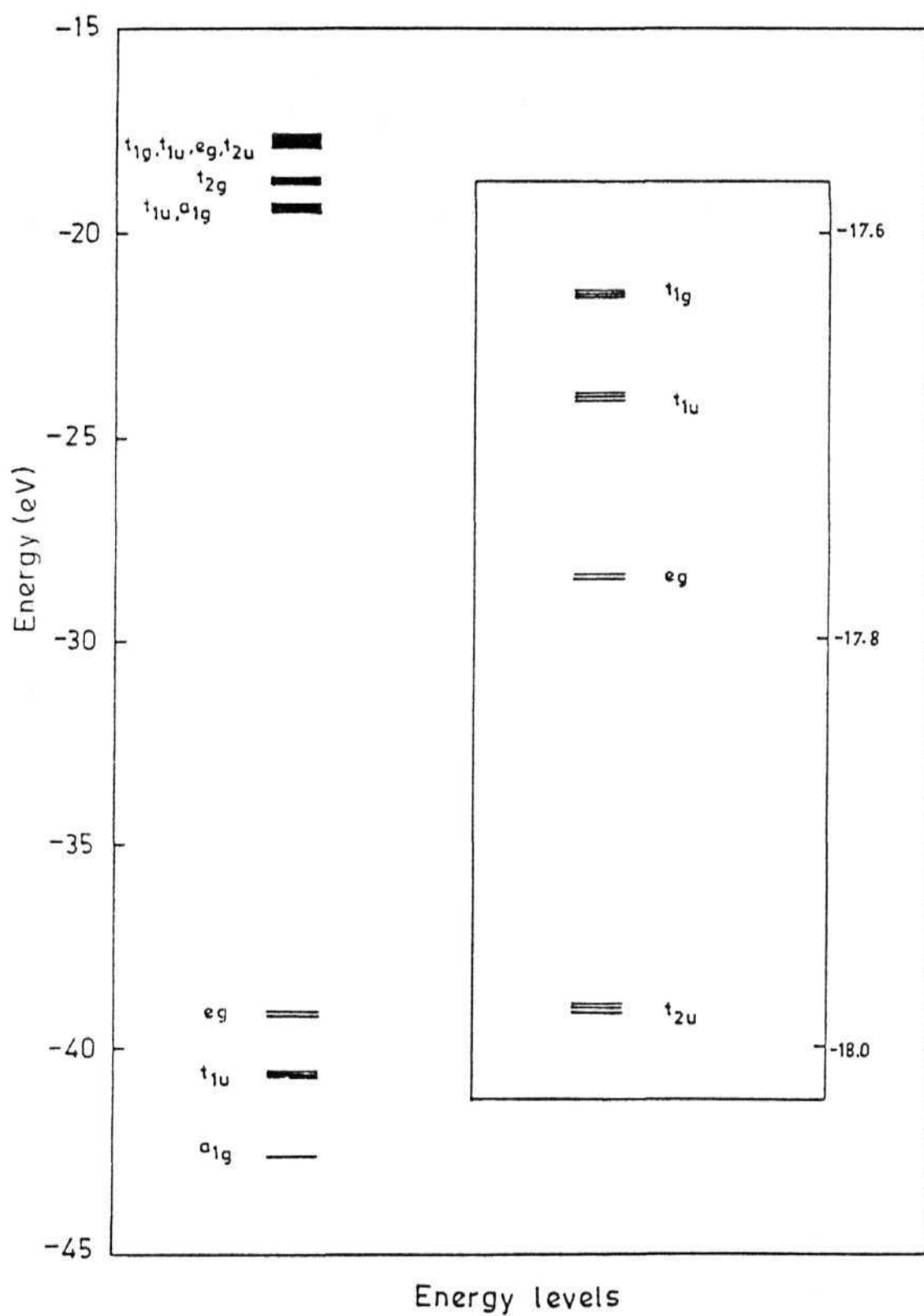
The double salt of dmp, did not give the radical signals. The Aq(II) spectra in it decayed with time but no new paramagnetic species was observed other than the single line of the organic radical which it initially contained (Figure 9). It is likely that the organic radical impurity destroyed any new radical formed by electron transfer. Attempts to purify the dmp ligand by recrystallisation from methanol were not successful.

3. 6. 3

The PF_6^\cdot radical:-

The PF_6^\cdot radical is interesting because it is expected to have an electronically degenerate ground state. One reason it has been eluding detection is the potential instability of the electronic state. γ -irradiation is expected to provide sufficient energy to dissociate one F atom from PF_6^\cdot leading to PF_5^\cdot . Any PF_6^\cdot formed by irradiation will also have sufficient kinetic energy to loose a fluorine atom to give the stable PF_5 molecule.

An energy level diagram for the PF_6^\cdot obtained using the Extended Hückel molecular orbital (EHMO) method is shown in Figure 18. It is seen that the ground state is ${}^2\text{T}_{1g}$, and there are three more degenerate states within about 2800 cm^{-1} of the ground state. The total energy vs distortion along an e_g mode was found to have a very shallow minimum. The vibronic interactions are expected to be complicated by multimode coupling effects. No attempt will be made here to treat this problem here. However, the above obser-



vations show a possible method to search for PF_6 radical in other systems, preferably in single crystals, where Ag^{2+} sites with a high redox potential is in proximity of a PF_6^- ion for a facile electron transfer to occur.

3. 7 Comparison between Copper and Silver complexes of hindered ligands:-

The bidentate N-heterocyclic ligands increased the $\text{Cu}^+ / \text{Cu}^{2+}$ potential⁴³ from 0.167 V to 0.251 V in the case of bpy and to ≥ 0.75 V for dmbp. The same ligands reduce the $\text{Ag}^+ / \text{Ag}^{2+}$ potential from 1.9 V to 1.45 V (bpy)⁴⁴ and to ≥ 1.7 V (dmbp,dmp). The major reason for the increase of the $\text{Cu}^+ / \text{Cu}^{2+}$ potential is the tetrahedral distortion of the CuL_2^{2+} ions, especially for the hindered ligands²⁸. The unhindered ligands tend to form cis-octahedral $\text{CuL}_2(\text{H}_2\text{O})_2^{2+}$ species in aqueous solution which lowers the potential. On the other hand, the reduction in the $\text{Ag}^+ / \text{Ag}^{2+}$ potential appears to be due to the extensive delocalisation of charge via π -bonding interaction. Here again the tetrahedral distortion in the case of dmbp and dmp complexes tend to raise the potential.

REFERENCES

1. N.N. Greenwood and A. Earnshaw, "Chemistry of the Elements", Pergamon Press, (1984).
2. F.A. Cotton and G. Wilkinson, "Advanced Inorganic Chemistry", Interscience, (1980).
3. K.C. Dash, Proc. Nat. Sym. Unusual Valency States Coord. Chem., BARC, Bombay (1987).
4. (a) H.N.Po, Coord. Chem. Revs.,20(1976)171.
(b) J.A.Mc Millan, Chem. Revs.,62(1962)65.
(c) P. Ray and D.Sen, "Chemistry of Bi and Tri-positive silver", Nat. Inst. Sciences of India, (1960).
5. W. Levason and M.D. Spicer, Coord. Chem. Revs., 76(1987)45 and references therein.
6. G.A. Barbieri, Gazz. Chem. Ital., 42(1912)7; quoted in ref.(5).
7. (a) T.J. Smith and R.A. Walton, J. Inorg.Nucl.Chem., 39(1977)1331.
(b) T.J. Smith and R.A. Walton, Inorg.Nucl Chem. Lett., 11(1975)301.
8. J.C. Evans, R.D. Gillard, R.J. Lancashire and P.H. Morgan, J. Chem. Soc. Dalt. Trans.,(1980)1277.
9. (a) T. Halpern, W.D. Phillips and J.A. Mc Millan, J. Chem. Phys., 52(1970)5548.
(b) J.A. Mc Millan and B. Smaller, J. Chem. Phys., 35(1961)1698.

10. R.W. Mathews and R.A. Walton, *Inorg. Chem.*, 10(1971)1433.
11. H.G. Hecht and J.B. Frazier, III, *J. Inorg. Nucl. Chem.*, 29(1967)613.
12. R.S. Banerjee and S. Basu, *J. Inorg. Nucl. Chem.*, 26(1964)821.
13. J.R. Wasson, *J. Inorg. Nucl. Chem.*, 28(1966)2201.
14. (a) M.P. Heywood and C.F. Wells, *J. Chem. Soc. Dalt.*, (1981)431.
(b) T. Halpern, S.M. McKoskey and J.A. McMillan, *J. Chem. Phys.*, 52(1970)3526.
15. G.T. Morgan and F.H. Burstall, *J. Chem. Soc.*, (1930)2594; (1937)1649.
16. W.G. Thrope and J.K. Kochi, *J. Inorg. Nucl. Chem.*, 33(1971)3958.
17. J. Talamin, Y. Le Mest, M.L. Her and J. Courtot-coupez, *Elec. Act.*, 29(1984)957, 967.
18. J.L. Atwood, M.Z. Simms and D.A. Zatko, *Cryst. Struct. Comm.*, 2(1973)279.
19. I.M. Anderson and J.K. Kochi, *J. Org. Chem.*, 35(1970)986.
20. G.W. Bushnell and M.A. Khan, *Can. J. Chem.*, 50(1972)315.
21. C.W. Harris and T.N. Kockyer, *Aust. J. Chem.*, 23(1970)1125.
22. J.A. McMillan and B. Smaller, *J. Chem. Phys.*, 35(1961)1698.
23. D.P. Murtha and R.A. Walton, *Inorg. Nucl. Chem. Lett.*, 9(1973)819.
24. J.L. Pierce, K.L. Busch, R.G. Cooks and R.A. Walton, *Inorg. Chem.*, 22(1983)2492.

25. W.R. Schiedt, J.V. Mondal, C.W. Eigenbrot, A. Adler, L.J. Radonovich and J.L. Hoard, *Inorg. Chem.*, 25(1986)795.
26. (a) G.W.A. Fowles, R.W. Mathews and R.A. Walton, *J.Chem. Soc. A* (1968)1108.
(b) A. Kleinstein and G.A. Webb, *J. Inorg. Nucl. Chem.*, 33(1971)405.
27. J.F. Dobson, B.E. Green, P.C. Healy, C.H.L. Kennard, C. Pakawatchai and A.H. White, *Aust. J.Chem.*, 37(1984)649.
28. S. Kitagawa, M. Munakatar and A. Higashie, *Inorg. Chim. Acta.*, 84(1984)79.
29. J.A. Hall, R.A. Plowman and H.S. Preston, *Aust. J. Chem.*, 18 (1965)1345.
30. K.V. Goodwin, D.R. Mc Millin and W.R. Robinson, *Inorg. Chem.*, 25(1986)2033.
31. (a) K. Nakamoto, "IR and Raman Spectra of Inorganic and Coordination Compounds", Wiley, London (1978)p.244.
(b) G.G. Messmer and G.J. Palenik, *Inorg. Chem.*, 8(1969)2750 and reference therein.
(c) D.P. Murtha and R.A. Walton, *Inorg. Chem.*, 12(1973)368.
32. (a) A. Abragam and M.H.L. Pryce, *Proc. Roy. Soc. (London)*, A 205(1951)135.
(b) P.T. Manoharan and M.T. Rogers, "Electron Spin Resonance of Metal Complexes", T.F. Yen, Ed., Plenum Press, New York (1968).
33. B.A. Goodman and J.B. Raynor, *Adv. Inorg. Chem. Radiochem.*, 13(1970)134.

34. M.V. Rajasekharan, R. Bucher, E. Deiss, L. Zoller, A.K. Salzer, E. Moser, J. Weber and J.H. Ammeter, *J. Am. Chem. Soc.*, 105 (1983)7516.
35. T.G. Brown and B.M. Hoffman, *Mol. Phys.*, 39(1980)1073.
36. S.F. Sontum and D.A. Case, *J. Phys. Chem.*, 86(1982)1596.
37. T. Buch, *J. Chem. Phys.*, 43(1965)761.
38. A. Carrington and A.D. Mc Lachlan, "Introduction to Magnetic Resonance", Chapman and Hall, London (1978)p.129.
39. Yu.G. Kriger, S.G. Kozlova, P.P. Samoilov and S.P.Gabuda, *Sov. Phys. Solid State*, 28(1986)325.
40. J.R. Morton, K.F. Preston and S.J. Strach, *J.Phys. Chem.*, 83 (1979)3418.
41. (a) J.E. Wertz and J.R. Bolton, "Electron Spin Resonance, Elementary theory and Practical Applications", Mc Graw-Hill, London (1972), p.68.
(b) J.R. Morton, *Can. J. Phys.*, 41(1963)706.
(c) R.W. Fessenden, *J. Mag. Res.*, 1(1969)277.
42. J.R. Morton, K.F. Preston and S.J. Strach, *J. Mag. Res.*, 37 (1980)321.
43. B.R. James and R.J.P. Williams, *J. Chem. Soc.* (1961) 2007.
44. N.R. Thompson in "Comprehensive Inorganic Chemistry", Vol.3, A.F. Throtman-Dickenson, Ed., Pergamon Press, Oxford (1973)p.122.

SUMMARY AND CONCLUSIONS

Section I: Chemistry of mixed valence manganese (III, IV) complexes.

1. $(\text{Mn}_2\text{O}_2\text{L}_4)^{3+}$ complexes are found to be unstable in water at neutral pH as was reported by Cooper et al³⁶ and in contradiction to Ramaraj et al⁴⁵.
2. $(\text{Mn}_2\text{O}_2\text{L}_4)^{3+}$ complexes are found to be susceptible to substitution on the labile Mn(III)(d^4 , high-spin) site. They were substituted by dmf or py or another bidentate ligand.
3. The intensity of the IVTA band of dmf and py substituted complexes was very small compared to the parent complexes indicating reduced delocalisation.
4. The electronic spectra of substituted $(\text{Mn}_2\text{O}_2\text{bpy}_3\text{phen})(\text{ClO}_4)_3$ and the analogous substituted $(\text{Mn}_2\text{O}_2\text{phen}_3\text{bpy})(\text{ClO}_4)_3$ complex have shown almost identical spectra with band positions similar to those in parent complexes.
5. The e.s.r spectra of the powder samples for all, except the PF_6^- salts and $(\text{Mn}_2\text{O}_2\text{bpy}_3\text{phen})(\text{ClO}_4)_3$ complex, show a broad single signal. In most of the complexes broad bands are observed on the wings which are found decreasing in intensity on lowering the temperature. They are attributed to quartet state.
6. The PF_6^- salts and $(\text{Mn}_2\text{O}_2\text{bpy}_3\text{phen})(\text{ClO}_4)_3$ complex show resolved spectra showing upto 16 lines indicating magnetic dilution in the lattice. Spectrum of $(\text{Mn}_2\text{O}_2\text{phen}_4)(\text{PF}_6)_3$ complex was simulated.

7. The frozen solution e.s.r spectra of all the complexes in dmf or CH_3CN are similar. In CH_3CN they show 16 lines and in dmf further splittings are also observed. The spectra were simulated, including anisotropic terms, for $(\text{Mn}_2\text{O}_2\text{phen}_4)(\text{PF}_6)_3$ in dmf and $(\text{Mn}_2\text{O}_2\text{bpy}_4)(\text{PF}_6)_3$ in CH_3CN .
8. The e.s.r parameters of the Mn(III, IV) complexes are not very sensitive to the nature of the ligands. The g and hyperfine parameters are nearly same in all cases. The g-anisotropy is reduced because of the high values of optical transition energies and the A values are dominated by core polarisation.
9. There was no temperature dependent change in the spectrum either in the solid or in solution state which could be attributed to change in electron transfer rate. The thermal electron transfer in all cases is slow compared to the difference in hyperfine coupling of the two centres (i.e., $< 10^8 \text{ Hz}$). The temperature dependence is mainly due to the change in population of the ground doublet and the first excited quartet state.
10. All these complexes were observed to oxidise water in the presence of Ce(IV) into O_2 in heterogeneous medium. The unsymmetrical complexes are found to release more amount of oxygen, as indicated by larger turnover numbers. MnO_4^- ion is also detected in solution in presence of $(\text{NH}_4)_2\text{Ce}(\text{NO}_3)_6$ which complicates mechanistic discussion.

Section II: Chemistry of bivalent silver (II) complexes.

1. Silver (I) complexes of the type (AgLNO_3) were formed where $\text{L}=\text{dmbp}$, dmp , daf , daf-one and mmbp , while tmbp forms $(\text{AgL}_2\text{NO}_3)$.
2. The oxidised products of these complexes gave magnetically concentrated samples with all ligands and in addition magnetically dilute samples of the type $(\text{AgLNO}_3)\text{PF}_6 \cdot \text{NH}_4\text{PF}_6$ where $\text{L}=\text{dmbp}$ and dmp .
3. The magnetically dilute salts showed highly resolved e.s.r spectra at room temperature with increased intensity at low temperatures. Delocalisation of the unpaired electron of d_{xy} molecular orbital onto bidentate nitrate leads to distortion in the planar geometry towards tetrahedron.
4. The bidentate N-heterocyclic ligands increased the $\text{Cu}^+/\text{Cu}^{2+}$ potential⁴³ from 0.167V to 0.251V in the case of bpy and to $\geq 0.75\text{V}$ for dmbp . The same ligands reduce the $\text{Ag}^+/\text{Ag}^{2+}$ potential from 1.9V to 1.45V (bpy)⁴⁴ and to $\geq 1.7\text{V}$ (dmbp , dmp). The reason for increase in potential for $\text{Cu}^+/\text{Cu}^{2+}$ is the tetrahedral distortion of the CuL_2^{2+} ion while the reduction in the potential for $\text{Ag}^+/\text{Ag}^{2+}$ appears to be due to the extensive delocalisation of charge via π -bonding interaction.
5. The Ag(II) spectrum of the double salt from dmbp was replaced over a period of days, finally resulting in an uninterpretable spectrum consisting of very narrow ($\leq 2\text{G}$) lines spread over 5000G. The spectrum obtained could not be fit to any known radical

formed by γ -irradiating PF_6^- salts and is tentatively assigned to the PF_6 radical. Our EHMO calculations on PF_6 radical led to a very flat potential surface clustering all molecular orbitals at T_{1g} leading to a complex vibronic coupling situation.